FLORIDA INTERNATIONAL UNIVERSITY

Miami, Florida

SUCRALOSE, A UNIQUE TRACER FOR WASTEWATER INTRUSION

A thesis submitted in partial fulfillment of the

requirements for the degree of

MASTER OF SCIENCE

in

CHEMISTRY

by

Mark Jonathan Cejas

2010

To: Dean Kenneth Furton
College of Arts and Sciences

This thesis, written by Mark Jonathan Cejas, and entitled Sucralose, A Unique Tracer for Wastewater Intrusion , having been approved in respect to style and intellectual content, is referred to you for judgment.

We have read this thesis and recommend that it be approved.

Rudolf Jaffe

Kevin O'Shea

Piero R. Gardinali, Major Professor

Date of Defense: March 26, 2010

The thesis of Mark Jonathan Cejas is approved.

Dean Kenneth Furton
College of Arts and Sciences

Interim Dean Kevin O'Shea
University Graduate School

Florida International University, 2010

DEDICATION

This thesis is dedicated to my family, friends and my Pattiness. Without their strong support and love this work would have been impossible.

ACKNOWLEDGMENTS

First and foremost, I would like to thank my major professor Dr. Piero Gardinali for his patience, support and insight throughout this research experience. I would also like to thank my committee members Dr. Rudolf Jaffe and Dr. Kevin O'Shea for their constructive ideas, support, and time.

I give special thanks to Dr. Joseph Boyer and his group for collecting samples in Little Venice, Marathon Key.

Finally, I would like to thank all my coworkers for their help and support. Especially, Chengtao Wang, Luis Arroyo, Adolfo Fernandez, Ingrid Zamora-Ley, Elienai Veguilla, Cesar Ramirez, Sudah Rani, Venkat Panditi, Jian Wang and Nubia Heuett.

Thanks to everybody in SERC, and the Chemistry and Biochemistry department.

ABSTRACT OF THE THESIS

SUCRALOSE, A UNIQUE TRACER FOR WASTEWATER INTRUSION

by

Mark Jonathan Cejas

Florida International University, 2010

Miami, Florida

Professor Piero R. Gardinali, Major Professor

The vitality of the Florida Keys ecosystem has been impacted by various anthropogenic influences, whereas one of the significant influences is the local intrusion of untreated wastewater. Prior research has elucidated the unique stability of sucralose under human and microbial metabolic processes and low decay rates in water, sediment, soil and sewage compartments. The unique environmental stability of sucralose and its specificity to anthropogenic sources, served as a basis to assess it as an ideal molecular tracer for wastewater intrusion. This study presents the development and validation of two isotope dilution methods, sucralose i.e. Splenda®. One method applied ESI-LC-MSMS, while the other employed (GC-MS). Sucralose was discovered to be an ideal tracer occurring at higher concentrations than previously detected pollutants in the chosen study sites. Furthermore, the accuracy, precision and detection limits of both analytical methods were suitable for the environmental monitoring in coastal marine waters of the Florida Keys.

TABLE OF CONTENTS

CHAPTER PAGE

LIST OF TABLES

TABLE PAGE

LIST OF FIGURES

FIGURE PAGE

Chapter 1

Introduction

1.1 Anthropogenic Perturbations to the Coastal Marine Ecosystem

In 1974, a baseline study of coral reef community structure began at Carysfort Reef off Key Largo. The study spanned eight years and documented relatively rapid changes in the abundance and distribution of reef-building corals. Selective mortality of organisms were noted from the baseline investigation, where the most diverse regions of the reef changed the most and led to a more simplistic arrangement of species – a reduction in biodiversity and a shift in the zonation pattern of species assemblages (Dustan, 1987). The 1974 study was one of the first to document the regional shift in the zonation pattern of the Florida Keys coral reef tract; from one that was dominated by the foundation species: *Acropora palmata, A. cervicornis*, and *Montastraea annularis,* to a dominance of fleshy and filamentous macroalgae, see figure 1.1 (Precht, 2007).

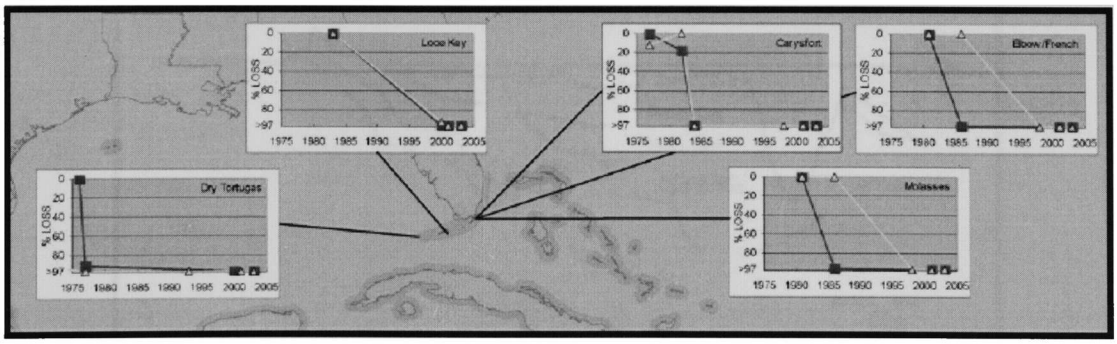

Figure 1.1. Loss of foundation species in the Florida Keys reef tract. Source: Dustan, 1987.

By the early 1980's, the coral zonation pattern once dominated by foundation coral species had essentially disappeared (Precht, 2007). This dramatic shift in the zonation pattern raised a question of great significance to scientists, managers and policy makers: were the recent changes something new or part of a long term pattern of repeated community shifts? Aronson and Precht viewed the recent demise of acroporid corals as a problem that required multiple scales of space and time to be investigated. Given that coral reefs are both geologic and biologic entities, Aronson postulated that it should be possible to observe the effects of various disturbances in ecological time, detect historical changes in the paleoecological record, and deduce the multiscale processes behind those patterns by comparing the structure and anatomy of the Holocene and Pleistocene reef building episodes with the modern coral reef communities, see figure 1.2 (Aronson and Precht, 2002).

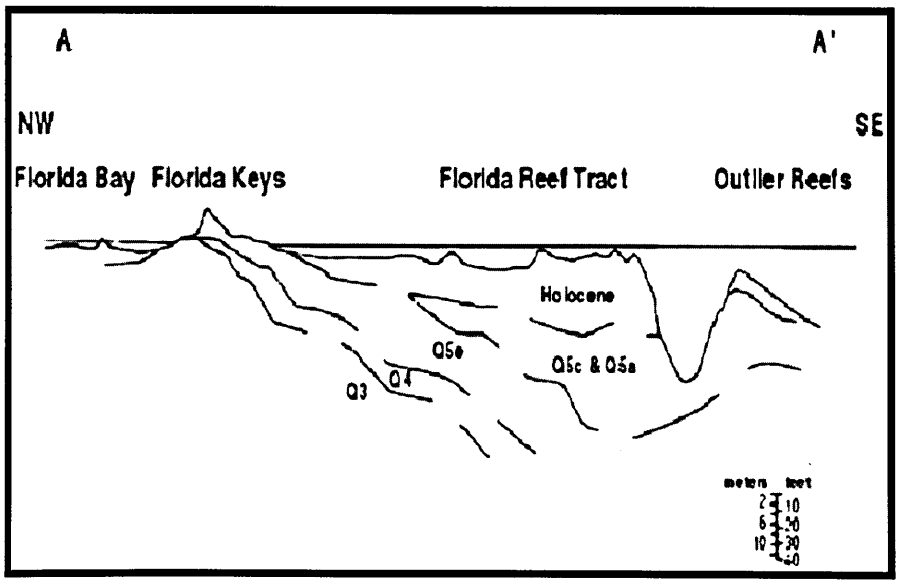

Figure 1.2. Stratigraphic cross section across the Florida Keys reef tract. Source: Aronson, et al. 2001b.

A multidisciplinary group of scientists joined Aronson in perusing the fossil record to study the ecological responses of coral reef systems (Jackson, 1992; Aronson and Precht, 2002). Their research explored locations throughout the Caribbean and concluded that the historical Pleistocene reef sections exhibited zonation patterns similar to modern reefs from the same locations. Furthermore, Pleistocene reef communities within the same environment were more distinct among reefs of the same age - from different places - than among reefs formed at different times at the same locations (Jackson, 1992). This commonality of coral zonation patterns showed that the shift in the zonation pattern was without geological precedent and solely related to perturbing anthropogenic factors (Stokstad, 2001).

Anthropogenic factors refer to the human perturbation as a whole, on observed changes to coral reef community structure. The scientific community has discovered many potential human induced causes in the breakdown of Caribbean reef zonation patterns and recent coral die-off. Among the postulated major causes are temperature - the condition of global warming - and poor water quality. The observed major effects are coral bleaching, disease and the displacement of foundation coral species by filamentous macroalgae communities (Aronson and Precht, 2002). However, the causal linkages are uncertain and addressed by many competing theoretical models. Two contending viewpoints of coral reef die off in the Florida Keys are cited as examples: (1) the primary cause of coral mortality is excessive levels of nutrients, which then stimulate the overgrowth and encroachment of macroalgae communities – bottom up model (Lapointe, 1997); (2) Recent reviews of the role of nutrient enrichment on coral reef decline (Szmant, 2002) and the relationships among nutrients, algae and competition between

algae and corals suggest that the increased abundance of algae is not because of enriched nutrients but is instead explained by the availability of new substrate for algal colonization following coral mortality from a complex interaction of causal mechanisms (Aronson and Precht 2002).

1.2 The Sewage Vector and Disease in Coastal Marine Waters

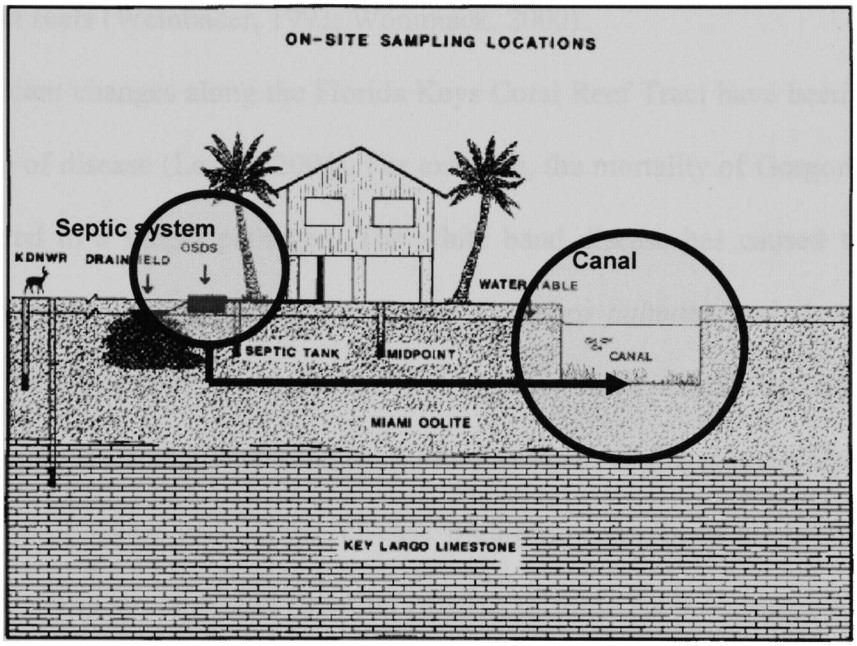

Figure 1.3. Local untreated sewage vector in the Florida Keys. Source: Lapointe, 1990.

Local land based sewage inputs are a major concern in the Florida Keys and postulated to be a significant cause of disease in coral reef communities of the Florida Keys. Untreated sewage effluent is dispersed into the marine environment via septic tanks, cesspits, and shallow injection wells, see figure 1.3 (Shinn, et.al. 1994; Paul, 1995) Approximately 65% of the wastewater in the keys is disposed in this fashion by some 30,000 on site sewage disposal systems (Lapointe, 1992). Moreover, evidence is

beginning to show direct links between the land based sewage source in the Florida Keys and disease outbreak. For instance, White Pox is caused by a marine invertebrate pathogen, a common fecal enterobacterium associated with sewage effluent (Patterson, 2002). Recent studies have revealed the correlation between wastewater derived nutrient gradients and the distribution of viruses in marine waters. The findings propose the sewage vector as a stimulus to viral development and a potential causal component of disease to coral reefs (Weinbauer, 1993; Wommack, 2000).

Significant changes along the Florida Keys Coral Reef Tract have been related to the emergence of disease (Lesser, 2004). For example, the mortality of Gorgonian corals has been related to a fungal pathogen. The white band disease has caused the almost complete decimation of two foundation species *Acropora palmata,* and *A. cervicornis* (Porter, 2001). Furthermore, populations of the shallow water Carribean Elkhorn coral *Acropora Palmata* are being devastated by White Pox, an emerging disease characterized by a rapid rate of tissue loss. These disease outbreaks have been major factors that influence community structure and zonation patterns of these reefs (Aronson and Precht, 2002).

A recent study in the Florida Keys assessed patterns, distribution and spread of coral disease. The authors noted that stations closest to densely populated environs, such as Key Largo, expressed a higher percentage of disease. The author claims: "This correlation suggests that proximity to human population centers may increase the likelihood of infection. One hypothesis is that poor water quality at these sites exacerbates disease virulence" (Porter, 2001). Downs, et al. (2005) applied a cellular biomarker approach to assess probable causes of coral stress in the Florida Keys. The

cellular diagnostic tool was used to measure changes in cellular parameters that include membrane integrity and composition, anti-oxidant redox status, protein metabolic condition, xenobiotic detoxification pathways, intra-cellular metal regulation, and genomic integrity. The diagnostics allowed: (1) assessment of cellular-physiological condition of an individual or population, (2) identification of stressors, either by direct measurement or by assessing stressor specific affects, and (3) forecasting behavior based on an understanding of cellular level processes. The results indicated that the distressed corals were afflicted with a severe oxidative damaging and protein denaturing stress; a condition that was associated with a significant xenobiotic detoxification response from exposure to synthetic chemicals.

The viewpoint supported from Aronson, et al. (2002) considers the synergistic relationship between nutrients and other disease causing factors as a significant cause of coral mortality. Bruno, et al. (2003) posited that the most important consequence of increased nutrification may lie in an increase in the severity and duration of coral diseases, not from the direct stimulation of macroalgae growth. The authors reported evidence from two field experiments that nutrient enrichment can significantly increase the severity of two important Caribbean coral epizootics: aspergillosis of the common gorgonian sea fan *Gorgonia ventalina* and yellow band disease of the reef building corals *Montastraea annularis* and *M. franksii.* They hypothesized that the experimental pathogenic species, *A. sidowii* and *Vibro* spp., utilized the additional nutrients in the enrichment treatments thereby increasing pathogen fitness and virulence. In light of the steadily growing discoveries, of the relationships between the declining health of the coastal marine ecosystem and anthropogenic factors, one can argue that the results are

converging and suggest a significant and deleterious impact by the sewage vector on the health of the coral reef ecosystem in the Florida Keys; signifying that a multidisciplinary dialogue - between marine biologists and marine chemists – must gain focus to study the relationship between coral die off and the myriad chemical stressors derived from the aquatic wastewater pollution vector.

1.3 Microconstituents in the Marine Environment

As Danovaro and Bruno suggest - from their reports of disease, viruses, and marine pollution - eutrophication acts synergistically with other anthropogenic factors and contribute to the creation of environmental conditions that favor the development of disease. The research of Danovaro, et al. research related to marine pollution on the bioactive effect of cosmetic sun products found an influence on microbial loop functioning and these products also induced viral development. The effect of cosmetic sun products on viral abundance was evident after a few hours and lasted for at least three months. These results indicate that bioactive pollutants released in coastal waters might have a significant impact on viral abundance, even at very low levels as observed for classical pollutants such as PCBs and pesticides (Danovaro, 2003; Cochran, et al. 1998). Danovaro's research is vital, for it increases the relevance of an anthropogenic induction of natural lysogenic viral production and supports a broader definition of 'water quality', one that considers the pollution stream as a source of bioactive emmerging pollutants (microconstituents) which can modify marine microbial communities. Furthermore, the studies by Downs, et al. and Bruno, et al. raise the attention that the wastewater vector could be a significant stimulus to coral disease in the marine environment and the

characterization of water quality should consider the most relevant microconstituents, in addition to nutrients and bacteriological indicators.

Endocrine disrupting effects by classical pollutants have been known since the end of the 1990's (Desbrow, et al. 1998). Since then, bioactive pharmaceuticals and personal care products (microconstituents) have emerged as important environmental pollutants as a result of their extensive presence in the environment. Their levels in the aquatic environment are usually on the order of ng-ug/L, and their effects not acute. Nonetheless, due to their continuous introduction into the environment, they may behave as a pseudo-persistent pollutant (Calamari, et al. 2003). Being biologically active substances, microconstituents are of concern because of their potential interaction with non-target organisms in the environment; but also because of their ability to be excreted unaltered or as toxic metabolites and move back up the aquatic trophic chain through surface, ground and drinking waters (Isidori, et al. 2009).

The prevalence of microconstituents was noted in a recent survey of U.S. surface and ground waters. The findings showed that one or more microconstituents were found in 80% of the 139 streams, and that steroids and non-prescription drugs were among the highest in concentration and frequency of detection. Their data are a strong indication that either treated or un-treated wastewater is the primary conduit for transmission of microconstituents into the aquatic environment (Koplin, 2002). A survey of microconstituents in marine and canal waters off the Florida Keys was recently conducted. The detection frequency for all hormones and fecal steroid contaminants was above 60% for 137 water samples off the Florida Keys. The concentration ranges for

these contaminants were as follows: estrone 0.7-16.4 ng/L, β-estradiol 2.5-4.6 ng/L, coprostanol 0.7-52.8, coprostanone n.d. - 40.4 ng/L (accepted for Ecotoxicology).

Irrespective of the model one applies to explain environmental degradation in the Florida Keys, three facts remain supported by the scientific community. (1) 'Local anthropogenic nutrient loads' derive from a complex sewage - wastewater vector (2) and the sewage vector is also a source of numerous chemical constituents (traditional hydrocarbon based pollutants, metals, pharmaceuticals, personal care products, nutrients, bacteria, etc.) that could introduce a wide range of stress to marine organisms (Depledge, 1999; Porter, 2003; Danovaro and Corinaldesi, 2003; Cochran et al, 1998). (3) Furthermore, to properly assess water quality in sensitive marine waters, bioactive microconstituents and molecular tracers that occur at higher concentrations - and share a common source - should be monitored.

Given the growing literature on the application of microconstituents as molecular sewage tracers, their effectiveness should be characterized as follows: (1) be ubiquitous and derive only from sewage. (2) Be persistent and present at high (detectable) concentrations in contaminated environmental samples. (3) Do not undergo extreme rates of degradation in wastewater/water, if so degradation rates should be known. (4) Chemical tracers should have high water solubility, low K_{OW} and low volatility (Hordern et al, 2009). Some proven tracers include compounds like linear alkylbenzenes, trialkylamines, fluorescent whitening agents a wide range of pharmaceuticals as well as caffeine and personal care products (Weigel, 2004, Glassmeyer, 2005, Hordern, et al, Singh and Gardinali, 2006, Gardinali, 2002).

After considering the current state of untreated sewage intrusion throughout the Florida Keys, empirical evidence indicates the need to properly monitor and assess the impact of the deleterious sewage intrusion with an ideal molecular tracer i.e., one that is ubiquitous in regards to the human condition, persistent at high detection levels, not prone to degradation by either human nor bacterial metabolism and highly soluble in water. The current research focused on the development and application of a trace level analytical method for an organic compound that meets the requirements as an ideal molecular tracer. The compound is the new artificial sweetner called sucralose, or by its trader name Splenda ®.

1.4 Sucralose: Chemical Properties, Kinetics, Toxicity and Persistence

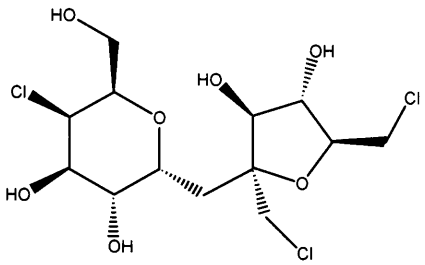

Figure 1.4. Molecular structure of sucralose. Molecular Mass: 397.64g/mol

Sucralose (1', 4', 6 trideoxy-trichloro-galactosucrose) is a substituted disaccharide synthesized by selective chlorination of sucrose at three of the primary hydroxyl groups, which involves inversion of configuration at carbon-4, from the gluco- to the galacto-analogue, see figure 1.4 (U.S. patent, 5,498,709). Sucralose is approximately 600 times sweeter than its natural sucrose analogue, without the bitter aftertaste often attributed to other non-nutritive sweeteners such as aspartame and saccharine (Wiet and Beyts, 1992;

Horne et al., 2002; Kuhn et al., 2004). Its intense sweetness is claimed to stem from the fructose moiety of the molecule.

Sucralose is commonly known under the trade name of Splenda® and was discovered in 1976 by scientists from Lyle & Tate Laboratories. The artificial sweetener was first approved for use in Canada - in 1991, Australia in 1993, and New Zealand in 1996. The U.S. followed in 1998 and the European Union only in 2004. By 2008 the sweetner was approved in over 80 countries (Grotz, et al. 2009). To give you an idea of Splenda's market dominance, according to the Wall Street Journal, Splenda sold $ 212 million in 2006 in the U.S. while Equal sold $ 48 million.

The safety of sucralose has been the subject of rigorous and extensive investigation (Grotz, et al. 2009). Consistent with regulatory requirements, the core safety research studies for sucralose were designed and conducted in accordance with recognized international standards. Critical safety studies are available in the following publications (Finn and Lord, 2000; Grice and Goldsmith, 2000; John et al., 2000a,b; Kille et al., 2000a,b; Mann et al., 2000a,b; Mc Lean Baird et al., 2000; Roberts et al., 2000; Sims et al., 2000; Wood et al., 2000). Examples of studies conducted included, but were not limited to:

- General physicochemical studies
- Genetic toxicity tests to consider mutagenic and clastogenic potential
- Metabolism and pharmacokinetic studies in five species, including humans
- Subchronic toxicity tests in several species
- Studies to confirm that sucralose is non nutritive

- Tests for potential metabolic interaction with carbohydrate regulation
- Specialized studies to assess immunotoxicity and neurotoxicity potential
- Studies to assess the likelihood for interaction with or induction of cytochrome P-450 enzymes
- Reproduction and development studies
- Chronic toxicity and carcinogenicity studies
- Human tolerance studies
- Studies in people with diabetes and in normoglycemic individuals to evaluate the potential to affect insulin sensitivity
- Bacterial, animal –model and human studies to investigate the potential to induce dental caries

Public health authorities worldwide, including, FDA – U.S., JMHW – Japan's ministry and health and welfare, SCF – the European Union's Scientific Committee on Health and Welfare, Canada's Department of Health and Welfare critically evaluated the information generated from the investigations listed above and concluded that sucralose is a safe food ingredient, that can be safely consumed for a lifetime (Grotz and Munro, 2009). Even though the critical safety studies represent one of the largest research programs ever conducted to investigate the safety of a new food additive, there is still new information being published in regards to the toxicity of sucralose mediated degradation products.

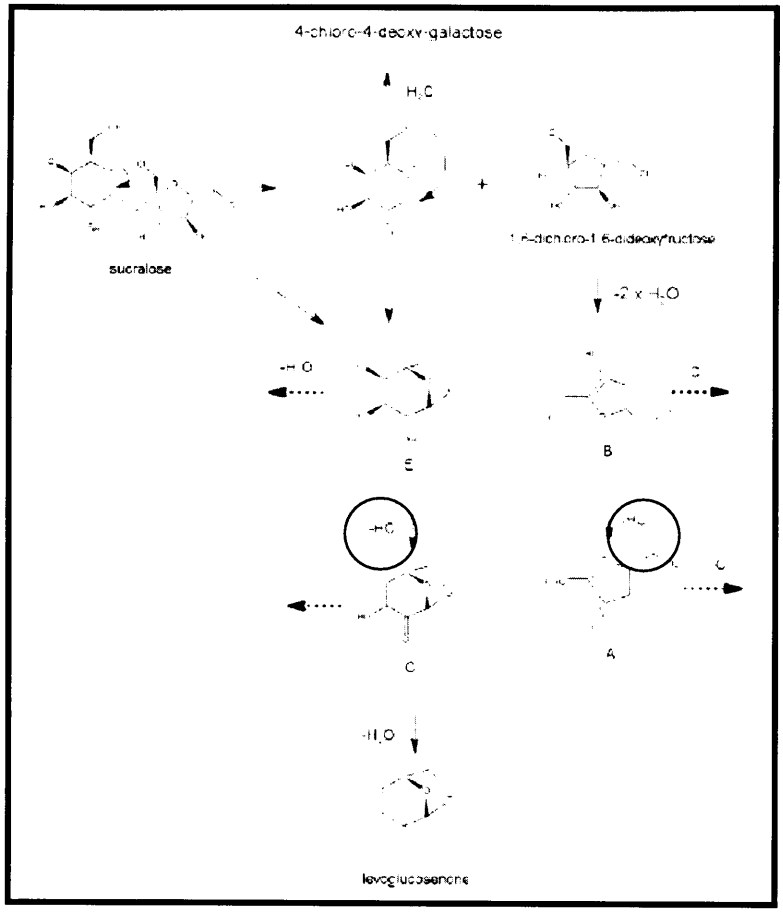

Fig 1.5. Proposed mechanism of degradation of sucralose and formation of compounds A,B,C,D and levoglucosenone. Source: Rhan and Laylayan, 2010.

For instance, Rhan and Yaylayan, 2009 investigated the thermal degradation and dehydrohalogenation reactions of sucralose in high temperatures and low moisture (baking) conditions: the authors examined the capacity of glycerol to capture the released hydrogen chloride and mediate its conversion into potentially toxic chloropropanol derivatives. The authors conclude that degradation of sucralose through the dehydrochlorination reactions (figure 1.5) generates two moles of hydrochloric acid per mole of sucralose through the transformations from E→C and from B→A. In the presence of glycerol, the hydrochloric acid generated a significant amount of the following three chloropropanols, 3-monochloropropanediol (3-MCDP), 1,2-

dichloropropanol (1,2-DCP) and 1,3-dichloropropanol (1,3-DCP). The authors close their report with the caution:

> "Degradation of sucralose in the presence of glycerol may generate different chloropropanols in addition to levoglucosenone, a well documented degradation product of sucrose and glucose. Caution should be exercised in the use of sucralose as a sweetening agent during baking of food products containing glycerol and or lipids due to the potential formation of toxic chloropropanols."

The pharmacokinetics of sucralose plays a strong role when characterizing it as a potential and powerful sewage tracer. Consistent with the no-calorie claim, the results of many studies confirmed that sucralose is only passively absorbed in limited amounts and consequently excreted in urine and feces as essentially "unaltered" sucralose. The total recovery of radiolabeled sucralose averaged 93%, 14% from urine and 78% from feces. Only 2-3% of the oral intake undergoes common phase II metabolism, specifically, glucuronidation (Roberts, et al., 2000). Glucuronide conjugates are also excreted in urine and readily eliminated with no measurable bioaccumulation (Grice and Goldsmith, 2000 John et al., 2000a; McLean Baird et al., 2000; Roberts et al., 2000; Sims et al., 2000; Wood et al., 2000). In addition to being extremely stable and virtually unaltered by human metabolic processes, sucralose proved to be stable under bacterial metabolism. According to a study on carbohydrate utilization (Young, 1990), 11 microorganisms could not utilize sucralose as a carbohydrate source, only one of the strain's tested displayed slight growth, but not reproducibly.

Aside from being very stable, not metabolized, nor readily transformed by the human body, sucralose exhibits strong stability in environmental samples. Measurements have been made of the biodegradation of sucralose in water, soils, sediment and sewage. Mineralization half life ($t_{1/2}$) of sucralose in various soils ranged from 60 -100 days. In sewage, 23% was mineralized in 123 days. In lake sediment, 5% was mineralized in 126 days. In lake water, approximately 2% was mineralized in 100 days (Labare, 1993). Even though these sucralose degradation rates are comparatively lower than the half life for most organic environmental contaminants, these studies are significant, for they show that sucralose is not biologically "inert" in the environment.

The environmental impact of sucralose was explored by Reinders et al., 2006. The authors presented a kinetic analysis of plant sucrose transporters (SUT's) SUT ShSUT1 from sugarcane and demonstrated that high concentrations of sucralose decreases sucrose transport in grasses such as sugarcane and possibly in other monocotyledons, such as sea grasses.

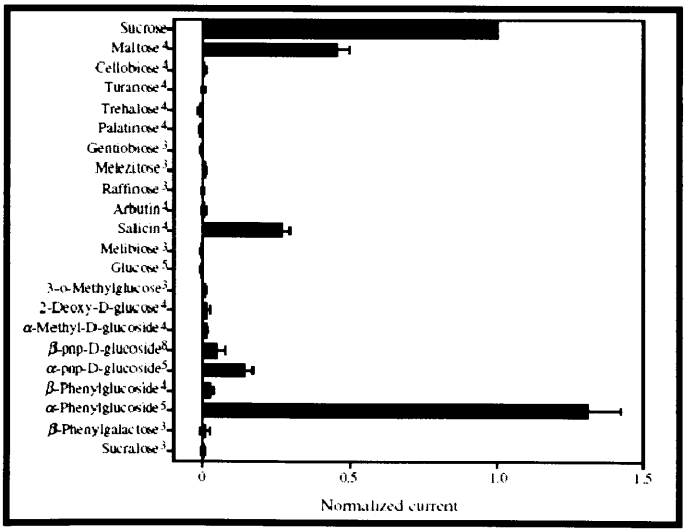

Figure 1.6. Bar chart showing the substrate specificity of ShSUT1. Substrate dependent currents from the kinetic analysis are presented as mean ± SE. Source: Reinders, et al. 2006.

Even though sucralose itself was not transported across the cell membrane, (Figure 1.6) their results indicate that sucralose can bind to the ShSUT1 binding site with about half the affinity of sucrose. The results from the Michaelis-Menten enzyme kinetics analysis (Shwartzenbach, et al. 2003) is summarized below (Figure 1.7) and indicated that sucralose is a 'competitive inhibitor' of sucrose. The inhibition constant K_I for sucralose was calculated in the following manner. The $K_{0.5}$ for sucrose was calculated from measurements taken in the presence of three different concentrations of sucralose (0,8 and 30mM), by applying the Michaelis-Menten equation at a membrane potential of -137 mV (figure 1.7-left). The $K_{0.5}$ "half saturation constant" values were multiplied by the inverse of V_{max} "the maximum rate of reaction", and then plotted as a function of the inhibitior (sucralose) concentration [I]. (figure 1.7-right).

Finally, the inhibition constant K_I was calculated by linear regression and equal to $K_I = 16.5mM = 6.55\times10^{9} ngL^{-1}$. The highest concentration of sucralose in surface water to date is 4374.04 ng/L (Mead, et al. 2009), thus, this concentration of sucralose inhibition is not yet environmentally relevant. Nonetheless, the research is important for it is another study showing that sucralose is not biologically "inert" in the environment. The author's research objective was to gain deeper insight into sucrose transport in plants, but also their research elucidates the potential environmental impact in the coastal marine waters of the Florida Keys, where the seagrass meadows, monocotyledons like the sugarcane, are one of the most abundant habitats.

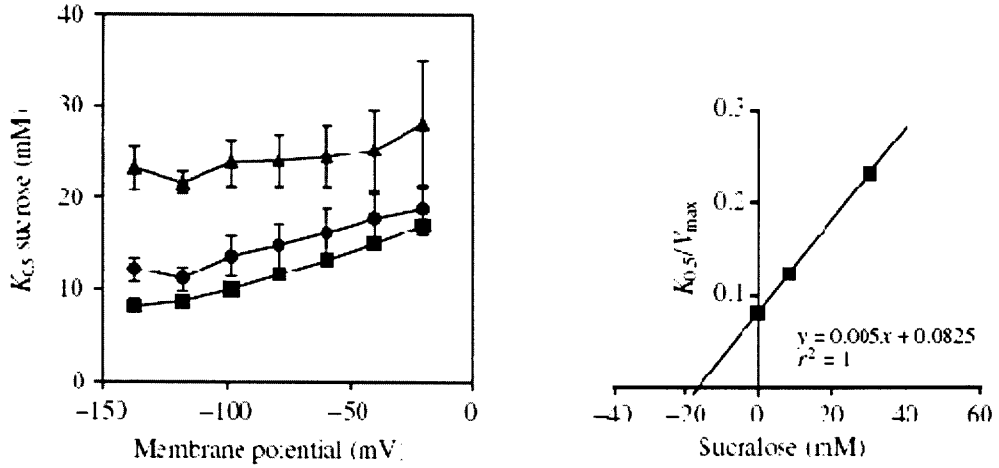

Figure 1.7. Determination of the K_I for sucralose. Left – sucrose dependent currents in the presence of 0,8 and 30 mM of sucralose. Right - $K_{0.5}/V_{max}$ was plotted as a function of the inhibitor (sucralose) concentration [I]. Source: Reinders, et al. 2006.

In view of the research findings presented in this section: sucralose is "specific" and a good descriptor of a sewage source; sucralose is present in the environment at high concentrations - relative to other microconstituents (This study; Mead, et al, 2009; Loos, et al. 2009); in addition, sucralose is a polar substance that displays a high aqueous solubility of 110 g/L, consequently a low estimated log K_{OW} value of -1 that prevent accumulation in fat tissues or other hydrophobic compartments in the environment. Thus, sucralose appears to have ideal physico-chemical properties to serve as a dissolved phase tracer of sewage intrusion in the near-shore Florida Keys.

1.5 Research Objectives

My research hypothesis is: can an analytical method be developed for the trace determination of sucralose from sea water. If so, can the method be applied to determine their occurrence and source from nearshore waters of the Florida Keys?

1.6 Research Outline

Chapter 1: Sucralose: A Unique Tracer for Wastewater Intrusion is made up of five parts:

- Part one focuses on introducing certain historical aspects of the human impact on the Florida Keys coral reef ecosystem.
- Part two is a literature review of the potential impacts of the sewage vector in the Florida Keys and its relation to disease and coral reefs.
- Part three delves into a discussion about the sewage vector as a source of bioactive pollutants in the sensitive marine waters of the Florida Keys and introduces the concept of applying molecular tracers to assess their impacts.
- Part four transitions into the introduction of sucralose to serve as an ideal dissolved phase molecular tracer. Chemical properties, toxicity, uses and environmental fate are reviewed.
- Part five lists the research objectives and outlines the complete body of the report.

Chapter 2: Negative Ion Electrospray ionization of Sucralose: Ion formation and ion source tuning is a comprehensive evaluation of the electrospray ionization (ESI) of sucralose with the purpose of discovering the optimal signal response for the sucralose based ions, to afford the development of an LC/MSMS based trace level analytical method. In this research it was discovered that sucralose is a polar compound that readily forms adduct ions with water or anions of organic modifiers. Thus the objective of this chapter is to optimize the electrospray ionization efficiency (or ion desolvation) of the three dominant ion signals: the deprotonated molecular ion $[M\text{-}H]^-$ – 397 m/z, hydrated adduct $[M+2*H_2O\text{-}H]^-$ – 433 m/z and acetate adduct $[M+C_2H_3O_2]^-$ – 457 m/z. Ionization

efficiency of the three sucralose ions were explored by a systematic study of signal response as it relates to various combinations of ESI parameters of the ion acceleration region. The optimization strategy was accomplished with response surface methodology (RSM) – a second order design of experiments technique. Furthermore, upon having knowledge of the optimal parameter values for the dominant sucralose ions, their relative responses were compared with various mobile phase conditions.

- The first part is a brief introduction.
- The materials and methods section is the second part while the third section is the results and discussion for this particular chapter. The results are separated into two parts. The first part presents the results of the RSM application for three sucralose adduct ions. The second part is a study that applies the optimal ESI parameters from the RSM study to compare the sucralose ion responses from various mobile phase compositions.
- The chapter finishes with the conclusion.

Chapter 3: Trace Determination of Sucralose in Coastal Waters of the Florida Keys. This chapter applies the ESI parameter settings optimized in chapter two and focuses on method development, validation and trace investigation of sucralose from sea water samples in the nearshore environment of the Florida Keys. There are three objectives for this chapter. Given the low retention of sucralose on the reverse phase HPLC column, the coelution of matrix derived polar constituent proved to be a significant cause of ionization suppression. Consequently, a major objective was to minimize this form of matrix effects by either modifying the organic strength of the elution step or increasing

the chromatographic retention factor. The primary objective was to develop an analytical method for sucralose sensitive enough to detect its occurrence from coastal marine environs. To ensure sub parts per trillion detection limits, pre-concentration with solid phase extraction (SPE) was optimized and two analytical approaches were developed and compared: SPE-ESI-HPLC-MSMS and SPE-EI-GC-MS. Furthermore, for both analytical approaches, robust statistically supported detection limits were calculated with weighted least squares regression and variance modeling.

- The methods section is comprised of four sections: The first part covers the SPE protocol for both instrumental approaches, while the second part is an in depth discussion of the analytical procedure, which is sectioned into the following: calibration standard preparation, chromatography parameters, ionization source parameters, mass spectrometry parameters and isotope dilution quantitation method. The third part is the procedure for the matrix suppression study, while part 4 presents the procedure for the determination of detection limits.
- The results section is made up of 4 parts. The first section covers the optimization of the SPE protocol, while the second presents the experimental results from the matrix effects investigation. The third part presents the results for the calculation of detection limits. The fourth part presents our findings of sucralose in surface waters of the nearshore Florida Keys.

Chapter 2

Negative Ion Electrospray Ionization of Sucralose: Adduct Formation and Ion Source Tuning

2.1 Introduction

Prior to this report, there have been three articles published on the mass spectrometric detection of sucralose. The first was published exclusively in Japanese (Hatano and Nakao, 2002) and during the end of this research two articles were released (Loos, et al. 2009; Mead, et al. 2009). The former was published for sucralose in foods stuff and the latter two are the only publications of sucralose determination for environmental purpose. Even though the current research shares electrospray ionization (ESI)-mass spectrometry with 2 of 3 reports above, the current findings are characterized by quadrapole ion trap mass spectrometry interfaced with 60° ion source geometry. As the published articles employ tandem quadrapole mass analysis interfaced to orthogonal geometry sources. Their findings report negative ionization and quantitation on the sucralose molecular ion chlorine cluster: 395 m/z, 397 m/z and 399 m/z (figure 2.1) without reference to adduct formation. This fact indicates that the molecular ion of sucralose was the dominant signal generated by both ESI – tandem MSMS systems.

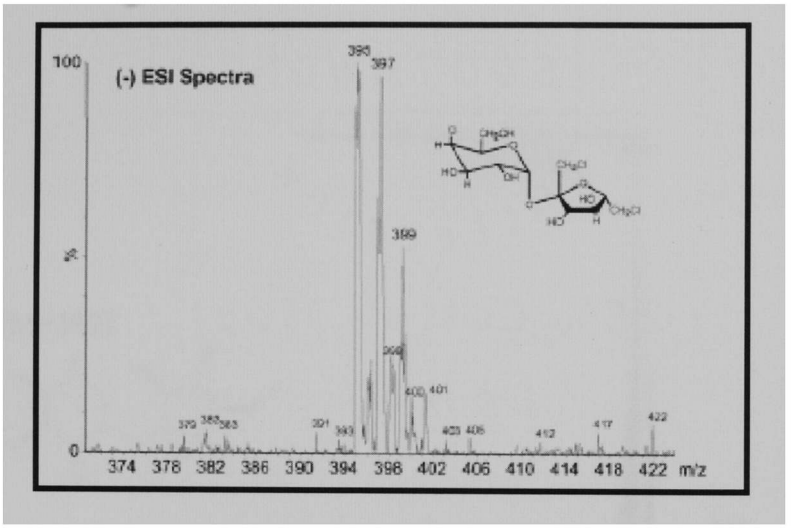

Figure 2.1. ESI spectra of sucralose: 395 m/z, 397 m/z, 399 m/z. Source: Loos, et al. 2009

Sucralose ($C_{12}H_{19}CL_3O_8$) accurate mass is 397.64 g/mol. Positive ions were not observed, thus we focused on the formation of negative ions (Hatano and Nakao, 2002; Loos et al., 2009). The current research reports the negative ionization of two sucralose adducts in lieu of the molecular ion signal. The ions are: deprotonated molecular ion $[M-H]^-$ – 397 m/z, dihydrate adduct $[M+2*H_2O-H]^-$ – 433 m/z and acetate adduct $[M+C_2H_3O_2]^-$ – 457 m/z. The figures 2.2 & 2.3 below are typical spectra for these ions.

This observation prompted a deeper investigation of sucralose electrospray ionization (ESI). The objective of this section is to establish ESI tuning parameters (e.g. voltage potentials and nebulizing gas flow) that optimize ion desolvation and maximize ionization production for the detection of sucralose. Two questions surfaced as a result of the observed ionization profile: First, is it possible to tune the electrospray parameters in the ion acceleration region to favor the molecular ion? Furthermore, if not, what are the ESI parameter values that optimize ionization efficiency for the dominant sucralose-adduct?

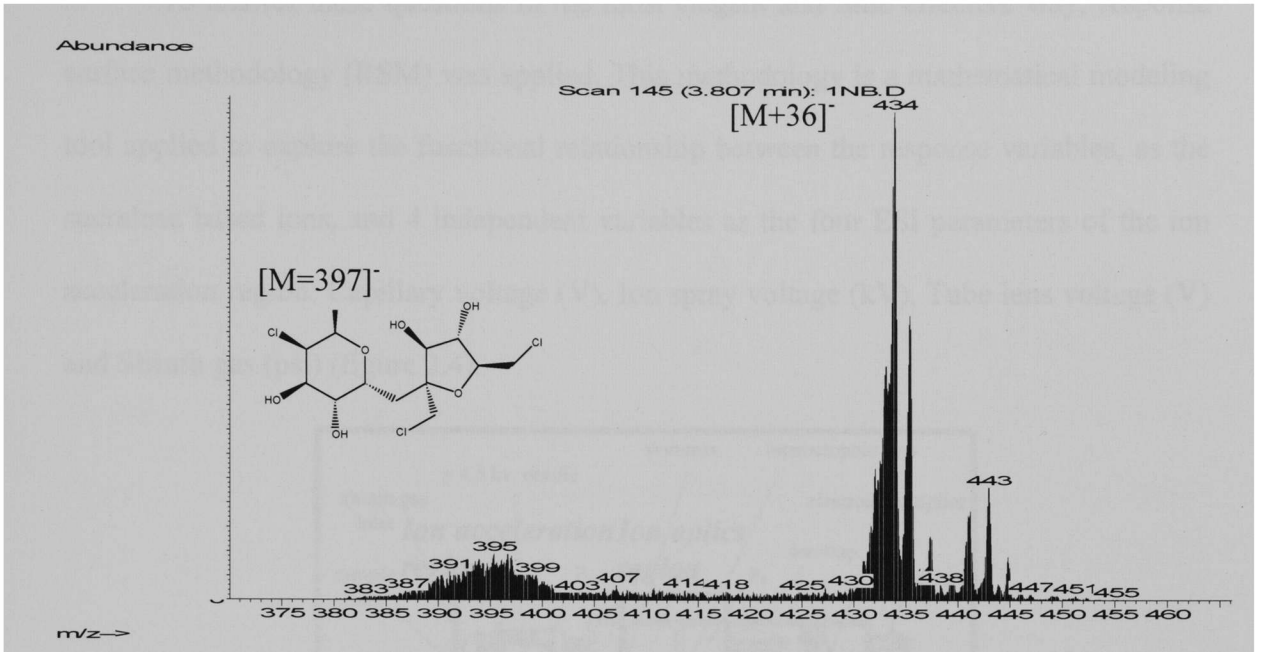

Figure 2.2. Spectra of sucralose molecular ion [M=397]- and sucralose – water adduct [M+36]-. Mobile phase composition is 3% HPLC grade water: acetonitrile

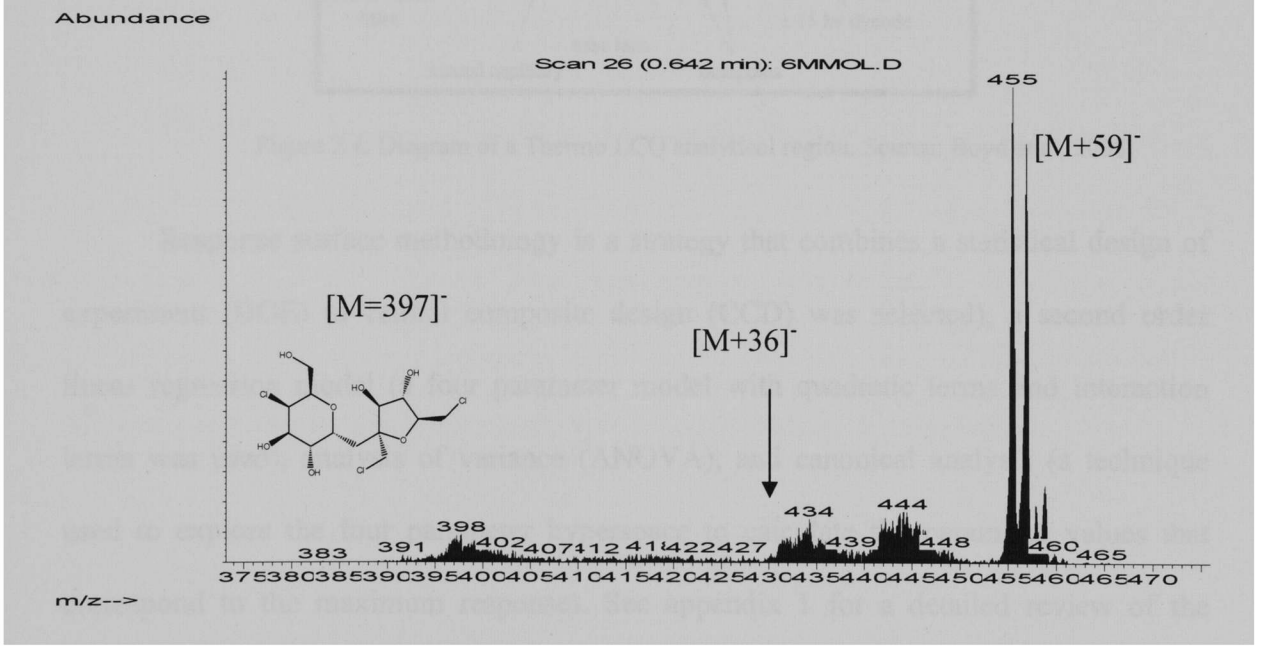

Figure 2.3. Spectra of sucralose molecular ion [M=397]- and sucralose – water adduct [M+36]- and the sucralose-acetate adduct. Mobile phase composition is 3% Ammonium acetate (4mmol): acetonitrile.

To answer these questions in the most elegant and time effective way, response surface methodology (RSM) was applied. This methodology is a mathematical modeling tool applied to explore the functional relationship between the response variables, as the sucralose based ions, and 4 independent variables as the four ESI parameters of the ion acceleration region: Capillary voltage (V), Ion spray voltage (kV), Tube lens voltage (V) and Sheath gas (psi) (figure 2.4).

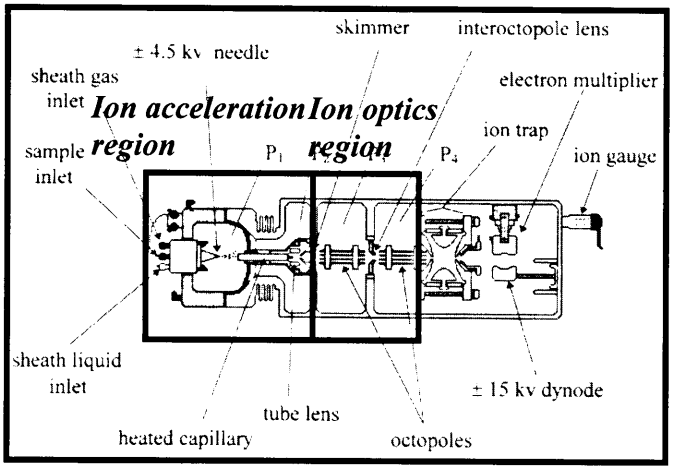

Figure 2.4. Diagram of a Thermo LCQ analytical region. Source: Boyd et al, 2008.

Response surface methodology is a strategy that combines a statistical design of experiment (DOE) (a central composite design (CCD) was selected), a second order linear regression model (a four parameter model with quadratic terms and interaction terms was used), analysis of variance (ANOVA), and canonical analysis (a technique used to explore the four parameter hyperspace to calculate the parameter values that correspond to the maximum response). See appendix 1 for a detailed review of the response surface methodology that was applied for this research. Response surface methodology facilitated the analysis of the relationships between a range of values for

four chosen parameters of the ion acceleration region and the response of the three dominant ions in a time and cost effective manner.

2.2 Materials

2.2.1 Chemicals

Sucralose ($C_{12}H_{19}Cl_3O_8$) was obtained as a solid in 99% purity from Toronto Research Chemicals, Inc. (North York Ontario, Canada). Deuterium Oxide (D_2O) was obtained in 98% purity from Acros Organics (Morris Plains NJ, USA). HPLC grade water was obtained from Pharmco (Brooksfield CT, USA). Acetonitrile (C_2H_3N), Ammonium Acetate ($C_2H_3O_2NH_4$) and Acetic Acid ($C_2H_4O_2$) were obtained from Fisher Scientific (Fairlawn NJ, USA).

2.2.2 Instrumentation

The liquid chromatograph-mass spectrometer system used in this investigation included a Thermo-Finnigan (Therno-Finnigan San Jose CA, USA) Surveyor Plus, quaternary pump, a Surveyor Plus auto-sampler, and a LCQ Advantage MAX quadrapole-ion trap mass spectrometer (QIT) (50-2000 Da.). The LC/MS was run under negative ion Electrospray Ionization (ESP-) for the sucralose signals studied.

2.3 Methods

Optimal ionization conditions for each sucralose ion, the deprotonated molecular ion $[M-H]^-$ – 397 m/z, dihydrate adduct $[M+2*H_2O-H]^-$ – 433 m/z and acetate adduct $[M+C_2H_3O_2]^-$ – 457 m/z were effectively revealed in the following five steps:

(1.) The range, as shown in table 2.1 below, was selected for each ion source parameter of the ion acceleration region.

Variable	Symbol	Coded variable level				
		Lowest	Low	Center	High	Highest
		$-\beta$	-1	0	+1	$+\beta$
Capillary voltage (V)	X1	-25	-15	-5	5	15
Ion Spray voltage (kV)	X2	2	3	4	5	6
Tube lens voltage (V)	X3	-20	-5	10	25	40
Sheath gas (psi)	X4	15	25	35	45	55

Table 2.1. Independent variables and their levels for the CCD

2.) An orthogonal central composite design matrix was constructed to manage the four variables in a short number of analytical runs (36). The table 2.2 below contains the orthogonal rotatable central composite design matrix (CCD) used for this experiment. It shows the design matrix in two forms. One form corresponds to the instrument values, while the other corresponds to the coded variables - which are equivalent values calculated by the equations shown in the table A.2 of Appendix 1. This design matrix was then used to construct the analytical sequence of 36 runs. Whereas each analytical run incorporated a dedicated tune file with ion acceleration region values that were prescribed by the levels of the CCD design matrix.

The HPLC column was bypassed for this experiment with a run time of 5 minutes, mobile phase flow rate of 0.600 ml min^{-1} and composition of 3% aqueous (2mmol/L ammonium acetate): 98% acetonitrile for the acetate adduct $[M+C_2H_3O_2]^-$ – 457 m/z and the deprotonated molecular ion $[M-H]^-$ – 397 m/z experiments. A mobile phase composition of 3% aqueous (HPLC water): 97% acetonitrile for the dihydrate adduct $[M+2*H_2O-H]^-$ – 433 m/z experiment. The concentration of sucralose was 500 ng ml^{-1}.

Test Number	Coded level of variables				Actual level of variables			
	X1	X2	X3	X4	Capillary Voltage (V)	Ion spray voltage (kV)	Tube lens voltage (V)	Sheath gas (kV)
1	0	0	0	0	-5	4	10	35
2	0	0	0	0	-5	4	10	35
3	0	0	0	0	-5	4	10	35
4	0	0	0	0	-5	4	10	35
5	0	0	0	0	-5	4	10	35
6	0	0	0	0	-5	4	10	35
7	0	0	0	0	-5	4	10	35
8	0	0	0	0	-5	4	10	35
9	0	0	0	0	-5	4	10	35
10	0	0	0	0	-5	4	10	35
11	0	0	0	0	-5	4	10	35
12	0	0	0	0	-5	4	10	35
13	-1	-1	-1	-1	-15	3	-5	25
14	1	-1	-1	-1	5	3	-5	25
15	-1	1	-1	-1	-15	5	-5	25
16	1	1	-1	-1	5	5	-5	25
17	-1	-1	1	-1	-15	3	25	25
18	1	-1	1	-1	5	3	25	25
19	-1	1	1	-1	-15	5	25	25
20	1	1	1	-1	5	5	25	25
21	-1	-1	-1	1	-15	3	-5	45
22	1	-1	-1	1	5	3	-5	45
23	-1	1	-1	1	-15	5	-5	45
24	1	1	-1	1	5	5	-5	45
25	-1	-1	1	1	-15	3	25	45
26	1	-1	1	1	5	3	25	45
27	-1	1	1	1	-15	5	25	45
28	1	1	1	1	5	5	25	45
29	-2	0	0	0	-25	4	10	35
30	2	0	0	0	15	4	10	35
31	0	-2	0	0	-5	2	10	35
32	0	2	0	0	-5	6	10	35
33	0	0	-2	0	-5	4	-20	35
34	0	0	2	0	-5	4	40	35
35	0	0	0	-2	-5	4	10	15
36	0	0	0	2	-5	4	10	55

Table 2.2. Central composite design - four experimental variables in coded and actual levels

3.) The analytical sequence was run, and then the peak areas were integrated. The signal areas, along with the design matrix in coded form, were exported to the SAS statistical analysis software; where the *proc rsreg* code was run to fit a second order linear equation, conduct analysis of variance to test the significance of each ESI parameter - i.e. variable of the second order linear equation - and analyze the shape of the response surface (to detect whether a saddlepoint, minimum or maximum), to determine the maximum response values of the three sucralose ions.

4.) The objective of the following step was to apply the derived optimal ESI settings for the three sucralose adducts, to evaluate and compare their responses with the following six mobile phase characteristics: 3% (HPLC grade water): 97% acetonitrile; 3% (0.2% acetic acid-ph3): 97% acetonitrile; 3% (1mmol/L ammonium acetate): acetonitrile; 3% (2 mmol/L ammonium acetate): 97% acetonitrile; 3% (4 mmol/L ammonium acetate): 97% acetonitrile; 3% (6 mmol/L ammonium acetate): 97% acetonitrile. To accomplish this task, sucralose and the corresponding mobile phase conditions were directly infused into the ESI source with a sucralose concentration of 500 ng ml^{-1}. The response of all three sucralose ions were tested with the six mobile phase conditions

5.) The MATLAB model based calibration toolbox was applied to generate contour and surface plots for each sucralose adduct experiment to aid in visualizing the four parameter hyperspace of the second order linear equation.

2.4 Results

2.4.1 Application of Response Surface Methodology for Ionization Tuning of Sucralose Adduct Ions

The results will be presented in the following way. The central composite design will be displayed along with the actual response data. Model coefficients, goodness of fit statistics and a full analysis of variance will be analyzed for the fitted response system. The response system – relationship between ion source parameter values and target analyte response - will then be assessed by canonical analysis to calculate the optimal conditions. A graphical representation of the optimal response system will be presented as contour and surface plots.

2.4.1.1 Sucralose Molecular Ion 397 m/z

The column on the right of table 2.3 is a vector that contains the responses for the sucralose molecular ion – 397 m/z (actual response variable). Linear regression, analysis of variance (ANOVA) and canonical analysis has been applied in this experiment to systematically investigate the functional relationship between the independent variables and the response variable.

$$Y = \beta_0 + \beta_1 X_1 + \beta_2 X_2 + \beta_3 X_3 + \beta_4 X_4 + \beta_{11} X_{11}^2 + \beta_{22} X_{22}^2 + \beta_{33} X_{33}^2 + \beta_{44} X_{44}^2$$
$$+\beta_{12} X_1 X_2 + \beta_{13} X_1 X_3 + \beta_{14} X_1 X_4 + \beta_{23} X_2 X_3 + \beta_{34} X_3 X_4 + \varepsilon$$

The coefficients of the fitted linear model are provided in table 2.4. The contribution of linear, quadratic and crossproduct terms to the total regression model will be reviewed first. Subsequently, the contribution of each independent variable (including

all order terms) will be evaluated. Finally, the contribution of each coefficient term will be evaluated.

Test Number	Coded level of variables				Actual level of variables				
	X1	X2	X3	X4	Capillary Voltage (V)	Ion spray voltage (kV)	Tube lens voltage (V)	Sheath gas (kV)	Signal
1	0	0	0	0	-5	4	10	35	14.35
2	0	0	0	0	-5	4	10	35	13.01
3	0	0	0	0	-5	4	10	35	14.46
4	0	0	0	0	-5	4	10	35	13.78
5	0	0	0	0	-5	4	10	35	12.90
6	0	0	0	0	-5	4	10	35	15.03
7	0	0	0	0	-5	4	10	35	13.05
8	0	0	0	0	-5	4	10	35	15.07
9	0	0	0	0	-5	4	10	35	15.63
10	0	0	0	0	-5	4	10	35	13.87
11	0	0	0	0	-5	4	10	35	14.10
12	0	0	0	0	-5	4	10	35	14.66
13	-1	-1	-1	-1	-15	3	-5	25	9.41
14	1	-1	-1	-1	5	3	-5	25	11.77
15	-1	1	-1	-1	-15	5	-5	25	16.78
16	1	1	-1	-1	5	5	-5	25	20.67
17	-1	-1	1	-1	-15	3	25	25	7.16
18	1	-1	1	-1	5	3	25	25	8.50
19	-1	1	1	-1	-15	5	25	25	12.82
20	1	1	1	-1	5	5	25	25	13.12
21	-1	-1	-1	1	-15	3	-5	45	4.78
22	1	-1	-1	1	5	3	-5	45	6.44
23	-1	1	-1	1	-15	5	-5	45	10.83
24	1	1	-1	1	5	5	-5	45	11.40
25	-1	-1	1	1	-15	3	25	45	4.66
26	1	-1	1	1	5	3	25	45	4.34
27	-1	1	1	1	-15	5	25	45	6.61
28	1	1	1	1	5	5	25	45	8.88
29	-2	0	0	0	-25	4	10	35	8.32
30	2	0	0	0	15	4	10	35	11.51
31	0	-2	0	0	-5	2	10	35	4.20
32	0	2	0	0	-5	6	10	35	12.13
33	0	0	-2	0	-5	4	-20	35	12.60
34	0	0	2	0	-5	4	40	35	5.42
35	0	0	0	-2	-5	4	10	15	5.91
36	0	0	0	2	-5	4	10	55	7.34

Table 2.3. Central composite design - four experimental variables in coded and actual levels with experimental results – 397 m/z

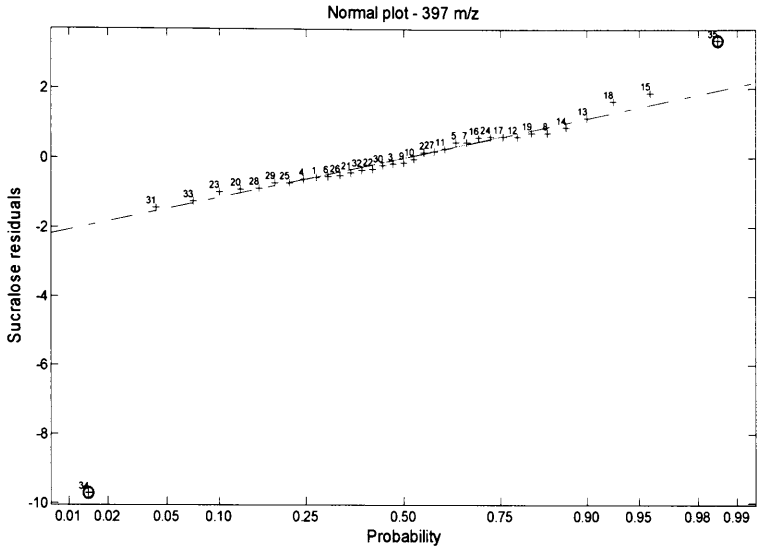

Figure 2.5. Normal plot of the residuals for 397 m/z

ANOVA and the Fisher's F-test indicate that the linear and quadratic terms have a significant contribution to the regression $\left[(P_{model} > F) < 0.0001\right]$. However, the cross product terms have a *p-value* of $\left[(P_{model} > F) < 0.53\right]$ and indicate an insignificant contribution of these terms to the regression model. The lack of fit test supports this result and concludes that there is significant lack of fit with the inclusion of the cross product terms - *p-value* $=\left[(P_{model} > F) < 0.0007\right]$. The insignificant cross product terms explain the source of the lack of fit error and indicate that a basic quadratic model should be fit instead as follows

$$Y = \beta_0 + \beta_1 X_1 + \beta_2 X_2 + \beta_3 X_3 + \beta_4 X_4 + \beta_{11} X_{11}^2 + \beta_{22} X_{22}^2 + \beta_{33} X_{33}^2 + \beta_{44} X_{44}^2 + \varepsilon .$$

When considering the sum of squares for regression of each variable, Fisher's F-test results indicate the following: Ion spray voltage and Sheath gas terms contribute

Response surface for variable Y					
Regression	d.f	SS	R-square	F-ratio	Prob>F
Linear	4	296.4392	0.5083	20.72	<.0001
Quadratic	4	192.9427	0.3308	13.48	<.0001
Cross-product	6	18.7456	0.0321	0.87	0.5307
Total regression	14	508.1277	0.8712	10.15	<.0001
Residual	d.f	SS	R-square	F-ratio	Prob>F
Lack of fit	10	66.5850	6.6585	8.58	0.0007
Pure error	11	8.5385	0.7762		
Total error	21	75.1236	3.5773		
Independent variable	d.f	SS	R-square	F-ratio	Prob>F
Capillary voltage X1	5	38.2737	7.6547	2.14	0.1003
Ion spray voltage X2	5	212.2627	42.4525	11.87	<0.0001
Tube voltage X3	5	115.3278	23.0655	6.45	0.0009
Sheath gas X4	5	161.0090	32.2018	9.00	0.0001
Quadratic model parameter	d.f	Coefficients	Standard Error	t Value	Prob> |t|
Intercept	1	-37.6572	9.6930	-3.88	0.0009
x1	1	0.0475	0.2583	0.18	0.8557
x2	1	15.0184	3.1934	4.70	0.0001
x3	1	0.0282	0.1728	0.16	0.8719
x4	1	1.1656	0.3059	3.81	0.0010
x1*x1	1	-0.0081	0.0033	-2.45	0.0232
x2*x1	1	0.0123	0.0472	0.26	0.7961
x2*x2	1	-1.2551	0.3343	-3.75	0.0012
x3*x1	1	-0.0020	0.0031	-0.65	0.5245
x3*x2	1	-0.0438	0.0315	-1.39	0.1784
x3*x3	1	-0.0046	0.0014	-3.12	0.0051
x4*x1	1	-0.0023	0.0047	-0.49	0.6274
x4*x2	1	-0.0565	0.0472	-1.20	0.2449
x4*x3	1	0.0036	0.0031	1.07	0.2977
x4*x4	1	-0.0164	0.0033	-4.91	<.0001

Table 2.4. ANOVA table for the full quadratic model – 397 m/z

significantly to the regression *p-value* $=\left[\left(P_{model} > F\right) < 0.0001\right]$. Tube voltage also contributes significantly with a *p value* of $\left[\left(P_{model} > F\right) < 0.0009\right]$. However, *F-test* results

indicate that Capillary voltage does not contribute significantly to the regression model unless the significance level for the test is > $\alpha = 0.10$ - $\left[\left(P_{model} > F\right) < 0.1003\right]$.

The fitness of the model was examined by the determination coefficient $\left(R^2 = 0.8712\right)$, which implies that 87% of the variance was attributed to regression, while 13% was not explained by the regression model. The normal plot of the residuals is shown in figure 2.5 and indicates that all points, except for 34 (see CCD matrix), fits reasonably well to a normal distribution. This point is an outlier and corresponds to the highest axial tube lens value of 40. This result implies that the model could benefit by a modification of the tube lens range in the X matrix.

The significance of each coefficient was determined by Student's *T*-test and the *P* value. The results are listed in Table 2.4 and indicate that the quadratic term is more significant than the linear term for capillary voltage. Both the quadratic and linear terms are significant for ion spray voltage.

Canonical analysis of response surface – 397 m/z

Independent variable	Critical value
Capillary voltage	6.1036
Ion spray voltage	5.7875
Tube voltage	-17.2050
Sheath gas	23.3376

Predicted value at stationary point: 19.306466

	Eigenvectors			
Eigenvalues	Capillary voltage	Ion spray voltage	Tube voltage	Sheath gas
-2.1369	0.5601	0.4536	-0.6170	-0.3155
-3.7644	0.8241	-0.3835	0.3859	0.1570
-5.9191	0.0524	0.7037	0.6750	-0.2152
-7.2159	0.0644	0.3896	-0.1208	0.9107

Stationary point is a maximum

Table 2.5. Canonical analysis of response surface – 397 m/z

The quadratic term is more significant than the linear term for tube voltage. Both the quadratic and linear terms are significant for sheath gas. All cross product terms are insignificant and indicate a lack of interaction effects between the variables.

Results for the canonical analysis are listed in Table 2.5. This technique facilitated the evaluation of the response surface to determine whether a maximum, minimum or saddle point was present. Also, the stationary point was derived and provided knowledge of the particular level for each factor that corresponds to the maximum response. The results show that all eigenvalues of the second order coefficients are of a negative sign, which means that the response system is a maximum see figure 2.6 – 2.11. The eigenvalues provided information to calculate the critical values for each variable. These critical values are the values that correspond to the maximum response of the system and are also listed in table 2.5. Each pair of figures below presents the effect of two variables on the response of the sucralose molecular ion – 397 m/z, while the other two variables were set at the critical values from canonical analysis. As such, these plots are three dimensional views of the multiparameter data set and provide a snapshot graphical representation of the hyperspace response surface.

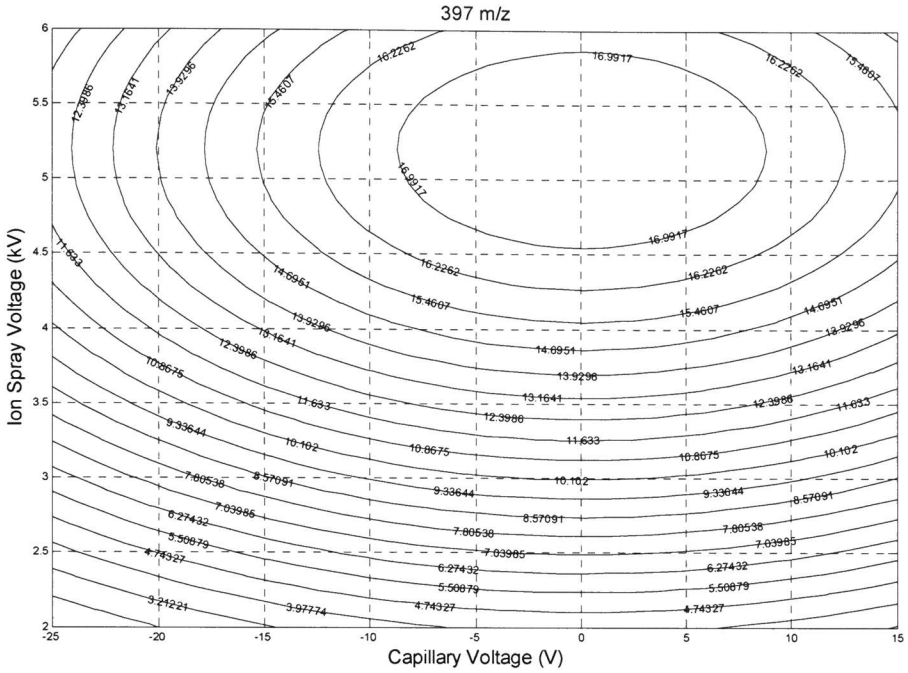

Figure 2.6. Contour plot of ion spray voltage vs. capillary voltage – 397 m/z

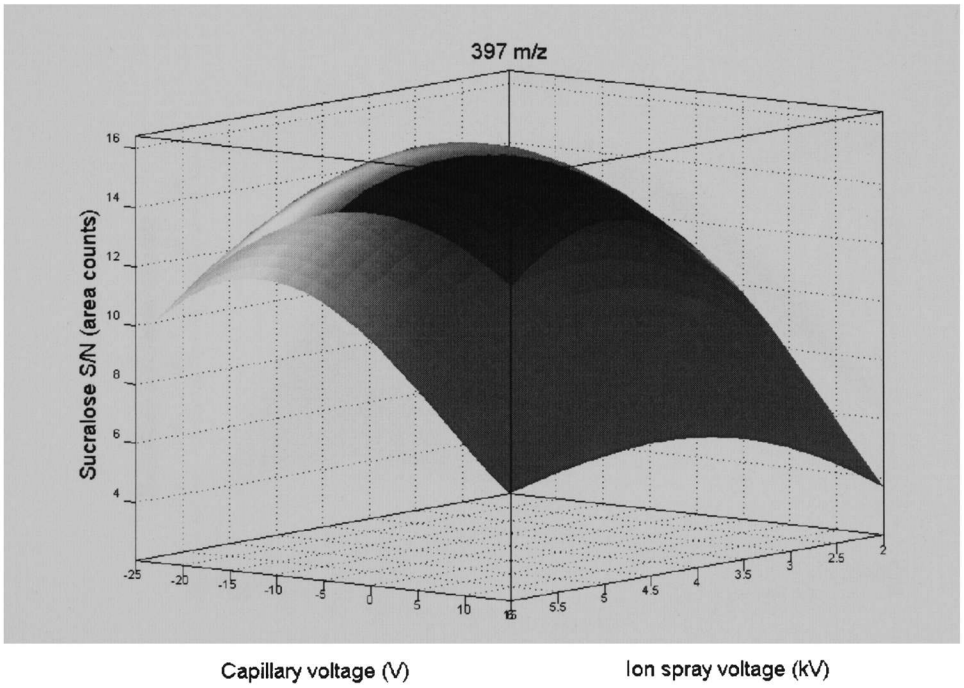

Figure 2.7. Surface plot of ion spray voltage vs. capillary voltage – 397 m/z

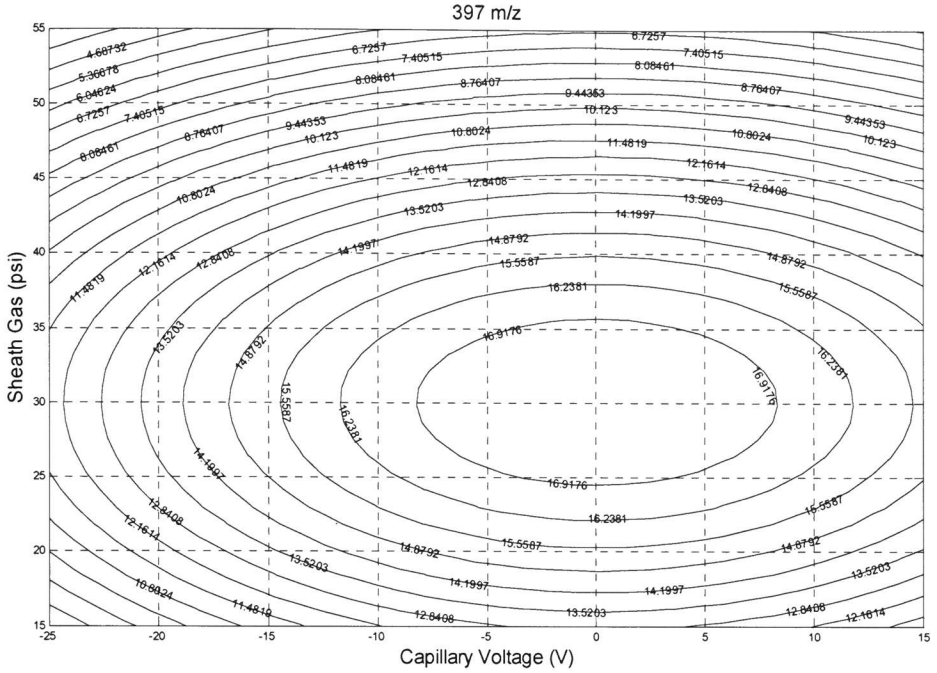

Figure 2.8. Contour plot of sheath gas vs. capillary voltage – 397 m/z

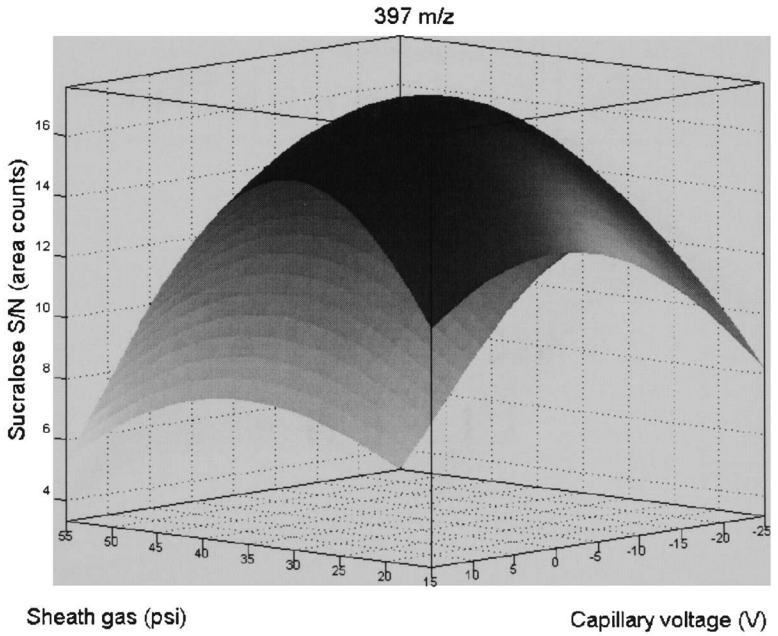

Figure 2.9. Surface plot of sheath gas vs. capillary voltage – 397 m/z

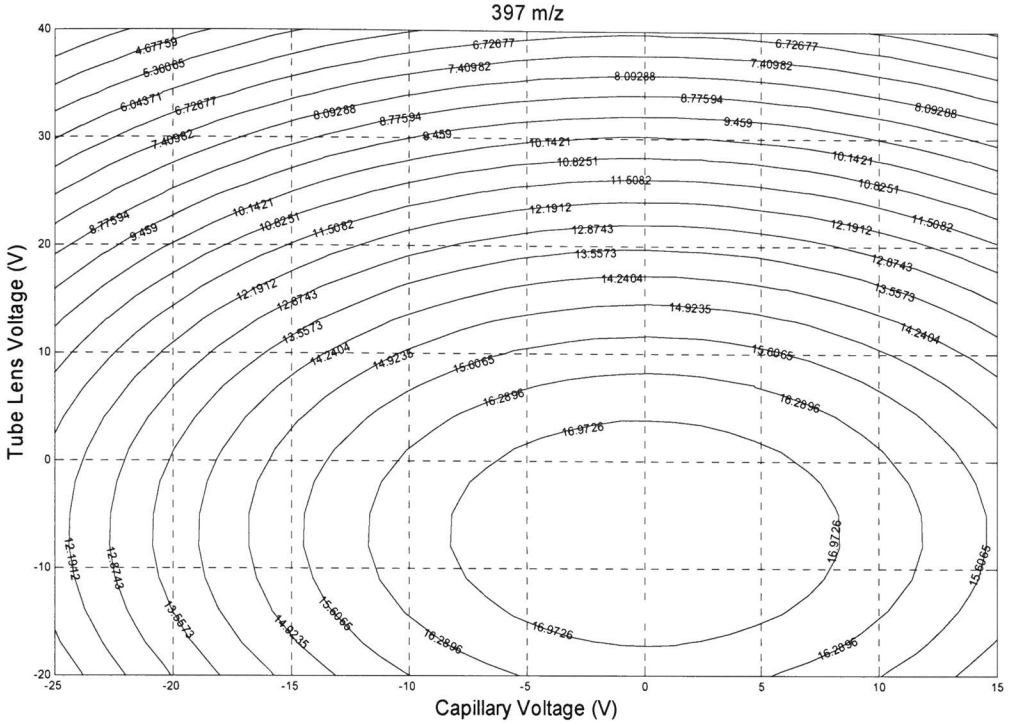

Figure 2.10. Contour plot of tube lens vs. capillary voltage – 397 m/z

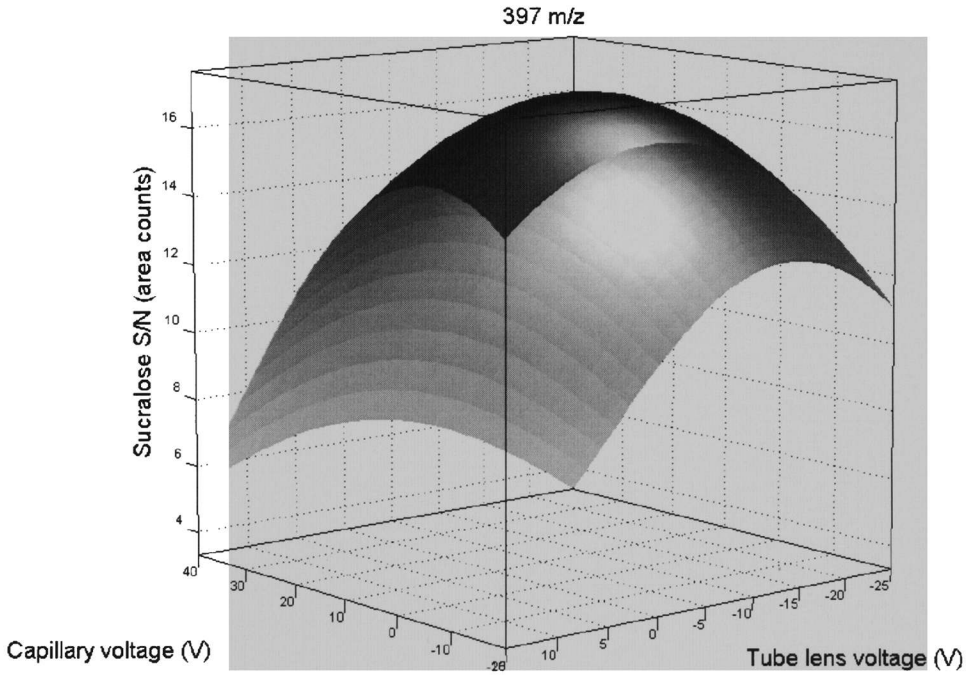

Figure 2.11. Surface plot of tube lens vs. capillary voltage – 397 m/z

2.4.1.2 Sucralose Acetate Adduct 457 m/z

The column on the right of table 2.6 is a vector that contains the responses for the sucralose molecular ion – 457 m/z (actual response variable). Linear regression, analysis of variance and canonical analysis has been applied in this experiment to systematically investigate the functional relationship between the independent variables and the response variable.

$$Y = \beta_0 + \beta_1 X_1 + \beta_2 X_2 + \beta_3 X_3 + \beta_4 X_4 + \beta_{11} X_{11}^2 + \beta_{22} X_{22}^2 + \beta_{33} X_{33}^2 + \beta_{44} X_{44}^2 + \beta_{12} X_1 X_2 + \beta_{13} X_1 X_3 + \beta_{14} X_1 X_4 + \beta_{23} X_2 X_3 + \beta_{34} X_3 X_4 + \varepsilon$$

The coefficients of the fitted linear model are provided in table 2.7. The contribution of linear, quadratic and cross-product terms to the total regression model will be reviewed first. Subsequently, the contribution of each independent variable - including all order terms - will be evaluated.

Test Number	Coded level of variables				Actual level of variables				Observed
	X1	X2	X3	X4	Capillary Voltage (V)	Ion spray voltage (kV)	Tube lens voltage (V)	Sheath gas (kV)	S/N
1	0	0	0	0	-5	4	0	35	3.33
2	0	0	0	0	-5	4	0	35	3.42
3	0	0	0	0	-5	4	0	35	3.62
4	0	0	0	0	-5	4	0	35	3.36
5	0	0	0	0	-5	4	0	35	3.65
6	0	0	0	0	-5	4	0	35	3.41
7	0	0	0	0	-5	4	0	35	3.27
8	0	0	0	0	-5	4	0	35	3.28
9	0	0	0	0	-5	4	0	35	3.11
10	0	0	0	0	-5	4	0	35	3.81
11	0	0	0	0	-5	4	0	35	3.02
12	0	0	0	0	-5	4	0	35	3.16
13	-1	-1	-1	-1	-15	3	-15	25	2.16
14	1	-1	-1	-1	5	3	-15	25	2.23
15	-1	1	-1	-1	-15	5	-15	25	3.72
16	1	1	-1	-1	5	5	-15	25	3.01
17	-1	-1	1	-1	-15	3	15	25	1.21
18	1	-1	1	-1	5	3	15	25	1.63
19	-1	1	1	-1	-15	5	15	25	1.87
20	1	1	1	-1	5	5	15	25	2.55
21	-1	-1	-1	1	-15	3	-15	45	1.98
22	1	-1	-1	1	5	3	-15	45	1.63
23	-1	1	-1	1	-15	5	-15	45	3.47
24	1	1	-1	1	5	5	-15	45	2.90
25	-1	-1	1	1	-15	3	15	45	1.00
26	1	-1	1	1	5	3	15	45	1.81
27	-1	1	1	1	-15	5	15	45	2.11
28	1	1	1	1	5	5	15	45	2.69
29	-2	0	0	0	-25	4	0	35	2.20
30	2	0	0	0	15	4	0	35	2.92
31	0	-2	0	0	-5	2	0	35	1.54
32	0	2	0	0	-5	6	0	35	3.84
33	0	0	-2	0	-5	4	-30	35	2.41
34	0	0	2	0	-5	4	30	35	1.75
35	0	0	0	-2	-5	4	0	15	1.97
36	0	0	0	2	-5	4	0	55	2.89

Table 2.6. Central composite design - four experimental variables in coded and actual levels with experimental results – 457 m/z

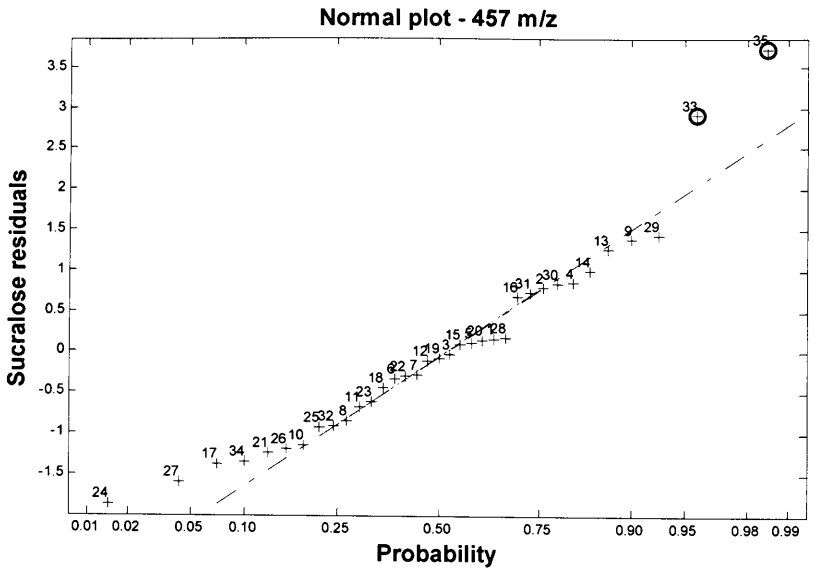

Figure 2.12. Normal plot of the residuals for 397 m/z

ANOVA and the Fisher's F-test indicate that the linear and quadratic terms have a significant contribution to the regression $\left[(P_{model} > F) < 0.0001\right]$. Also, the cross product terms have a *p-value* of $\left[(P_{model} > F) < 0.0316\right]$ and indicate a significant contribution by interaction effects, which were not observed for the de-protonated molecular ion $[M\text{-}H]^-$ – 397 m/z. Lack of fit test indicates no lack of fit *p-value* $=\left[(P_{model} > F) < 0.1203\right]$ if considering a low to stringent α level of significance - $\alpha < 0.10$. When considering the sum of squares for regression of each variable, Fisher's F-test results indicate the following: Ion spray voltage and tube lens voltage contributes significantly to the regression *p-value* $=\left[(P_{model} > F) < 0.0001\right]$. Capillary voltage also contributes significantly also contributes significantly to the regression model - $\left[(P_{model} > F) < 0.001\right]$.

Response surface for variable Y					
Regression	d.f	SS	R-square	F-ratio	Prob>F
Linear	4	9.9853	0.4438	30.81	<.0001
Quadratic	4	9.3960	0.4176	28.99	<.0001
Cross-product	6	1.4159	0.0629	2.91	0.0316
Total regression	14	20.7974	0.9244	18.33	<.0001
Residual	d.f	SS	R-square	F-ratio	Prob>F
Lack of fit	10	1.1160	0.111608	2.10	0.1203
Pure error	11	0.5856	0.053238		
Total error	21	1.7016	0.081033		
Independent variable	d.f	SS	R-square	F-ratio	Prob>F
Capillary voltage X1	5	3.072255	0.614451	7.58	0.0003
Ion spray voltage X2	5	8.909522	1.781904	21.99	<.0001
Tube voltage X3	5	7.720550	1.544110	19.06	<.0001
Sheath gas X4	5	2.511026	0.502205	6.20	0.0011
Quadratic model parameter	d.f	Estimate	Standard Error	t Value	Prob> |t|
Intercept	1	-4.663968	1.436522	-3.25	0.0039
x1	1	0.010589	0.038598	0.27	0.7865
x2	1	1.962139	0.478277	4.10	0.0005
x3	1	-0.008287	0.025623	-0.32	0.7496
x4	1	0.170514	0.045799	3.72	0.0013
x1*x1	1	-0.002340	0.000503	-4.65	0.0001
x2*x1	1	-0.006022	0.007117	-0.85	0.4070
x2*x2	1	-0.202723	0.050322	-4.03	0.0006
x3*x1	1	0.001689	0.000474	3.56	0.0018
x3*x2	1	-0.006450	0.004744	-1.36	0.1884
x3*x3	1	-0.001580	0.000224	-7.07	<.0001
x4*x1	1	0.000000284	0.000712	0.00	0.9997
x4*x2	1	0.005219	0.007117	0.73	0.4714
x4*x3	1	0.000618	0.000474	1.30	0.2070
x4*x4	1	-0.002672	0.000503	-5.31	<.0001

Table 2.7. ANOVA table for the full quadratic model – 457 m/z

The fitness of the model was examined by determination coefficient $\left(R^2 = 0.9244\right)$, which implies that 92% of the variance was attributed to regression, while 8% was not

explained by the regression model. The normal plot of the residuals is shown in figure 2.12 and indicates that all points fit reasonably well to a normal distribution. It is important to note that two points do deviate slightly from normality and correspond to points 33 and 35. These points correspond to extreme values of tube lens and sheath gas settings in the design matrix. This result implies that the model could benefit by a modification of the tube lens range and sheath gas ranges in the X matrix.

The significance of each coefficient was determined by Student's *T*-test and the *P* value. The results are listed in Table 2.7 and indicate that the quadratic term is more significant than the linear term for capillary voltage. Both the quadratic and linear terms are significant for ion spray voltage. The quadratic term is more significant than the linear term for tube voltage. Both the quadratic and linear terms are significant for sheath gas. All cross product terms are insignificant except for one - $x_1 * x_3$ - with a *p value* of 0.0018.

Independent variable	Critical value			
Capillary voltage	-9.344395			
Ion spray voltage	5.633949			
Tube voltage	-12.074816			
Sheath gas	36.015358			
Predicted value at stationary point: 19.306466				
	Eigenvectors			
Eigenvalues	Capillary voltage	Ion spray voltage	Tube voltage	Sheath gas
-0.482747	0.691121	-0.524564	0.493218	0.062611
-0.850280	0.340275	0.730564	0.230988	0.545100
-1.111919	-0.423449	-0.416960	0.047982	0.802828
-1.792657	-0.476714	0.131350	0.837304	-0.233265
Stationary point is a maximum				

Table 2.8. Canonical analysis of response surface – 457 m/z

This indicates that there is a significant interaction effect between capillary voltage and tube lens voltage. This relationship is observable in their plots (figures 2.16 & 2.17).

Results for the canonical analysis are listed in Table 2.8. The results show that all eigenvalues of the second order coefficients are of a negative sign, which means that the response system is a maximum see figure 2.13 – 2.18. The eigenvalues provided information to calculate the critical values for each variable. These critical values are the values that correspond to the maximum response of the system and are also listed in table 2.8. These critical values were then applied to the standard second order regression model to construct the following surface and contour plots. As such, these plots are three dimensional views of the multiparameter data set and provide a snapshot graphical representation of the hyperspace response surface.

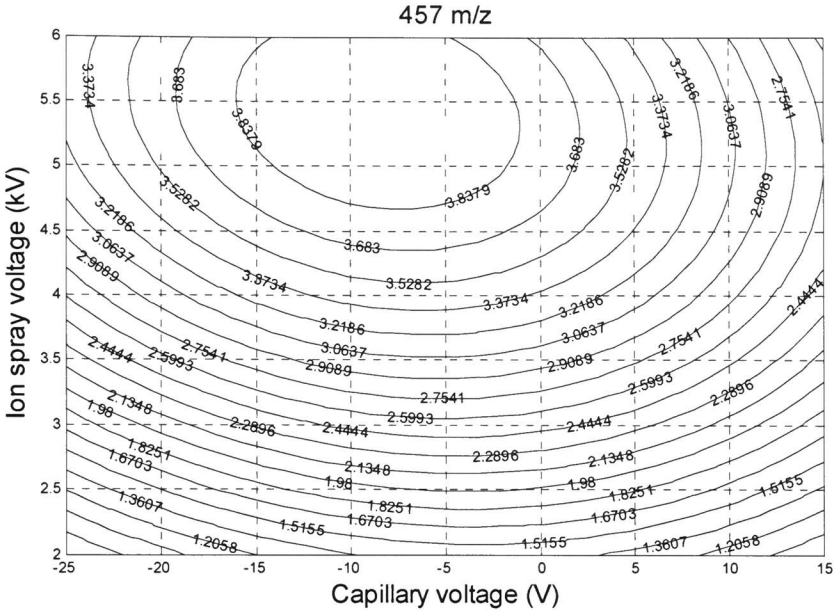

Figure 2.13. Contour plot of ion spray voltage vs. capillary voltage – 397 m/z

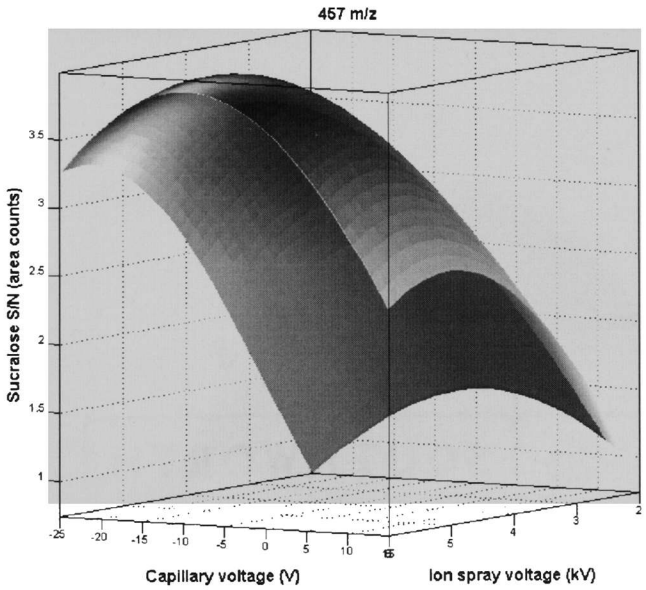

Figure 2.14. Surface plot of ion spray voltage vs. capillary voltage – 457 m/z

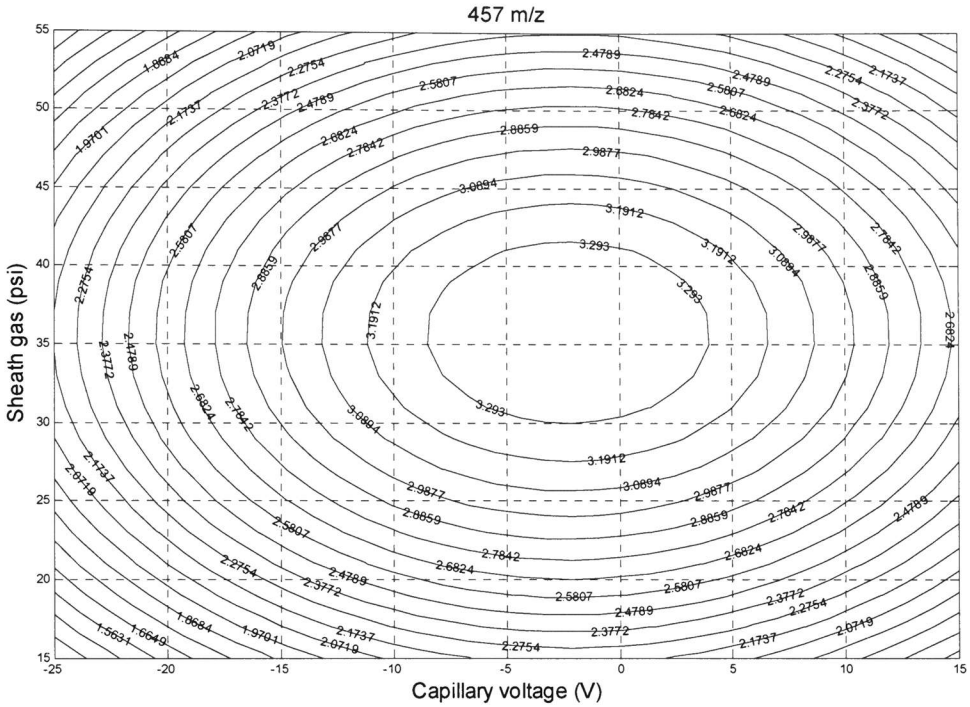

Figure 2.15. Contour plot of sheath gas vs. capillary voltage – 457 m/z

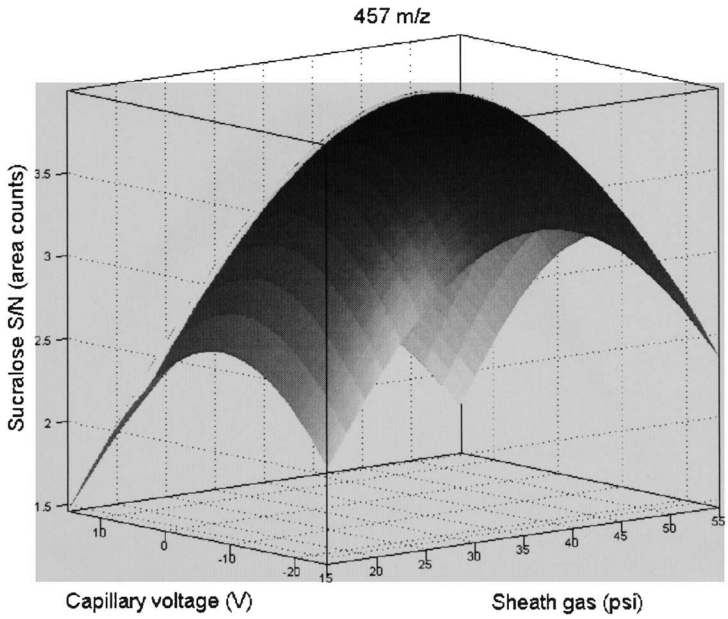

Figure 2.16. Surface plot of sheath gas vs. capillary voltage – 457 m/z

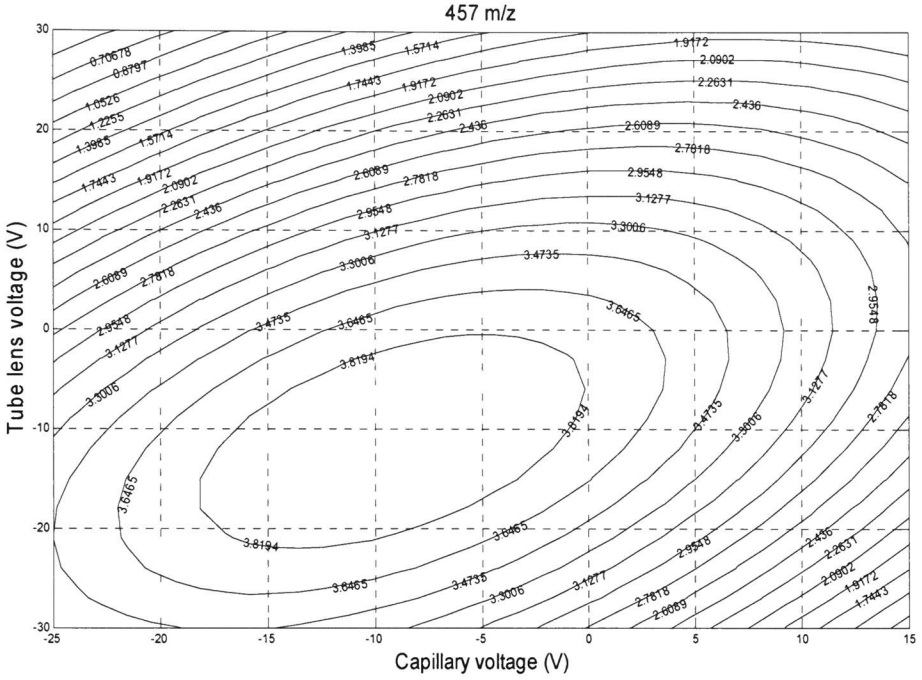

Figure 2.17. Contour plot of tube lens vs. capillary voltage – 457 m/z

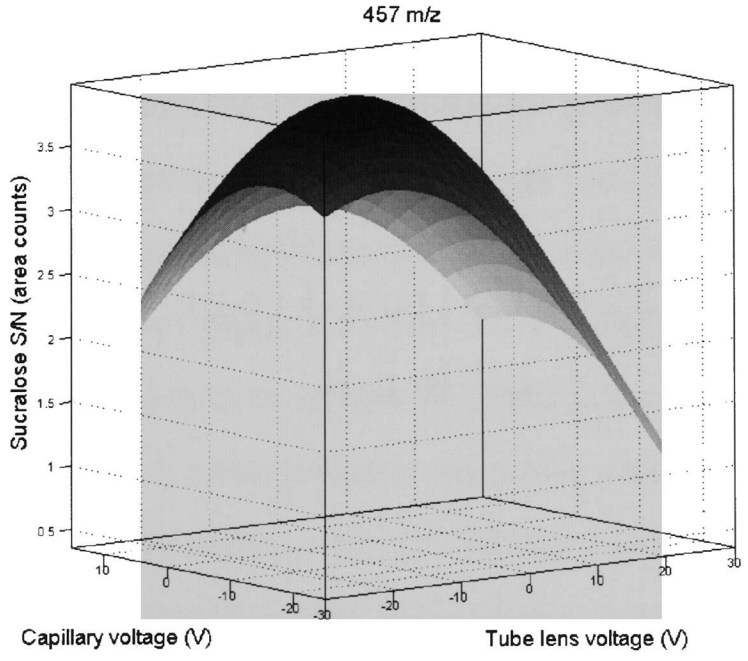

Figure 2.18. Surface plot of tube lens vs. capillary voltage – 457 m/z

2.4.1.3 Sucralose Dihydrate Adduct Ion 433 m/z

The water sucralose adduct signal was tuned in the same fashion as the molecular ion and the acetate based adduct ion. The optimal critical value for each parameter is as follows: sheath gas - 38 psi, ion spray voltage - 4.05 kV, tube lens voltage - -8 V, capillary voltage - 2.59 V.

2.4.2 Exploring Maximum Response of Sucralose Ions by Investigating Various Mobile Phase Conditions

This section is focused on the effect of mobile phase composition to the formation of either the deprotonated molecular ion chlorine cluster of sucralose $[M-H]^-$ - 395, 397, 399 m/z, the hydrated adduct of sucralose $[M+2*H_2O-H]^-$ - 431, 433, 435 m/z, or the corresponding acetate adduct $[M+C_2H_3O-H]^-$ - 455, 457, 459 m/z, see figure 2.3 & 2.4. The bar graph below (figure 2.19) is a summary of the experimental results. The formation of the sucralose deprotonated molecular ion is greatest - relative to its formation under all experimental conditions - when the mobile phase mixture is free of buffer additives. Nonetheless, even when the mobile phase condition promotes the greatest response for the deprotonated molecular ion, the water sucralose adduct response is well over twice as much (Figure 2.19). Thus, in the absence of buffer additives, the dominant sucralose response is in the form of a bi-molecular water-sucralose adduct. When acetic acid (pH 3) is incorporated to the mobile phase, the molecular ion is minimal while the acetate adducts - 455, 457, 459 m/z - are dominant. Furthermore, ammonium acetate has a significant effect on the response of sucralose as acetate adduct.

The effect of ammonium acetate is shown in the bar chart above and indicates that sucralose response is greatest with 4 mmol L^{-1} concentration of ammonium acetate.

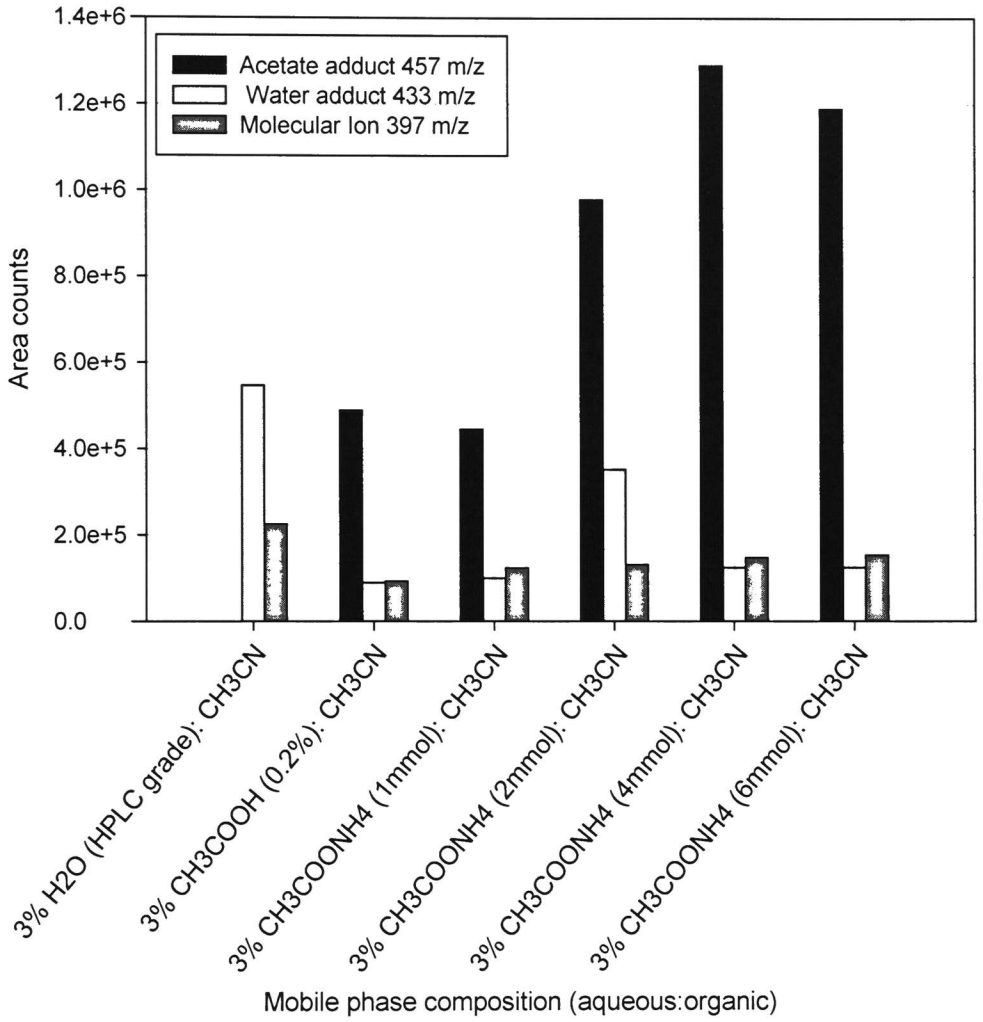

Figure 2.19: Response Distribution of the three Prevalent Ions/Adduct Ions: Sucralose Molecular Ion – 397 m/z, Water - Sucralose Adduct – 433 m/z and Acetate - Sucralose Adduct – 457 m/z.

2.5 Conclusion

There have been two previous publications concerning sucralose detection with a mass spectrometry system. In both instances, the molecular ion of sucralose yielded a suitable response for trace analysis and was the ion selected for quantitation. Also, both reports applied tandem mass spectrometry systems that were interfaced to orthogonal geometry ESI sources. This study is the first to report mass spectrometric detection of sucralose from 60° geometry ESI source – Thermo Ion Max – interfaced to a quadrapole ion trap system. Given this particular instrumental arrangement, this study reports the prevalence of sucralose adduct ESI response in lieu of the sucralose molecular ion. It was observed that sucralose adducts were preferentially ionized over the molecular ion, whether the aqueous component of the mobile phase involved an acetate based additive or not.

Three questions were posed to further validate these observed phenomena. The first question was - can tuning of ESI parameters of the acceleration region favor the ionization of the sucralose molecular ion over either sucralose based adducts? If not, what are the ESI parameter values that optimize ionization efficiency for the most intense adduct ion? The third question was what mobile phase condition maximizes the response of the most intense ion?

Sucralose response was explored with response surface methodology and canonical analysis. Experimental results from the ionization tuning experiments support the prevalence of adduct formation in lieu of the sucralose molecular ion. Thus, considering the optimal ionization conditions for the sucralose molecular ion, adducts were preferentially formed whether pure water was used or an acetate based additive was

involved with the aqueous component of the mobile phase. Furthermore, ESI tuning was applied to the sucralose water and acetate adducts. Their optimal settings were then applied to investigate ionization under various mobile phase conditions. It was concluded that in the absence of a buffer additive, the water sucralose adduct was the dominant signal. In the presence of an acetate based mobile phase system (0.2% acetic acid at pH 3 was considered) 4 mmol/L of ammonium acetate provided the maximum response for the sucralose acetate adduct.

In light of the 60° geometry based ESI source and QIT mass spectrometry system, it has been validated that the sucralose acetate based adduct provides the best quality signal - of course only when considering acetate based additives – for sucralose response. However, thus far we have only investigated the *quality* of sucralose response in an ideal solvent system. The next chapter will apply the tuned ESI signal to investigate system based minimum detection limits as well as consider the application of the technique to evaluate sucralose response from sea water samples.

Chapter 3

Trace Determination of Sucralose in Coastal Waters of the Florida Keys

3.1 Introduction

The previous chapter was dedicated to the tuning of the electrospray ionization (ESI) source for optimal sucralose response. In this study, two methods were developed for the determination of sucralose from sea water samples (HPLC/MSMS and GC/MS). Furthermore, their detection limits were calculated with statistical rigor and will be presented. The results and discussion of this chapter will be presented in the following manner. The report will begin with a procedural outline for both of the developed methodologies (HPLC/MSMS and GC/MS), including standard preparation, chromatography system parameters, ESI source parameters, mass spectrometry parameters – illustrating mass spectrometric transitions for sucralose, d-6 sucralose and the selected external standards. The experimental section will lead to the quantification method and representative calibration curves.

Chapter 2 covered issues regarding the tuning of the ionization source, thus information concerning ESI source parameters, as it relates to optimal sucralose response, will not be restated. The discussions and results section will be covered in the following manner. SPE validation will be presented, showing sucralose recovery as a function of sample volume and sample type – deionized water and sea water. The second part of the results and discussion will cover problems encountered by matrix suppression effects and how they were resolved by optimizing sucralose retention on the reverse phase HPLC

column. The third section will present statistically supported detection limits for the HPLC/MSMS and GC/MS methods. The fourth section presents data concerning the application of the developed methods, to assess the environmental occurrence of sucralose from two study sites in the coastal marine waters of the Florida Keys.

Our research employs the Zorn, et al. procedure to calculate detection limits. The Zorn approach could be considered a hybrid of the DIN 32545 and the EPA MDL, marrying the important and critical features the two approaches. The two critical features of the above approaches are, respectively, the replicate based calibration design from calibration standards and the inclusion of the analyte variance due sample preparation error – the Zorn approach is based on a calibration design from variably spiked samples using the complete analytical method. Furthermore the Zorn approach, which is thoroughly covered in Appendix 2, is based on the same detection limit theory as the DIN 32545 and EPA approaches, but improves upon it by applying the weighted variant of least squares analysis to correct for the heteroscedastic condition (non-constant variance) of analytical data.

The HPLC based approach remained the tool of choice for sucralose determination from sea water throughout the validation phases, up until the decision limits L_c for both instrumental approaches were compared – HPLC/MSMS: 35.17 ng/L; GC/MS: 5.014 ng/L. Even though the detection limit of the HPLC/MSMS system is suitable for screening purposes, we opted for the sub-trace level GC/MS system because of limited knowledge of sucralose occurrence in U.S. (Mead, et al. 2009). Our report is the first to document sucralose occurrence from near shore waters of the Florida Keys, supported by statistically determined detection.

Background modules were added to the appendix, to better comprehend the application of variance modeling and weighted least squares regression to calculate statistically supported detection limits.

3.1.1 Sampling Strategy and Study Sites

One liter water samples were collected at each station in amber bottles. Sampling bottles and all glassware used for sample collection and preparation were cleaned by washing with soap then rinsed with DI water and then combusting at 450 °C for 6 hours. Environmental descriptors such as pH, salinity, dissolved oxygen, surface water temperature, and site depth were also collected as part of the sampling protocol. Surface samples were collected, then stored in ice and shipped to the laboratory where they were maintained below 4°C until analysis.

3.1.1.1 Lake Largo Harbor

Key Largo is one of the largest islands in the Florida Keys and is known as the diving capital of the world. It has close to 12,000 residents and about 5,000 homes. Key Largo Harbor is located near the most populated area of Key Largo with hundreds of septic tank systems. This site is located along 25 ft. deep winding canals that were cut into the permeable limestone. The canals are surrounded by residential and commercial operations, with most of the waterfront properties served by old and aging septic tanks (Lapointe, 1992). Sampling sites are located on a canal system that is adjacent to Key Largo Harbor, a heavily populated commercial and residential sector of Key Largo.

Lake Largo Harbor sampling was done once, during September of 2008. The eight sites are shown in Figure 3.1. Site LLH-01 is the harbor mouth. LLH-03, LLH-05 and LLH-07 are at the dead end channels, while sites LLH-02, LLH-04 and LLH-06 are along the main channel and site LLH-08 is Lake Largo, at the source of the canal system.

The main target of sampling this area was to assess the contributions from septic tanks (residential).

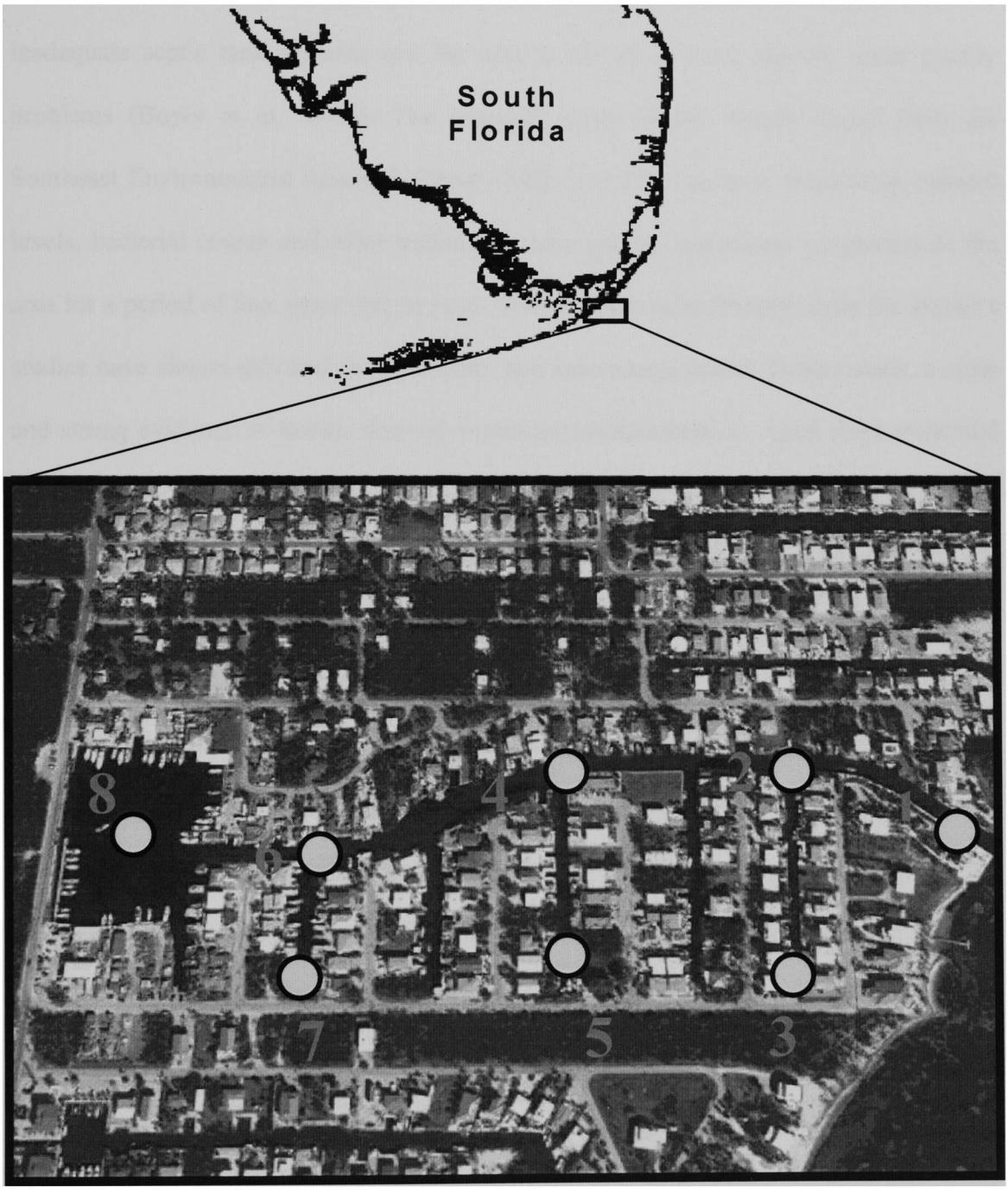

Figure 3.1. Satellite image of Lake largo Harbor

3.1.1.2 Little Venice, Marathon Key

The Little Venice area is on Marathon Key and has approximately 540 permanent residents living in densely populated areas. Most of these homes are still served by inadequate septic tank systems and the area is known to have chronic water quality problems (Boyer et al., 2004). The research group of Dr. Joseph Boyer from the Southeast Environmental Research Center (SERC) at FIU has been monitoring nutrient levels, bacterial counts and other traditional water quality assessment parameters in the area for a period of four years (Boyer et al., 2004). The results obtained from Dr. Boyer's studies have shown elevated fecal coliform and enterococci counts in the canals, a clear and strong evidence of human derived wastewater contamination. Apart from microbial indicators, high nutrient levels at the canals have also been documented. As a part of our group projects, emerging pollutants of concern (EPOC) monitoring was started in 2001 to increase the number of water quality based chemical tracers that could be used for environmental impact assessment.

The Little Venice sampling program includes ten sampling stations located in four different canals (Figure 3.2). Stations 1 and 3 are located in a "U-shaped" connected canal system located at 112th Street. These canals receive better tidal flushing than other canals because of their flow-through design and relatively short length. Also, the canals are surrounded by single-family residences that were built before 1970 and a high percentage of those residences are thought to have no sewage treatment systems (Boyer et al., 2004). Stations 2, 4, and 5 are located on the canal next to 100th Street and stations 6 and 7 are located on the canal adjacent to 97th Street. Both canals are dead-end canals that are surrounded by single-family houses and mobile homes. Many of these residences

are also thought to have poorly functioning old septic systems. Stations 8 and 9 are located next to the 91st Street canal, which is located outside the Little Venice Service Area (Boyer et al., 2004). Station 10 is located about 100 meters offshore on the remnants of a dredged canal area.

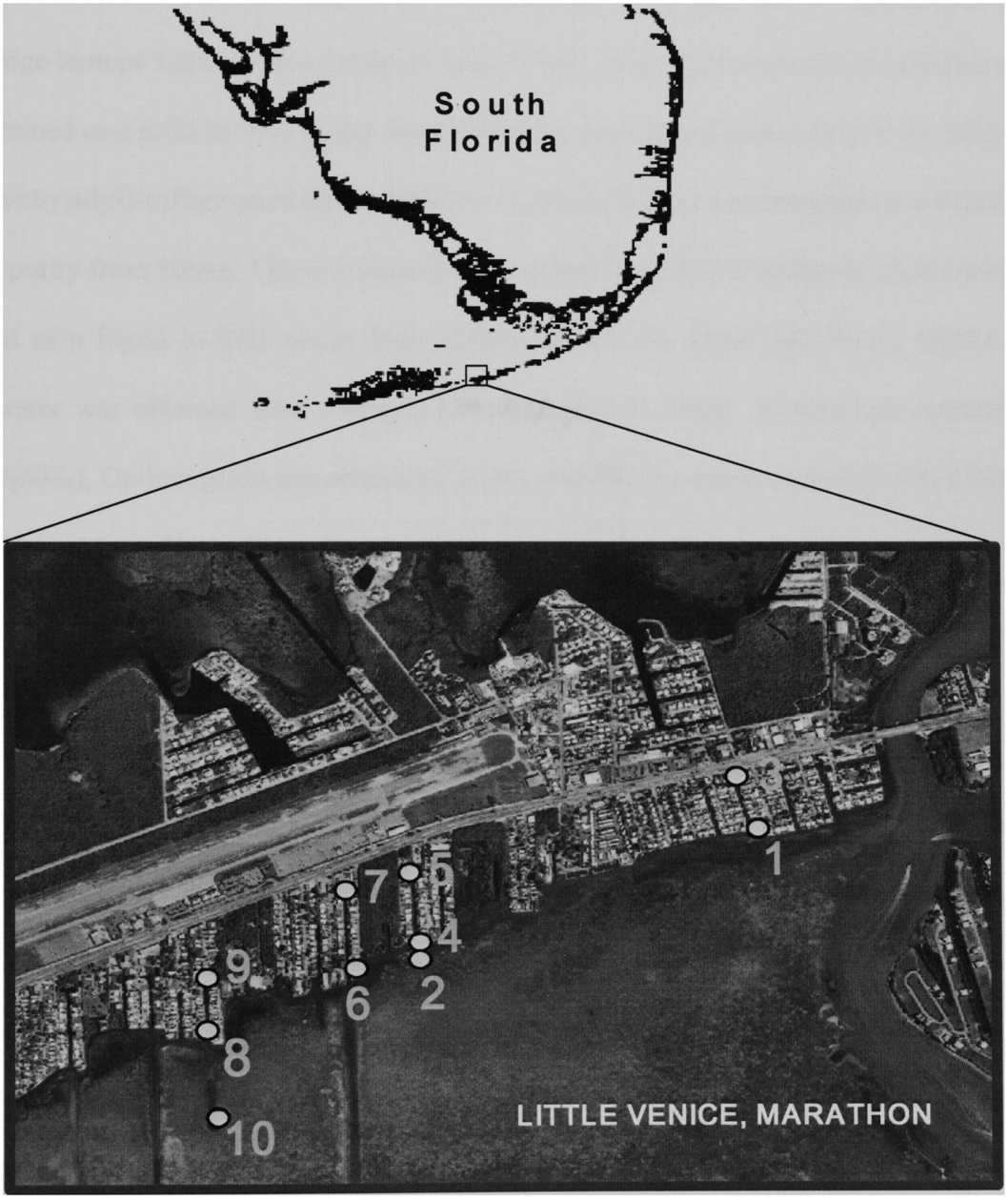

Figure 3.2 Satellite image of Little Venice, Marathon, FL.

3.2 Materials

3.2.1 Reagents and Solvents

Sucralose ($C_{12}H_{19}Cl_3O_8$) and sucralose-d6 ($C_{12}H_{13}D_6Cl_3O_8$) were obtained as a solid in 99% purity from Toronto Research Chemicals, Inc. (North York Ontario, Canada). Caffeine $3C^{13}$ ($C_3{}^{13}C_5H_{10}N_4O_2$) was obtained as a solid in 99% purity from Cambridge Isotope Laboratories (Andover MA, USA). 2,4,6-trichlorophenol ($C_6H_3Cl_3O$) was obtained as a solid in 99% purity from Chem Service (West Chester PA,USA). N,O-bis(trimethylsilyl)-trifluoroacetamide (BSTFA) ($C_8H_{18}F_3NOSi_2$) was obtained as a liquid in 99% purity from Pierce, Thermo Scientific (Rockford IL, USA). Pyridine (C_5H_5N) was obtained as a liquid in 99% purity from Sigma-Aldrich (St. Louis MO,USA). (HPLC grade water was obtained from Pharmco (Brooksfield CT, USA). Ammonium Acetate ($C_2H_3O_2NH_4$), Optima grade acetonitrile (C_2H_3N), and Optima grade methanol (CH_3OH) were obtained from Fisher Scientific (Fairlawn NJ, USA).

3.2.2 Chromatography Materials

I used a 0.45 um pore size, 25 mm diameter membrane filter obtained from Millipore (Billerica MA, USA). 250 mg Oasis HLB SPE sorbent was purchased from Waters (Milford MA, USA). Luna C-18 (2) 5 um particle size, 4.6 mm inner diameter, 150 mm length, Luna C-18 (2) 5 um particle size, 4.6 mm inner diameter, 250 mm length were purchased from Phenomenex (Torrance CA, USA). Zebron MR-1 fused silica capillary column – 0.25 um film thickness, 0.25 mm internal diameter and 30 m length from Phenomenex (Torrance CA, USA).

3.2.3 Instrumentation

The liquid chromatography-mass spectrometer system used in this investigation included a Thermo-Finnigan (Therno-Finnigan San Jose CA, USA) Surveyor Plus, quaternary pump, a Surveyor Plus auto-sampler, and a LCQ Advantage MAX quadrapole-ion trap mass spectrometer (QIT) (50-2000 Da). The LC/MS was run under negative ion Electrospray Ionization (ESP-) for the sucralose signals studied.

The gas chomatograph-mass spectrometer system used in this investigation included an Agilent HP 6890N gas chromatograph coupled to an Agilent HP 5973 mass spectrometer. Automated SPE preconcentration was facilitated by an Autotrace® SPE workstation from Zymark (Hopkinton MA, USA)

3.3 Methods

3.3.1 Solid Phase Extraction (SPE) for HPLC/MSMS and GC/MS

The 700 ml water samples were filtered through a 0.45 um membrane filter then amended with the suitable standards.

HPLC/MSMS analysis: For all samples including system blanks, 100 ul of a 200 ng/ul sucralose d-6 stock solution was added. For sucralose recovery QC samples i.e. laboratory spike samples (LBS) and matrix spiked samples MS, an additional 100 ul of a 200 ng/ul sucralose stock solution was added.

GC/MS analysis: For all samples including system blanks, 50 ul of a 200 ng/ul sucralose d-6 stock solution was added. For sucralose recovery QC samples i.e. laboratory spike samples (LBS) and matrix spiked samples MS, an additional 50 ul of a 200 ng/ul sucralose stock solution was added.

Samples (700 ml) were automatically processed on an Oasis HLB SPE cartridge by means of an Autotrace® SPE workstation. The following table 3.1 describes the method program for automated SPE analysis.

Autotrace SPE procedural program for sucralose preconcentration from sea water
1.) System lines were flushed with a 20% methanol: 80% water solution.
2.) Syringe washed with 5 ml. of methanol
3.) Syringe washed with 5 ml. water
4.) Column was conditioned with 5 ml. of methanol
5.) Column was conditioned with 5 ml. of water
6.) 700 ml of the sample was loaded
7.) Syringe was washed with 5 ml of water
8.) Column was rinsed with 4 ml. of water
9.) Column was rinsed with 2 ml. of 5% methanol:95% water
10.) Column was dried for 12 minutes with nitrogen
11.) Column was eluted with 10 ml of acetonitrile
- Conditioning flow rate: 5 ml/min - Loading flow rate: 3 ml/min - Column rinse flow rate: 3 ml/min - Nitrogen flow pressure: 12 psi

Table 3.1. SPE procedure for sucralose preconcentration from sea water.

Following sample elution, SPE extracts were evaporated to dryness by applying a gentle stream of nitrogen.

HPLC/MSMS analysis: the extract was then enriched with 200 ul of a 100 ng/ml 2,4,6 trichlorophenol external standard solution that was prepared in a 90% water: 10% acetonitrile solvent system. The extract was then transferred to a 250 ul borosilicate glass insert and stored in a freezer at -20 ° C.

GC/MS analysis: the extract was then amended with 200 ul of a 100 ng/ml caffeine $3C^{13}$ external standard solution that was prepared in 100% acetonitrile. The extract was then quantitatively transferred to a 250 ul borosilicate glass vial insert and evaporated to dryness with a gentle stream of nitrogen. 100 ul of BSTFA and 50 ul of pyridine were added to the dry extract. The solution was mixed well then heated for 40 minutes at 70° C. After completing the reaction, the extract was evaporated to dryness under a gentle stream of nitrogen then reconstituted in 200 ul of dichloromethane.

3.3.2 HPLC/MSMS Calibration Standards

A series of stock solutions were prepared in acetonitrile from 99% pure neat solids of sucralose, sucralose d-6, caffeine $3C^{13}$ and 2,4,6-trichlorophenol (table 3.2). Calibration solutions for HPLC/MSMS analysis were prepared in 90% water: 10% acetonitrile system. To ensure a delivery volume >15 ml, a low concentration stock solution of sucralose was prepared at 200 ng/ul. The rest of the calibration standards were prepared from the following stock solutions: Caffeine $3C^{13}$ -100 ng/ml; 2,4,6-trichlorophenol - 96.3 ug/ml; sucralose – 20 ug/ml; sucralose d-6 – 20 ug/ml.

Calibration standards for HPLC MSMS analysis

Solution component	Calibration Solution 1 (ng/ml)	Calibration Solution 2 (ng/ml)	Calibration Solution 3 (ng/ml)	Calibration Solution 4 (ng/ml)	Calibration Solution 5 (ng/ml)
Internal standard: 2,4,6-trichlorophenol	200	200	200	200	200
Surrogate internal standard: sucralose d-6	200	200	200	200	200
Target compound: Sucralose	20	60	120	400	900

Table 3.2. Calibration standards for HPLC/MSMS analysis.

3.3.3 GC/MS Calibration Standards

The GC/MS standards were prepared without caffeine $3C^{13}$. The external standards were added prior to derivitization. Derivitization was done prior to instrumental analysis in the following manner. 200 ul of the following calibration standards and 200 ul of a 100 ng/ml caffeine 3C13 stock solution were delivered to a borosilicate glass insert then evaporated to dryness under a gentle stream of nitrogen. 100 ul of BSTFA and 50ul of pyridine were added to the calibration standards. Along with the corresponding unknown and QA samples, the calibration standards were heated for 40 minutes at 70°C. The standards were allowed to cool 20 minutes then evaporated to dryness with nitrogen. Finally the extracts were reconstituted in 200 ul of dichloromethane (table 3.3).

Calibration standards for GC/MS analysis

Solution component	Calibration Solution 1 (ng/ml)	Calibration Solution 2 (ng/ml)	Calibration Solution 3 (ng/ml)	Calibration Solution 4 (ng/ml)	Calibration Solution 5 (ng/ml)	Calibration Solution 6 (ng/ml)
Internal standard: Caffeine $3C^{13}$	100	100	100	100	100	100
Surrogate internal standard: sucralose d-6	100	100	100	100	100	100
Target compound: sucralose	5	20	60	150	500	900

Table 3.3. Calibration standards for GC/MS analysis.

3.3.4 HPLC Parameters

The high pressure liquid chromatography parameters were designed as follows: The mobile phase flow rate was 600 ul/min throughout the complete analytical run. The initial mobile phase condition was 98% of 4 mM ammonium acetate: 2% acetonitrile. This condition was held constant for 1 minute and followed by a ramp that changed the mobile phase composition to 98% acetonitrile: 2% 4mM ammonium acetate, this

condition was held for 5 minutes and twenty seconds. The ramp was then brought back to the initial condition over the span of 1 minute. Re-equilibration of the reverse-phase column was achieved after 17 minutes. Sample injection volume was 25 ul (table 3.4).

HPLC gradient, flow rate and injection parameters

Time (min)	Flow rate (ml/min)	Acetonitrile (%)	4 mM Ammonium acetate (%)
0.00	0.6	2	98
1.00	0.6	2	98
6.80	0.6	98	2
12.00	0.6	98	2
13.00	0.6	2	98
31.00	0.6	2	98
Injector conditions: Injection Volume (ul): 25			

Table 3.4. Chromatography parameters for HPLC analysis.

3.3.5 GC Parameters

The gas chromatography parameters were designed as follows: The initial oven temperature was 50°C and was held constant for 1 minute. Then a temperature ramp of 8° C/min. raised the temperature to 265°C. A second temperature ramp of 2°C/min. brought the temperature to 280°C, and then a third temperature ramp of 10°C/min. raised the temperature to 300°. The final temperature was held constant for 5 minutes. Refer to the table 3.5 for the injection port, transfer line and source temperatures.

GC temperature gradient, gas flow rate and injector parameters

Initial temperature: 50° C ; Initial time: 1.00 minute			
Ramp number	Temperature rate (°C/min)	Final temperature (°C)	Final time (min)
1	8	265	0
2	2	280	0
3	10	300	5
Splitless injection. Inlet flow on at 1 min Constant gas flow at 1.2 ml/min Injection vol.: 2 ul; Total run time: 46 min		Inlet temp.: 260° C; Transfer line temp.: 280° C MS source temp.: 250° C; Quadrapole temp.: 150° C Solvent delay of 10 minutes	

Table 3.5. Chromatography parameters for GC analysis.

3.3.6 ESI Source, Ion Optics and Mass Spectrometry Parameters

The purpose of chapter 2 was to find optimal conditions for the electrospray ionization of sucralose, thus the optimization strategy will not be restated. However, all ionization parameters, including the ion optics parameters (octapoles and interoctapole lenses) will be listed. The energy values for the ion optics are important to focus the ions towards the mass analyzer (figure 3.3 & table 3.6) and were established with an optimization algorithm supplied by the instrumental acquisition software. The ESI probe position was set at the D position and the probe z-axis was set at 1.5 cm to ensure an offline path for uncharged and oppositely charged microdroplets.

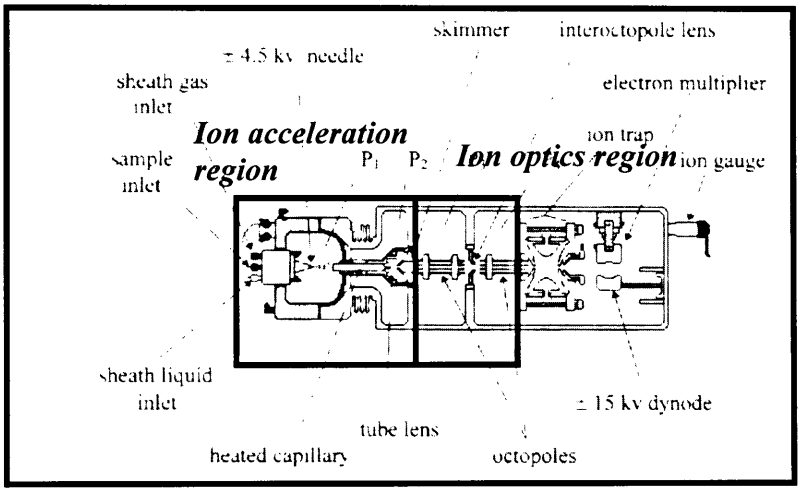

Figure 3.3. Diagram of a Thermo LCQ analytical region. Source: Boyd et al, 2008.

ESI source parameters of the ion acceleration region	ESI source parameters of the ion optics region
Sheath gas: 36 psi Auxiliary gas: 2 psi Ion spray voltage: 5.5 V Capillary temperature: 320° C Capillary voltage: -8 V Tube lens voltage: -12 V	Multipole offset 1: 3.10 V Lens voltage: 30 V Multipole offset 2: Multipole RF amplitude: 290 Probe position: D Z-axis probe position: 1.5 cm

Table 3.6. ESI source parameter

3.3.6.1 Mass Spectrometry Parameters for QIT-MSMS – Scan Segments

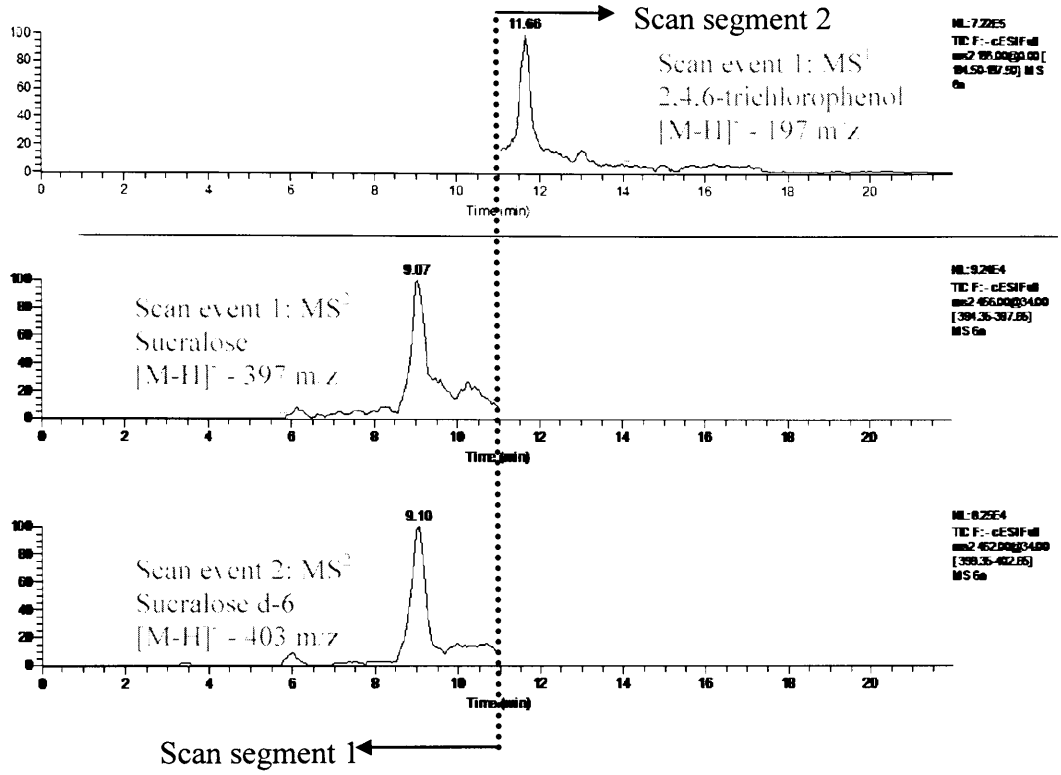

Figure 3.4. QIT-MSMS scan segments.

The above chromatograms are representative of MS^2 sucralose analysis. The QIT mass spectrometry system is limited for trace analysis, in the sense that greater that two scan events per scan segment dramatically reduces the response ion current. As a means to maximize instrument sensitivity, two scan segments were designed. The first scan segment was dedicated for sucralose and d-6 sucralose scan events and range from 6-11 minutes (figure 3.4), while the second scan segment ranges from 11-14 minutes and was dedicated for the 2,4,6-trichlorophenol scan event (figure 3.4). The following section presents information about the ion transitions that occurred in the particular QIT scan events. MS^2 and MS^3 scan events were used for the trace analysis of sucralose and its deuterated analog.

3.3.6.2 Mass Spectrometry Parameters for QIT-MSMS – MS^2 Scan Transition Events

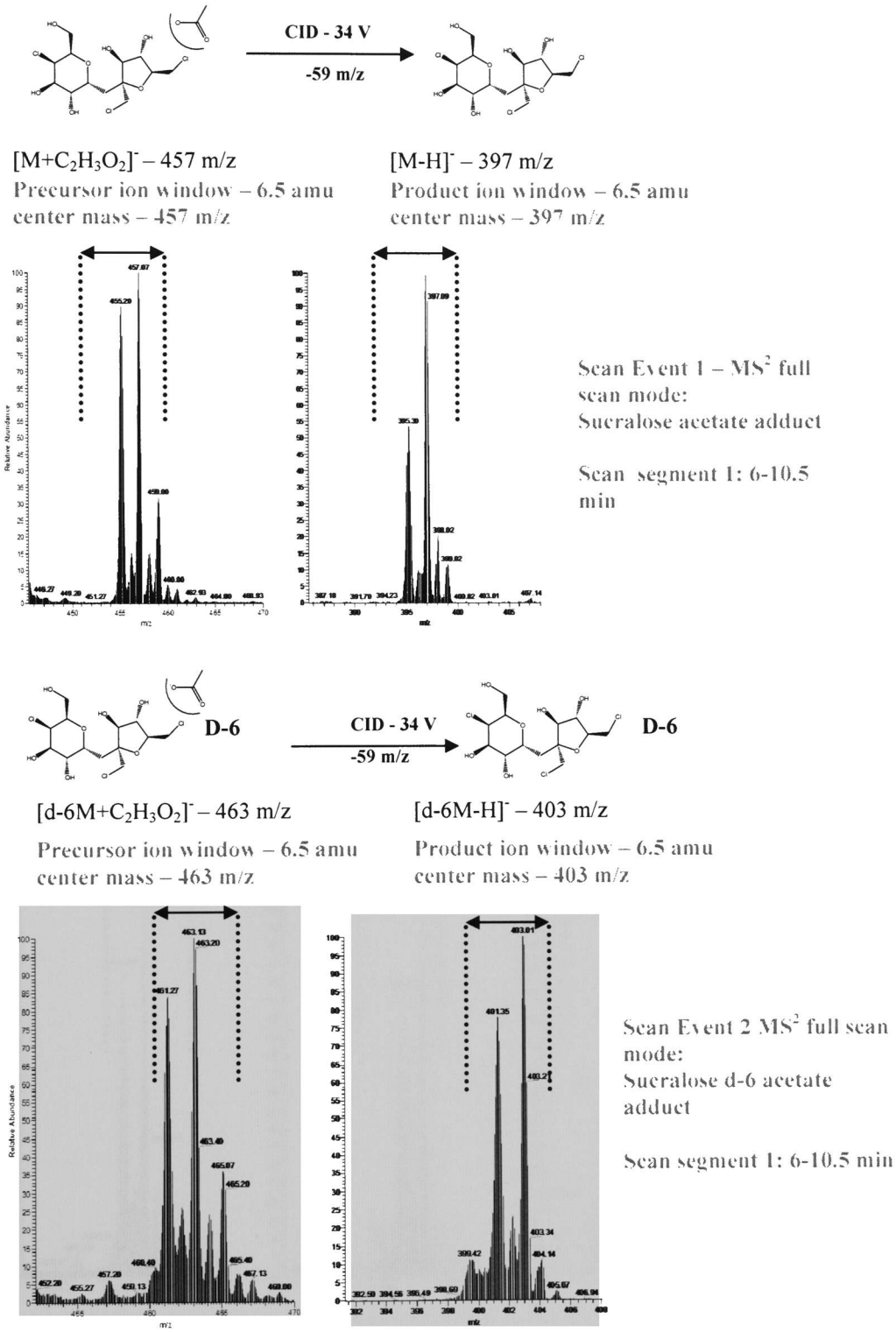

Figure 3.5. Quadrapole ion trap MS^2 mass transitions for sucralose and d-6 sucralose.

3.3.6.3 Mass Spectrometry Parameters for QIT-MSMS – MS^3 Scan Transition Events

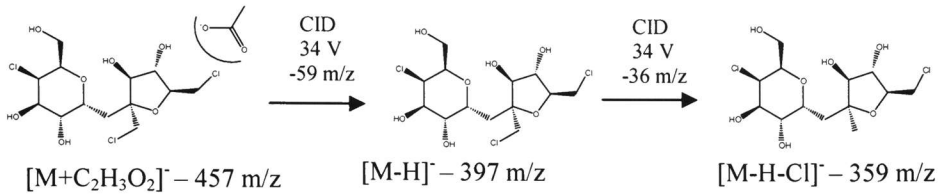

$[M+C_2H_3O_2]^-$ – 457 m/z

Precursor ion window – 6.5 amu
center mass – 457 m/z

$[M-H]^-$ – 397 m/z

Product 1 window – 6.5 amu
center mass – 397 m/z

$[M-H-Cl]^-$ – 359 m/z

Product 2 window – 6.5 amu
center mass – 461 m/z

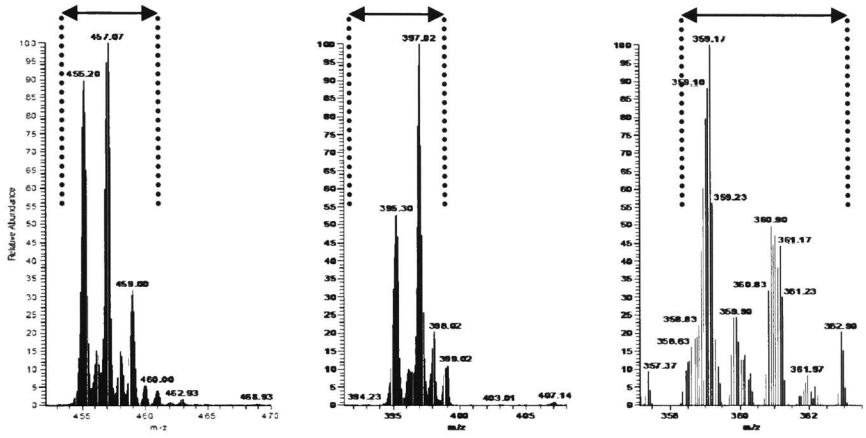

Scan Event 1 – MS^3 CRM mode: Sucralose acetate adduct

Scan segment 1: 6-10.5 min

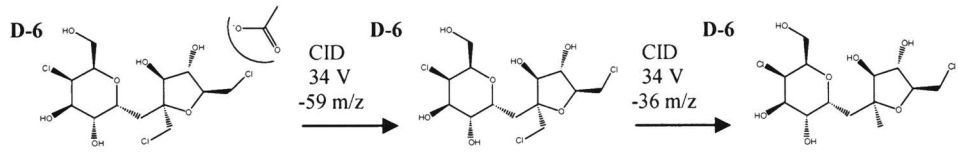

$[d\text{-}6M+C_2H_3O_2]^-$ – 463 m/z

Precursor ion window – 6.5 amu
center mass – 463 m/z

$[d\text{-}6M-H]^-$ – 403 m/z

Product 1 window – 6.5 amu
center mass – 403 m/z

$[d\text{-}6M-H-Cl]^-$ – 367 m/z

Product 2 window – 6.5 amu
center mass – 367 m/z

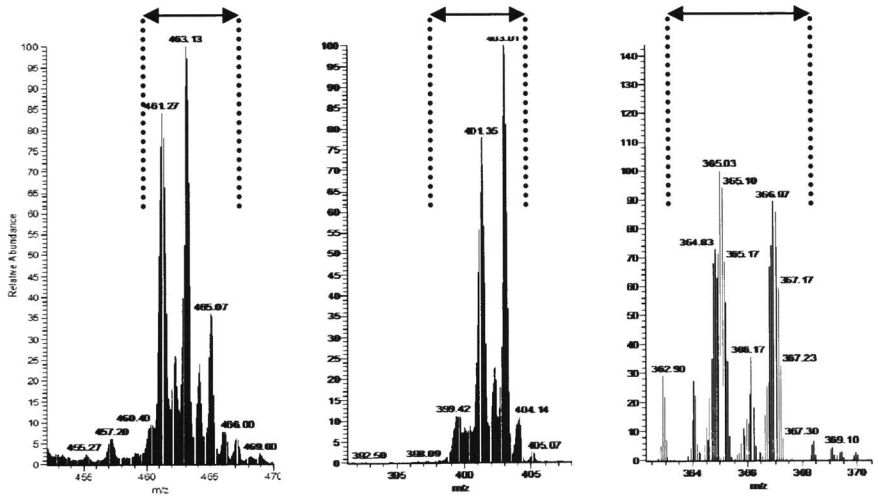

Scan Event 2 MS^3 CRM mode: Sucralose d-6 acetate adduct Scan segment 1: 6-10.5 min

Figure 3.6. Quadrapole ion trap MS^3 mass transitions for sucralose and d-6 sucralose.

3.3.6.4 Mass Spectrometry Parameters for QIT-MSMS – Internal Standard MS Transition

Two,4,6-trichlorophenol was the selected internal standard for quantitation of the d-6 sucralose surrogate internal standard from actual environmental samples. The analyte signal was acquired in the MS^1 full scan mode. The molecular ion for 2,4,6-trichlorophenol was $[M-H]^-$ - 197 m/z. The scan event parameters are as follows: The scan event for the external standard occurs on scan segment 2 (figure 3.4). The ion window is centered at 196 m/z with a scan width of 3 amu. Fragmentation of this compound did not occur – CID = 0V, thus the product scan settings are equivalent to the precursor ion scan settings above.

3.3.6.5 Mass Spectrometry Parameters for QIT-MSMS – Ion Detection

The ion detection parameters were: Automatic gain control was set to the on position (AGC on), with an MS^n max ion time of 1600 ms. MS^n scan rate was set to 1 microscan. The target MS^n AGC value was set to 8E07.

3.3.6.6 Mass Spectrometry Parameters for Electron Impact–MS – SIM Segments

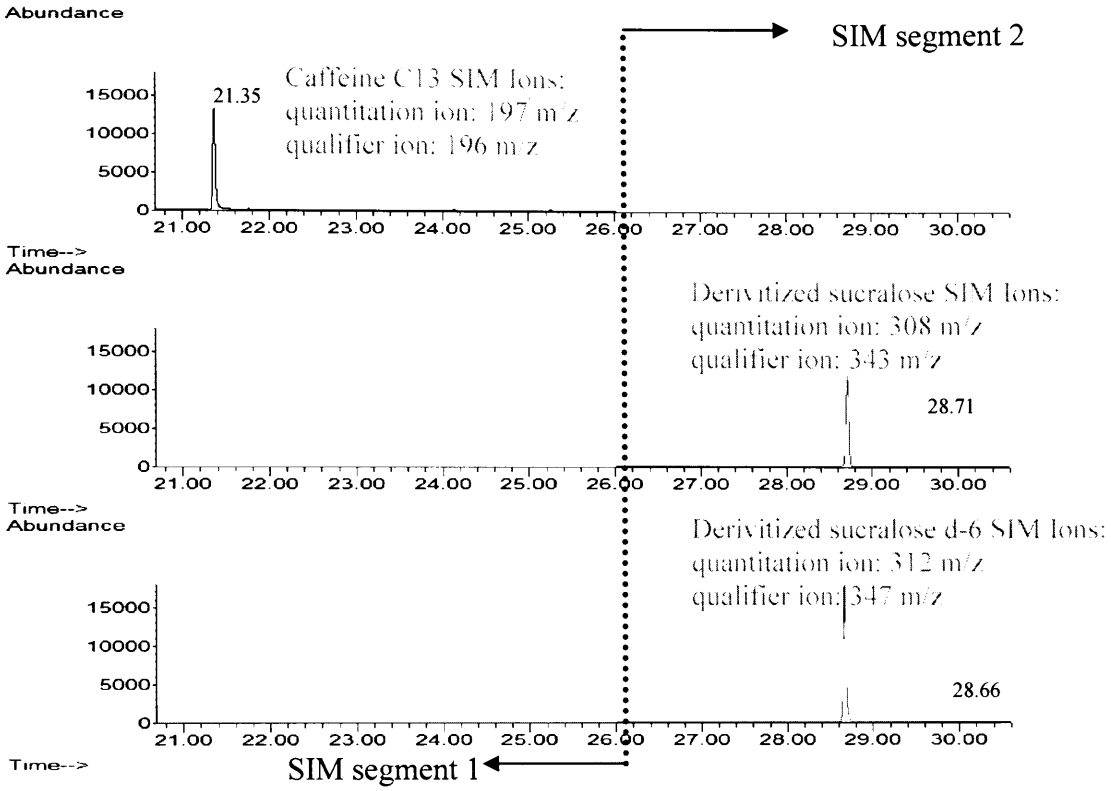

Figure 3.7. GC/MS chromatograms and SIM segments for sucralose and d-6-sucralose.

The chromatograms above in figure 3.7 represent a typical elution pattern for sucralose, the surrogate internal standard - sucralose d-6 and the $^{13}C_3$ caffeine internal standard. The acquisition method was designed with 2 SIM segments. As illustrated above, the first SIM segment spans from 20 minutes thru 26 minutes, while the second SIM segment begins at 26 minutes and spans the remainder of the analytical run. The first SIM segment is dedicated for specific scans of the $^{13}C_3$ caffeine, while the second SIM segment for sucralose and sucralose d-6.

3.3.6.7 Mass Spectrometry Parameters for Electron Impact–MS - SIM Quantitation and Qualifier Ions

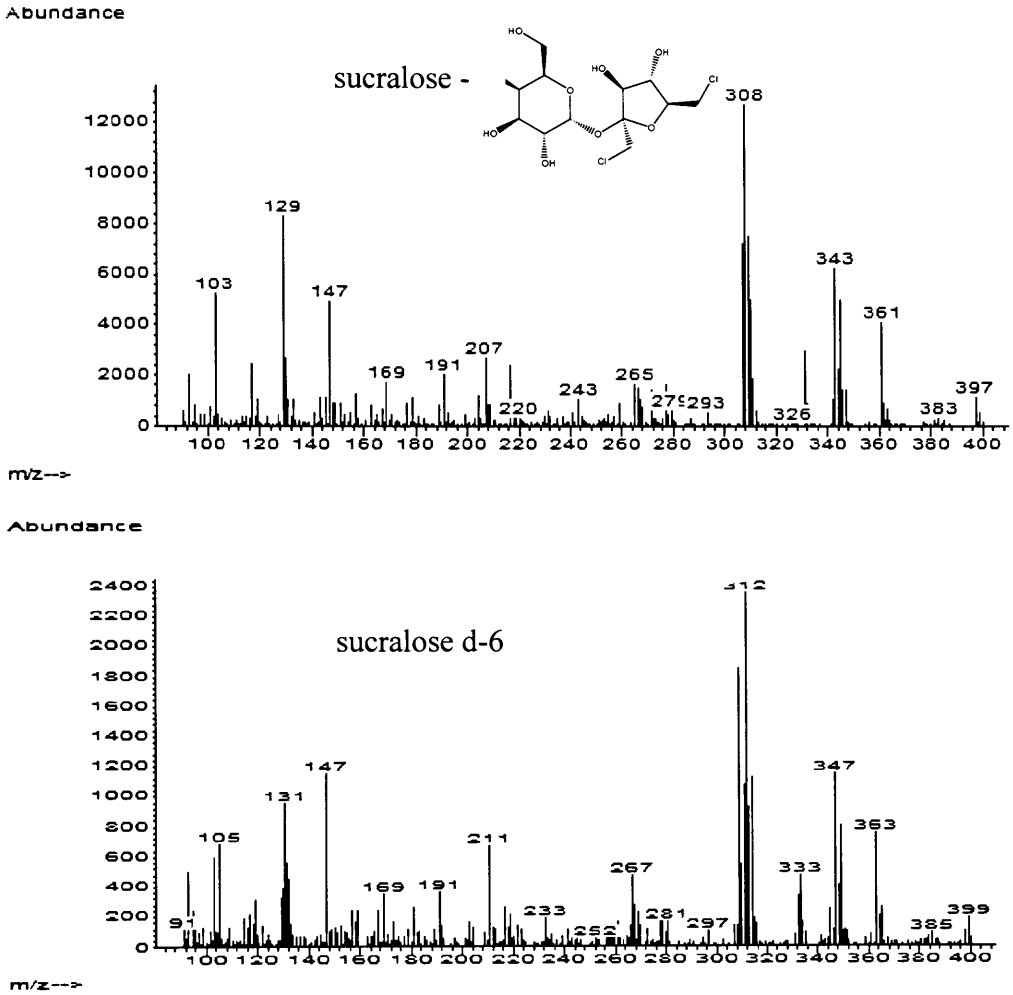

Figure 3.8. EI full scan spectra for the TMS ether of sucralose (top) and sucralose d-6 (bottom).

The above figures 3.8 are electron impact (EI) full scan mass spectra for the TMS ether of both sucralose (top) and the sucralose d-6 (bottom). Work by Qiu, et al. reported a detailed explanation of fragmentation pathways and particular structures of the dominant ions for the TMS ether of sucralose. The base peak of both mass spectra are **308 m/z** for sucralose and **312 m/z** for its labeled analog, these ions were the quantitation

ions. The qualifier ions are **343 m/z** for sucralose and **347 m/z** for sucralose d-6. A dwell time of 40 ms was set for all mass scans.

3.3.7 Isotope Dilution Determinations for Sucralose

For both analytical approaches, GC/MS and HPLC/MSMS, sucralose was analyzed by isotopic dilution. Ion abundance ratios, minimum detection levels, signal to noise levels, and retention times were evaluated using authentic standards of the target analyte prior to each analytical run. Calibration of the instrument was performed by the internal standard method (figure 3.9) and isotope dilution-average response factors were used to quantify the analyte in each sample. This was achieved by adding a known amount of a deuterated sucralose standard to every sample prior to extraction. Consequently, relative response factors are used in conjunction with the initial calibration data to determine concentrations directly by using the following equation:

(1) $$C_x = \frac{(Area_x)C_{IS}}{(Area_{IS})RRF} * \frac{1}{S_{Volume}}$$

where C_x = the concentration (ng/L) of sucralose in the sample, $Area_x$ = the area of the chromatographic peak of sucralose, $Area_{IS}$ = the area of the chromatographic peak for the d-6 sucralose, C_{IS} = the amount (ng) of the labeled standard added prior to extraction. S_{Volume} = The sample volume (L).

(2) $$RRF = \frac{(Area_x)}{(Area_{IS})} * \frac{C_{IS}}{C_x} * \frac{1}{S_{Volume}}$$

and the relative response factor (RRF) is defined as the average relative response factor from the calibration curve. The chemical composition and concentrations of the calibration solutions, for both analytical approaches are listed in the tables 3.2 & 3.3.

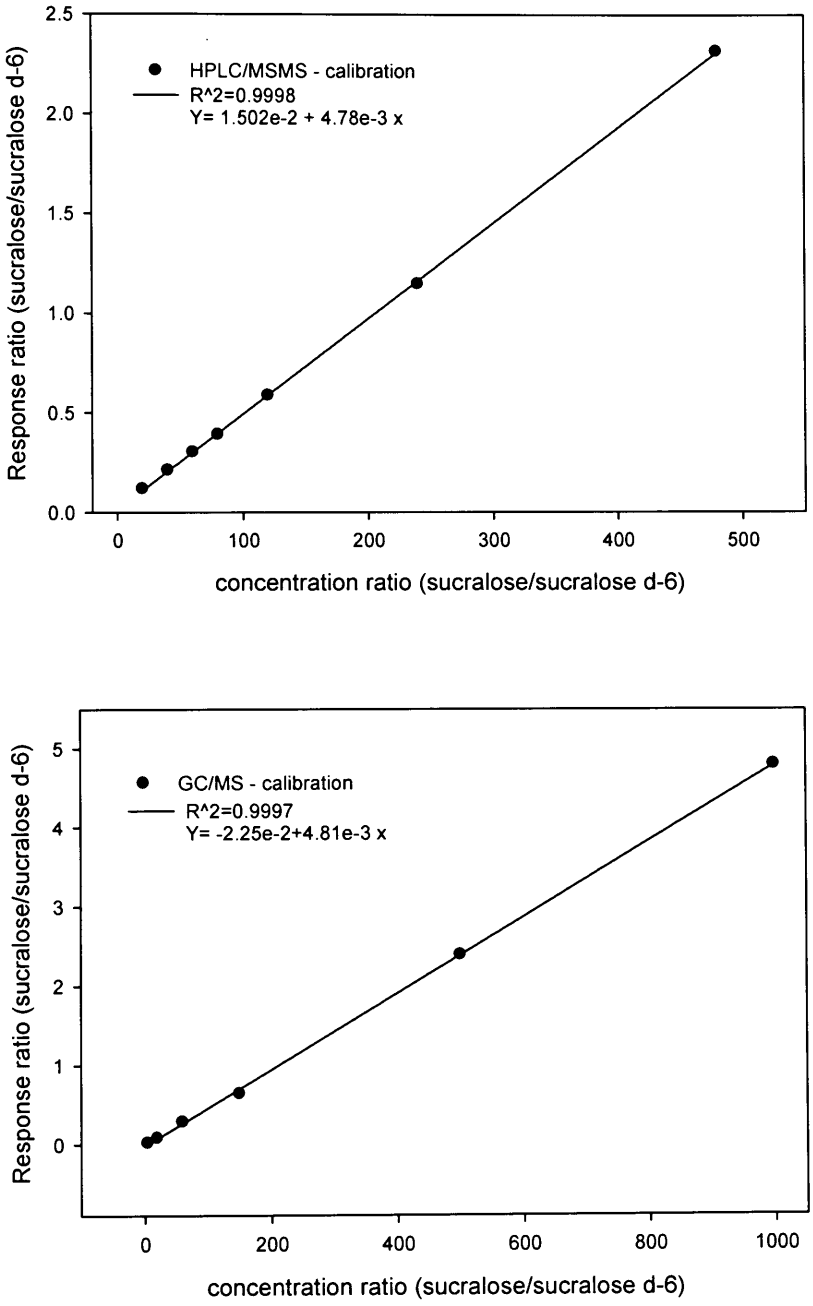

Figure 3.9. Typical calibration curves produced by HPLC/MSMS (top), GC/MS (bottom).

3.3.8 Solid Phase Extraction - Breakthrough Volume Experiment

Several sets of experiments were conducted to assess the recovery of sucralose from deionized water and sea water at different loading volumes. The breakthrough volume of sucralose was assessed by spiking 600 ng of both sucralose and sucralose d-6 into three replicate samples of the appropriate matrix, containing the increasing volumes (300, 500, 700, 900 ml.). Aside from the variation of the loading volume, the samples were then processed by the SPE procedure described in the HPLC/ MSMS portion of section 3.3.1. See sections 3.3.4 and 3.3.6 for the applied HPLC and MS parameters.

3.3.9 Assesment of ESI Suppression Effects on Sucralose

Overcoming matrix suppression of sucralose proved to be a major hurdle for the development of a trace level LC/MSMS methodology. The works by Matuszewski, et al. 2003, and Fu et al. 1998 supported that kind of behavior. In our study, variations of their approaches were applied to identify, and eliminate the matrix suppression effects of the sea water matrix on sucralose response. The following experimental approach is divided in two parts. Part A is focused on evaluating the suppression effects introduced by the organic solvent strength of the SPE elution step; while part B addresses matrix suppression as a function of chromatographic retention of sucralose on the HPLC column.

In part A, two sets of seven sea water samples and two matrix-free deionized water samples were analyzed. Set 1 (black bars) was fortified with sucralose and sucralose d-6 ***prior*** to the SPE extraction process, while set 2 (grey bars) was fortified with equivalent concentrations of the standards ***after*** the SPE extraction process. Aside

from the pre/post fortification difference between sets 1&2, the sample treatments between both sets were identical and differences due to an incremental change in the solvent composition for the SPE elution step, i.e. 0% acetonitrile thru 100% acetonitrile in 20% increments. Furthermore, for both sets, the deionized water (matrix free) sample (cross hatched bars) was extracted with a solvent composition of 100% for the SPE elution step. Matrix effect (ME%) was evaluated as the ratio of the peak area of the analyte spiked into a real sample extract post SPE (A), over the peak area of the analyte spiked directly into a matrix free pure solvent sample *100.

(22) $$ME\% = \frac{A}{B} \times 100$$

Sucralose recovery (RE %) was calculated by isotope dilution – internal standard method (section 3.3.7) and is the ratio of sucralose concentration determined from a sea water sample that was spiked prior to extraction, over the expected concentration *100. The HPLC and mass spectrometry parameters applied in this experiment are described, respectively in sections 3.3.4 and 3.3.6.

In part B, matrix suppression effects of sucralose was evaluated by studying the retention of sucralose by varying the HPLC mobile phase flow rate and the HPLC column length. Sucralose was introduced into the HPLC-ESI-MSMS system at a concentration of 500 ng/ml. Three runs were conducted on the shorter Luna column (see section 3.2.2), respectively with the following mobile phase flow rates - 400, 600 and 800 ul/min. The flow rate that provided the best retention and sucralose response was then used to conduct one run with the longer HPLC column (see section 3.2.2).

3.3.10 Determination of Sucralose Detection and Quantification Limits

Detection limits were calculated for two analytical approaches: HPLC/MS-MS and GC/MS. For both analyses, the experimental procedures were as follows. Six 500 ml deionized water samples were fortified with the appropriate concentrations of both sucralose and sucralose d-6 standards (Table 3.7). The samples were then processed with the optimized sucralose method (see methods 3.3). Six extracts were then analyzed.

For the HPLC/MS-MS strategy, the MS^2 scan transitions were applied (figure 3.5). An instrument acquisition sequence was then designed with seven randomized replications of each sample concentration. This dataset was then quantified by isotope dilution with the appropriate analytical software – HP Chemstation for the GC/MS data and Thermo Xcalibur for the HPLC/MS-MS dataset. Response and amount ratios were then exported to the MATLAB® technical computing environment for weighted least squares analysis and modeling of the response variance.

The first step was to calculate the weighted least squares estimates by applying equations 2-14 of appendix 2. Upon calculating the weighted least squares estimates, the next step was to model the variability (s^2) of sucralose by fitting a suitable regression equation (figures A.8, 3.16). The first application of the variance model was to extrapolate the weight (w_o) at the lowest detectable concentration (X=0) (figure 3.17).

The lowest detectable concentration (X=0) was effectively estimated from the lowest concentration of the calibration design as 5 ng/L (figure 3.17). The weight (w_o) was then calculated as the inverse of the variance (s^2) for this concentration and applied to equation 15 of Appendix 2 - along with the weighted regression estimates - to calculate the critical level in response units R_c. This level is the concentration that corresponds to *a*

decision limit and has a specifically defined false positive (type 1) error rate (α) that results from the hypothesis test H_0: X=0 (see figures A.6 & A.9). The critical level in concentration units L_C was calculated with equation 16 (Appendix 2).

The next step was to calculate the detection limit L_D from a second hypothesis test. The second level is a detection limit (L_D); Currie defined this as "the true concentration at which a given analytical procedure may be relied upon to lead to detection". At the detection limit, a second hypotheses test H_0: $X=L_D$ allows the false negative error rate (β) to be set at the critical level (L_C), from the overlap of its probability distribution with the distribution at X=0 (see figure A.6). As the Figure A.6 illustrates, the detection limit L_D is established by setting the false negative error rate (β) equal to the false positive error rate (α).

The following procedure explains how (β) is set equal to (α): the calculated critical level (L_C) was multiplied by a factor of two ($2*L_C$) (Currie L.A., 1968). At concentration ($2*L_C$), the variance model was then applied to extrapolate the corresponding weight (w_{LD}). Consequently, the detection limit L_D was calculated by applying w_{LD}, $2*L_C$ and the weighted least squares parameters to equation 17.

3.4 Results

3.4.1 Solid Phase Extraction - Breakthrough Volume Experiment

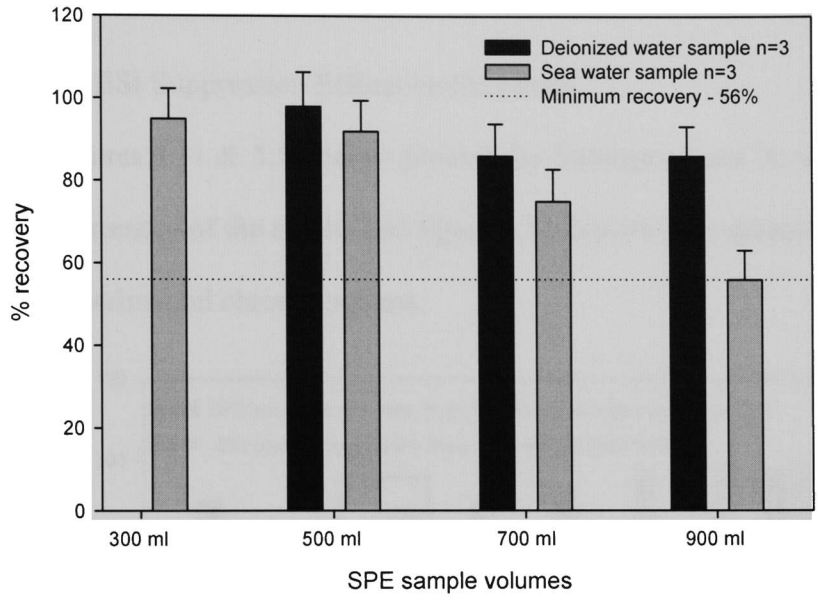

Figure 3.10. SPE breakthrough volume experiment from a sea water and deionized water matrix.

The Figure 3.10 illustrates the results for the breakthrough volume experiment. For the deionized water sample, the results indicate a small but significant breakthrough of sucralose for sample volumes between interval of 500 to 700 ml, respectively with mean recoveries and relative standard deviations of 98 %, 86 % and 8.4%, 7.8 %. Furthermore, it was observed that the mean recovery of sucralose remained approximately constant when the sample loading volume was increased from 700 to 900 ml. However, the breakthrough trend increased upon introducing the complexity of real world sea water samples. For such matrix, the capacity of the SPE cartridge appears to be suitable at loading volumes < 500 ml. The degredation of performance continues for the sample loading volume interval from 500 to 900 ml, respectively, with recoveries and

relative standard deviations of 92%, 75 % and 7.5% and 7.8%. In consideration of these results, 700ml was selected as the method loading volume.

3.4.2 Assesment of ESI Suppression Effects on Sucralose

The two figures 3.11 & 3.12 below present the findings of part A, whereas figure 3.11 illustrates a summary of the results and figure 3.12 depicts the suppression effects as observed in the experimental chromatograms.

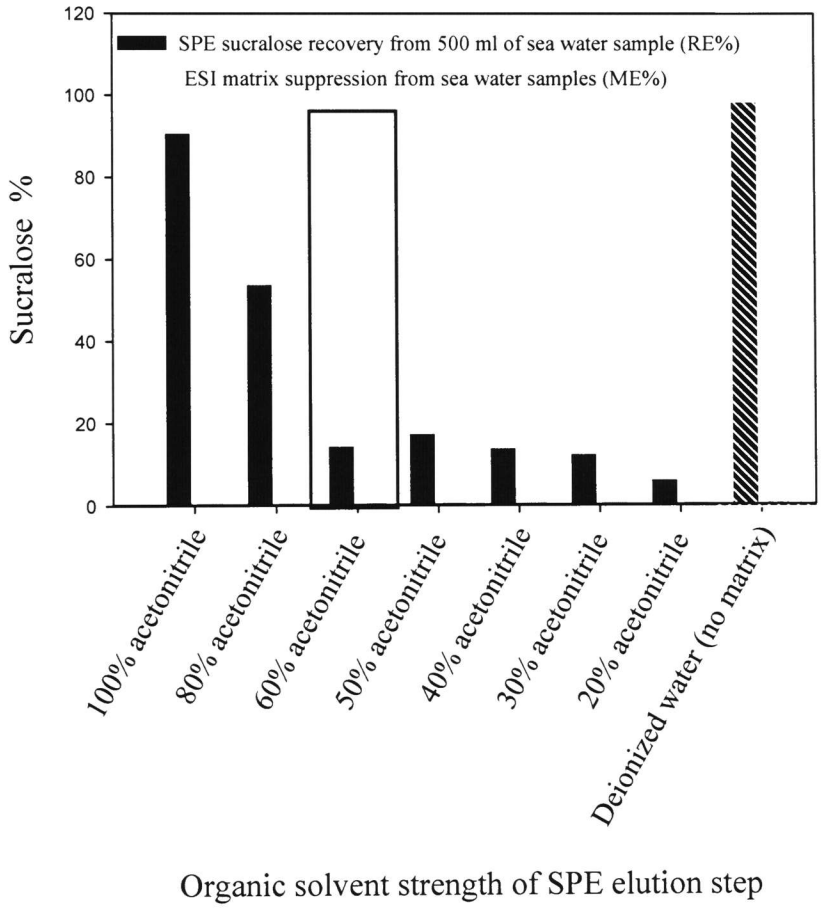

Figure 3.11. Comparison of sucralose SPE recovery (RE %) with sucralose suppression effects (ME %). 500 ml sample, 500 ng spike, but different elution solvent

The figure 3.11 summarize the experimental results for part A and shows how matrix suppression effects (ME%) diminish (thus signal intensity rises) as the organic strength of the elution step decreases (set 2 – grey). The bar chart also depicts how the recovery of sucralose from the SPE process, decreases as the organic strength of the elution step decreases (set 1 – black). The quality of the extraction and ionization process can be assessed by comparing a given treatment to the ideal matrix free deionized water sample.

The results indicate that matrix suppression is dramatically reduced at an organic solvent strength of < 60% acetonitrile. However, it is evident in the plot that the reduced suppression is achieved at the expense of a significant decrease in sucralose recovery from the SPE extraction process. Accordingly, as matrix suppression is significantly reduced, process efficiency for the extraction of sucralose is also reduced. This finding demonstrates that the matrix suppression of sucralose is caused by endogenous matrix components that could not be resolved and eliminated by means of SPE reverse phase chromatography. It is evident that a different approach must be considered to minimize the ionization suppression effect of sucralose.

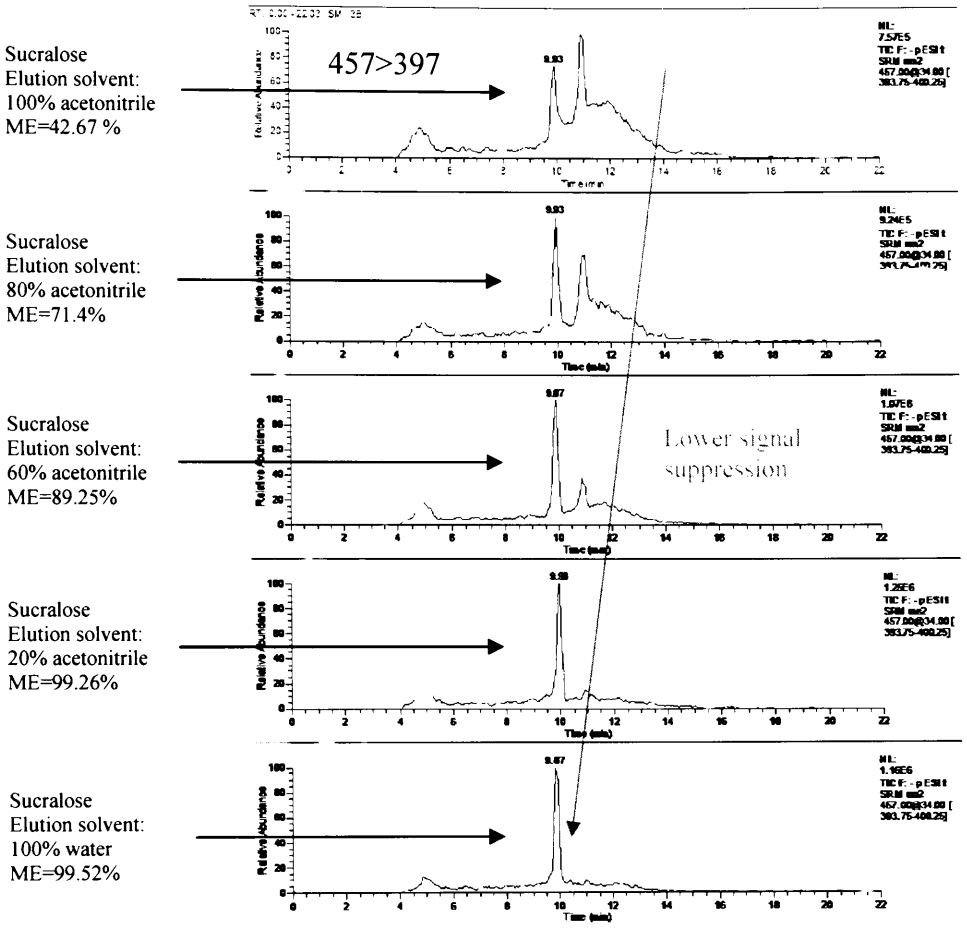

Figure 3.12. Sucralose chromatograms from the (ME%) experiment (set 2 – grey bars in figure 3.11) showing the reduction of ionization suppression with lower organic solvent strength of the SPE elution step.

Figure 3.13 below presents the experimental results for part B and shows how sucralose response and resolution are optimized from the endogenous matrix components by varying the HPLC chromatographic parameters. The top three chromatograms are elution profiles of sucralose, acquired with the shorter 150 mm Luna C18(2) column and three flow rates: 400 ul/min, 600 ul/min and 800 ul/min. The bottom chromatogram was acquired with the longer 250 mm Luna™ column at a flow rate of 600 ul/min.

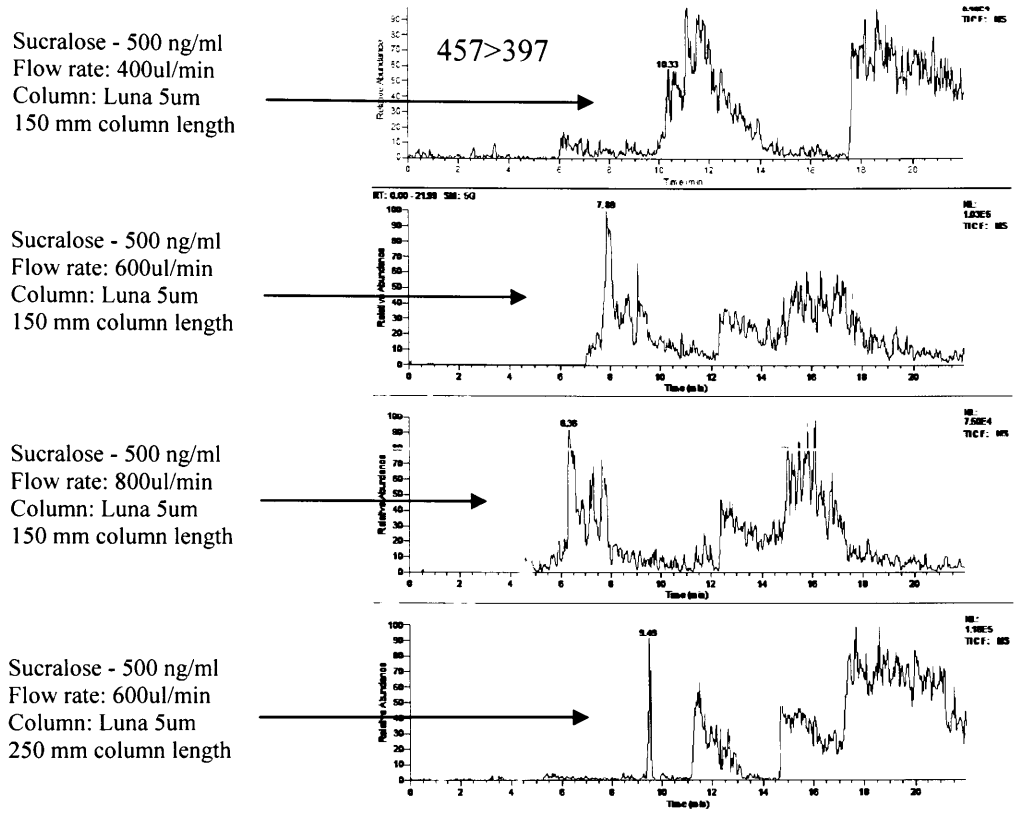

Figure 3.13. Chromatograms showing sucralose response from a typical sea water sample extract with varying flow rate and HPLC column length.

As flow rate is increased, the matrix suppression of sucralose is reduced. The lower chromatogram shows the effect of greater efficiency provided by a longer chromatography column – length increased from 150 to 250 cm. At these conditions, sucralose is entirely resolved from the dominant endogenous matrix components and ionization suppression is significantly reduced. This result indicates that the ionization suppression was caused by polar matrix component(s) that like sucralose are lowly retained in the selected C-18 based media. Trace determination of sucralose was afforded by maximizing column efficiency for the particular 5 micron particle size technology.

3.4.3 Determination of Sucralose Detection and Quantification Limits

3.4.3.1 HPLC/MSMS

The figure 3.14 shows two variations of least squares regression, unweighted (top) and weighted (bottom). The prediction intervals were also generated for each case, and illustrate the non-constant variance, and how the condition is accounted for in the weighted variant of least squares regression.

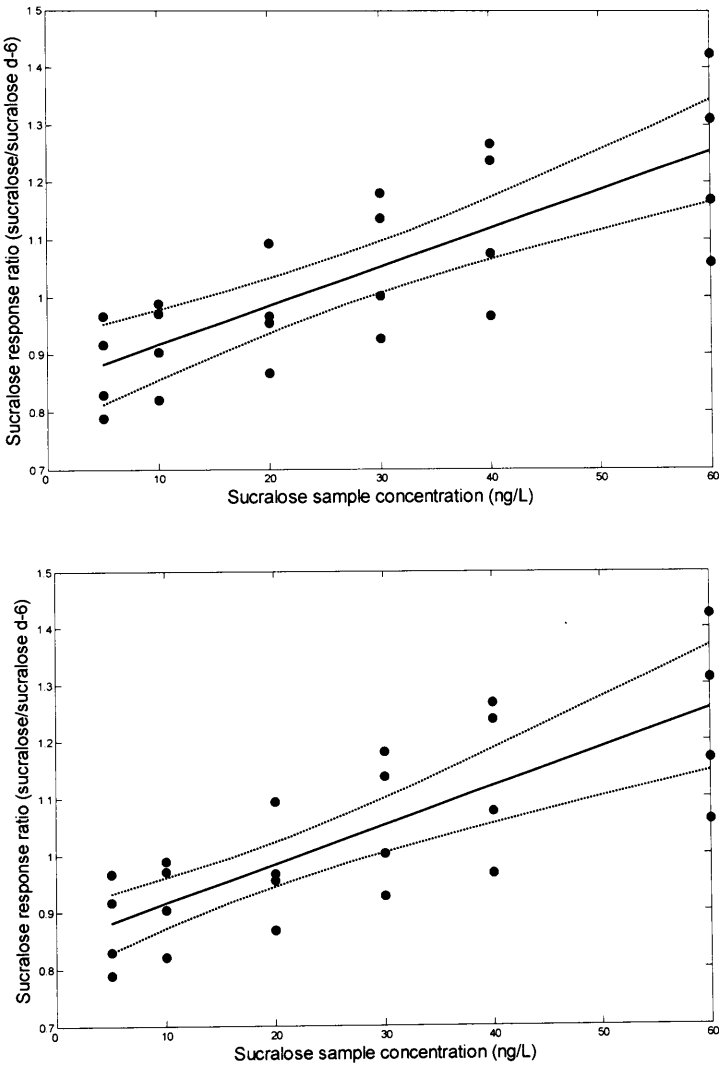

Figure 3.14. Variance structure, least squares regression with prediction intervals of HPLC/MSMS data. Unweighted least squares regression (top). Weighted least squares regression (bottom).

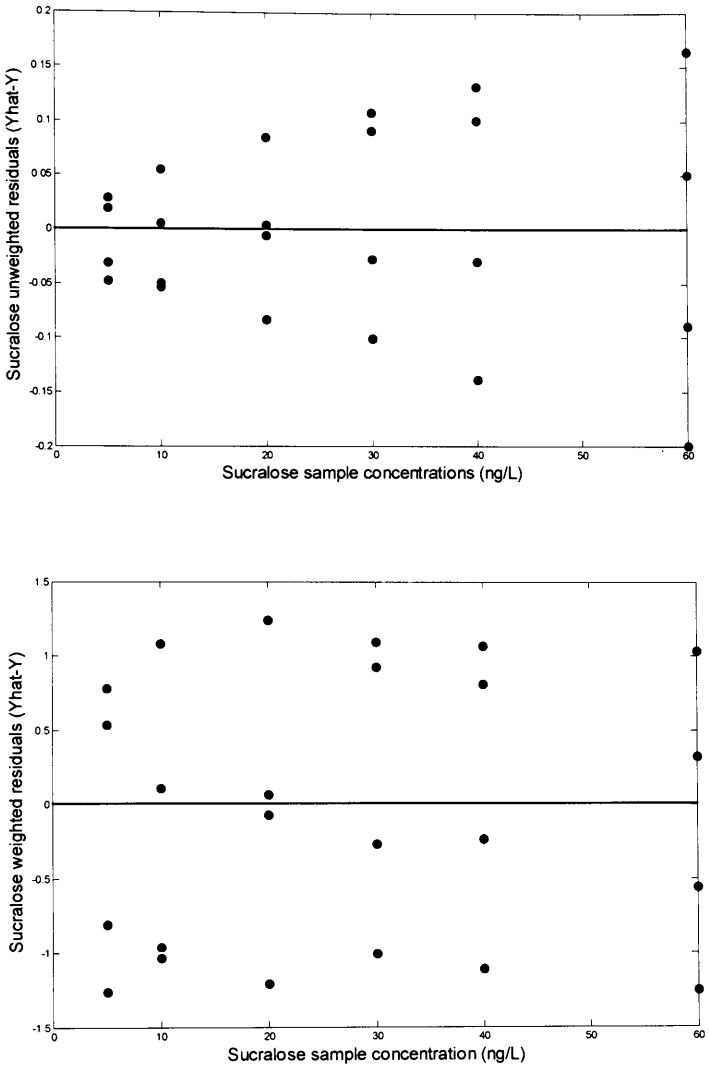

Figure 3.15. Residual plots for sucralose HPLC/MSMS data. Unweighted case (top), weighted case (bottom).

In the case of chemical data, the weighted correction of the regression procedure validates one of two primary assumptions necessary for least squares regression, which is constant variance. Figure 3.15 shows the residual plots of sucralose for the two variants of regression and proves how the condition of constant variance is met for the case of weighted least squares regression.

The following table shows the response ratios and weighted least squares estimates that were generated from the HPLC/MSMS calibration design.

Variance analysis of sucralose calibration design - labeled sucralose d-6 at (10 ng L^{-1})

Replicate Number	Area ratio (5 ng L^{-1})	Area ratio (10 ng L^{-1})	Area ratio (20 ng L^{-1})	Area ratio (30 ng L^{-1})	Area ratio (40 ng L^{-1})	Area ratio (60 ng L^{-1})
1	0.865	0.825	0.956	1.121	1.207	1.424
2	0.806	0.880	0.947	1.138	1.239	1.171
3	0.856	0.930	1.037	1.002	0.967	1.060
4	0.789	0.822	0.869	0.928	1.077	1.311
Statistics						
$SS_{pure\ error}$	0.0042	0.0079	0.0141	0.0297	0.0468	0.0762
$MS_{pure\ error}$ (s^2)	0.0014	0.0026	0.0047	0.0099	0.0156	0.0254
$(\hat{w}_i = 1/s^2)$	714.0413	378.9217	212.3098	100.8488	64.0836	39.3874

Table 3.7. Response ratios and weighted least squares regression estimates for HPLC/MSMS calibration design.

The following figure 3.16 is a plot constructed from the weight values of the above table 3.7 vs. their respective sample concentrations. Note the heteroscedastic condition (non constant variance). As evident in figure 3.16, a two component exponential model provided a good fit to model the non-constant variance and was used to extrapolate the weights w_o and w_{LD} $(\hat{w}_i = 1/s^2)$. The equation parameters for the model are provided in table 3.8.

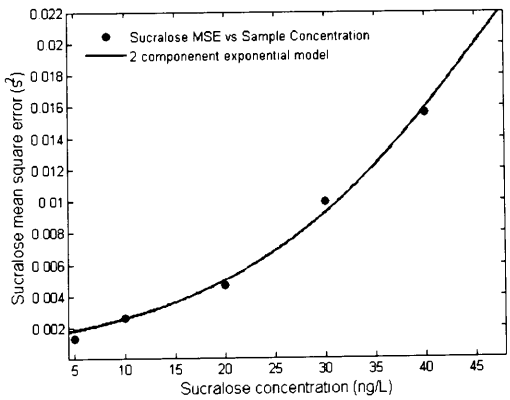

Figure 3.16. Variability model for the HPLC/MSMS sucralose real sample calibration data.

The figure 3.17 below is a chromatogram of sucralose (top) and the surrogate internal standard d-6 sucralose (bottom), from the lowest concentration of the calibration design. This concentration is approximately 2.5 times the instrumental noise value and was defined as the lowest detectable concentration (X=0). Furthermore, it is important to re-iterate that this response of sucralose has been processed by the complete method from a spiked 500 ml water sample. However, even though detection is evident at this concentration, it cannot be relied upon to confirm detection.

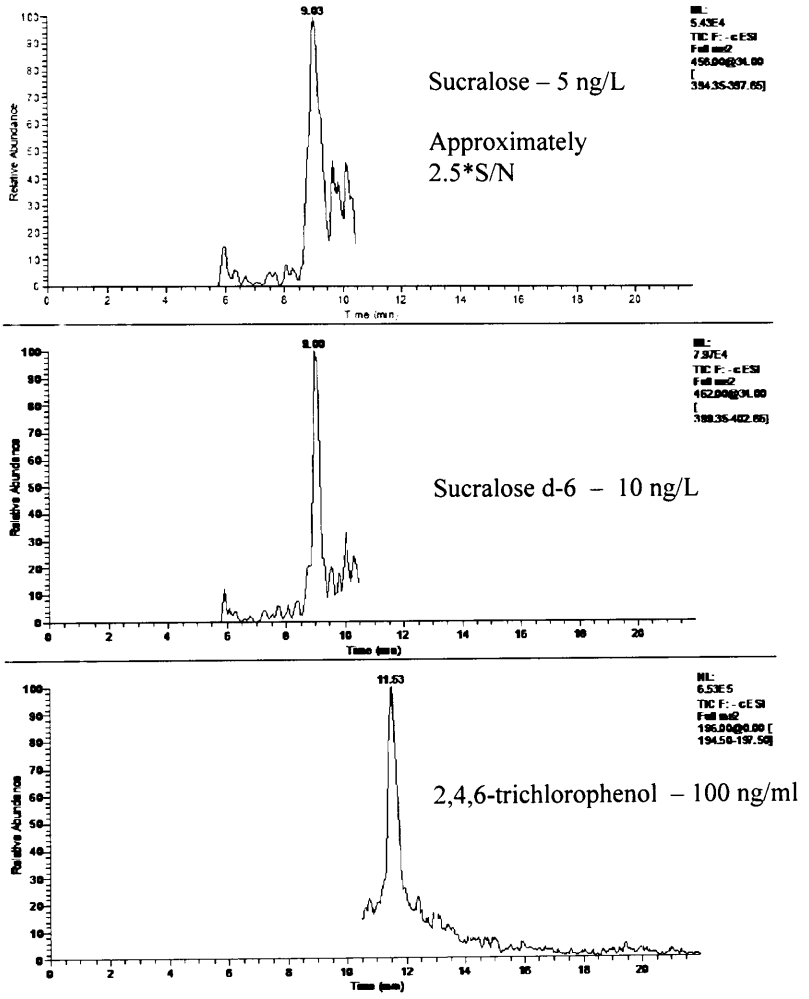

Figure 3.17. Low level sample chromatogram. Sucralose at 5 ng/L, sucralose d-6 at 50 ng/L and 2,4,6-trichlorophenol at 100 ng/ml - MS^2 transitions.

The weight (w_o) corresponds to the response variability at the lowest detectable concentration (X=0) and was estimated from the exponential variance model above. This weight value of 1.565e+3, along with the weighted regression estimates from table 3.8, were applied to calculate the critical level in response units R_c (equation 15 of appendix 2). The critical level Lc was then easily calculated from R_c by equation 16 of appendix 2. The value was determined as 11.831 ng/L (table 3.8).

The weight at the detection level (w_d) was estimated from the variance model and along with the weighted regression estimates, applied to equation 17 of appendix 2. The detection limit Ld is presented in table 3.8 and calculated as 35.176 ng/L.

Variability models for complete method detection limits

Weighted sum of squares estimates					Assay limits by criteria	
Intercept β_0	Slope β_1	Residual Standard Deviation s_W	$\hat{w}_0$ critical	$\hat{w}_d$ detection	L_C critical level[a] (ng/L)	L_d detection limit[b] (ng/L)
0.7887	0.0081	0.9129	1.565e+03	6.311e+03	11.831	35.176

[a] $\alpha = 0.01$, one sided test statistic. [b] $\alpha = \beta = 0.01$, one sided test statistic.

Table 3.8. Variability model parameters and detection limits of sucralose for the HPLC/MSMS method

3.4.3.2 GC/MS

The same sequence of equations, and procedure was applied to calculate the detection limits of sucralose for the GC/MS methodology. The following table 3.9 & 3.10 summarize the weighted least squares parameters and detection limits.

Variance analysis of sucralose calibration - labeled sucralose d-6 as internal standard (100 ng L^{-1})

Replicate Number	Area ratio (1.6 ng L^{-1})	Area ratio (2.4 ng L^{-1})	Area ratio (5 ng L^{-1})	Area ratio (12 ng L^{-1})	Area ratio (24 ng L^{-1})
1	0.1216	0.1120	0.1404	0.2406	0.4927
2	0.1206	0.1177	0.1349	0.2331	0.4738
3	0.1161	0.1145	0.1305	0.2354	0.4823
4	0.1158	0.1147	0.1348	0.2338	0.4908
5	0.1164	0.1134	0.1349	0.2343	0.4907
6	0.1158	0.1111	0.1379	0.2440	0.4971
7	0.1211	0.1118	0.1381	0.2426	0.4954
Sum of squares statistics					
$SS_{pure\ error}$	0.00005	0.00003	0.00006	0.00012	0.00040
$MS_{pure\ error}$ (s^2)	7.517E-06	5.228E-06	1.022E-05	2.078E-05	6.748E-05
Weights $\left(\hat{w}_i = 1/s^2\right)$	133022.366	191278.302	97859.841	48121.838	14817.326

Table 3.9. Response ratios and weighted least squares regression estimates for GC/MS calibration design

Variability models for complete method detection limits

Weighted sum of squares estimates					Assay limits by criteria	
Intercept β_0	Slope β_1	Residual Standard Deviation s_W	$\hat{w}_0$ critical	$\hat{w}_d$ detection	x_C critical level[a] (ng/L)	x_d detection limit[b] (ng/L)
0.1021	0.0053	2.0953	1.990e+05	1.311e+005	2.246	5.0137

[a] $\alpha = 0.01$, one sided test statistic. [b] $\alpha = \beta = 0.01$, one sided test statistic.

Table 3.10. Variability model parameters and detection limits of sucralose for the GC/MS method

The following chromatogram represents the lowest concentration of the calibration design for the GC/MS method – 1.6 ng/L (Figure 3.18), which is approximately 10 times the noise level. Three times the noise level is approximately 0.48 ng/L.

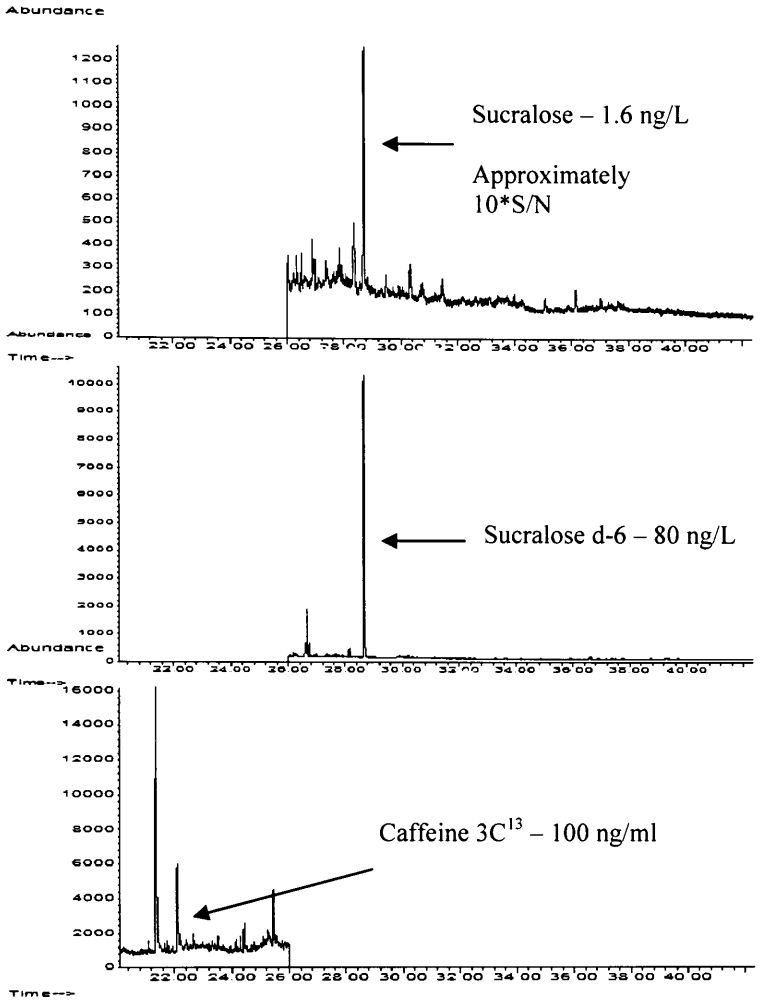

Figure 3.18. Low level sample chromatogram. Sucralose at 1.6 ng/L, sucralose d-6 at 80 ng/L and caffeine $3C^{13}$ at 100 ng/ml

The following tables 3.11 summarize the various derivations of detection limits for sucralose,

	S/N of 3 from an extracted sample (ng/L)	S/N of 10 from an extracted sample (ng/L)	Critical value L_C (ng/L)	Detection limit L_D (ng/L)
HPLC/MSMS	5	16.6	11.8	35.2
GC/MS	0.48	1.6	2.24	5.01

Table 3.11. Summary of various detection limit derivations for our HPLC/MS-MS sucralose method

3.4.4 Occurrence of Sucralose from Coastal Waters of the Florida Keys

The following section summarizes a literature survey of the occurrence of sucralose from the U.K. (Loos, et.al. 2009), Norwegian waters (Die, et.al. 2007) and U.S. waters (Mead, et. al. 2009), and compares them with our results for the environmental occurrence for sucralose in surface water samples of the Florida Keys. Each section will elaborate and discuss the corresponding occurrence data in terms of descriptive statistics and summarized here as box plots (figures 3.19. & 3.23)

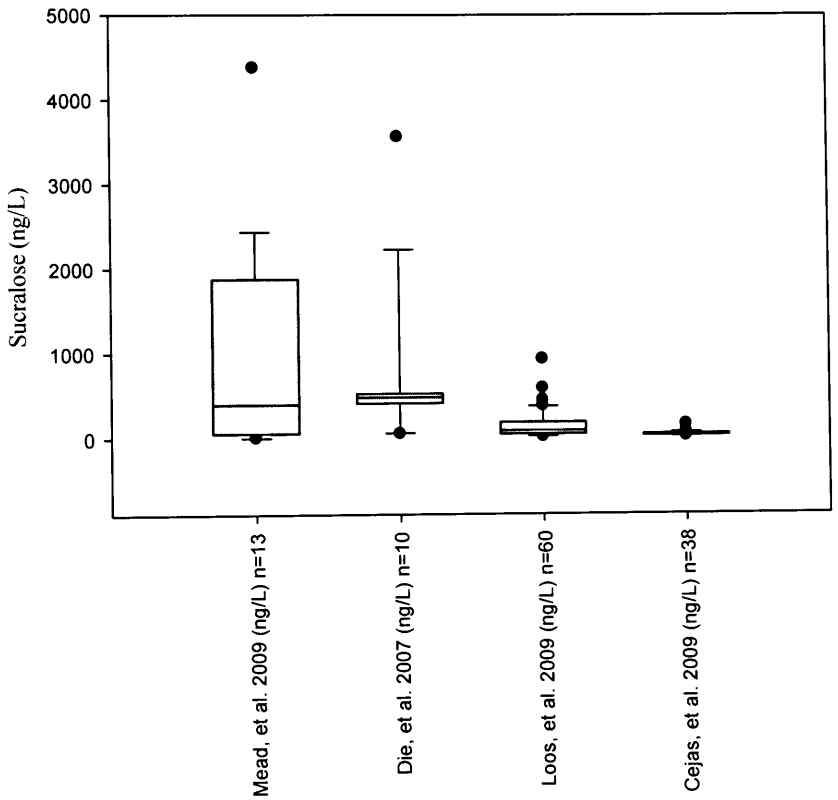

Figure 3.19. Literature survey of sucralose occurrence from surface water samples.

As previously discussed two analytical approaches, HPLC/MS-MS and GC/MS based, were successfully developed and validated for the trace analysis of sucralose from sea water samples. The following chromatograms depict typical results from both analytical approaches.

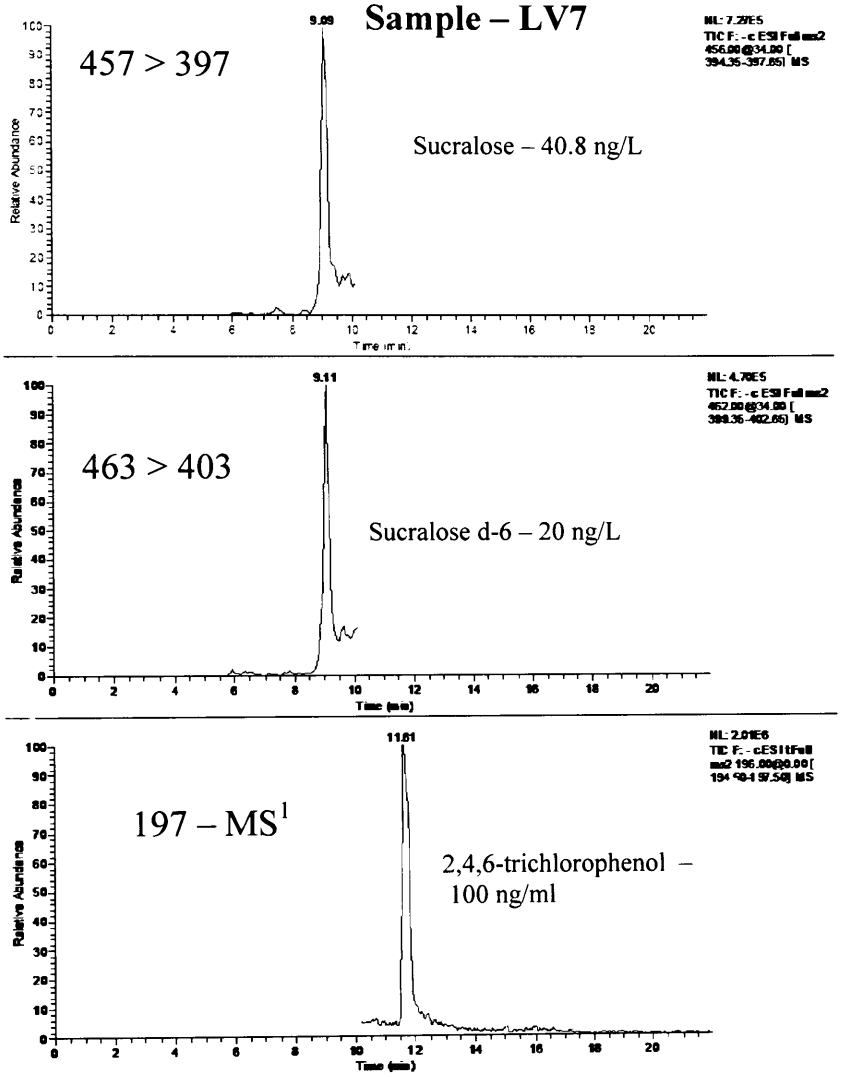

Figure 3.20. Sample chromatogram of sucralose analyzed with HPLC/MSMS – MS^2 transitions. April 2008 Little Venice (LV7) sample.

The figure 3.20 above shows a chromatogram of sucralose occurrence from a sea water sample (LV7) that was acquired with an MS^2 scan transition (figure 3.5). The top

chromatogram illustrates sucralose at a concentration of 40.7 ng/L; a level that is near the 70th percentile - 40.2 ng/L - from our sucralose dataset. The next chromatogram (figure 3.21) depicts the analysis of sucralose from the same surface water samples as in figure 3.20, but acquired with the greater selective power of MS^3 under consecutive reaction monitoring mode (CRM) scan transitions (figure 3.6). The CRM mode exploits the selective power of the quadrapole ion trap and further confirms the presence of sucralose in the surface water samples.

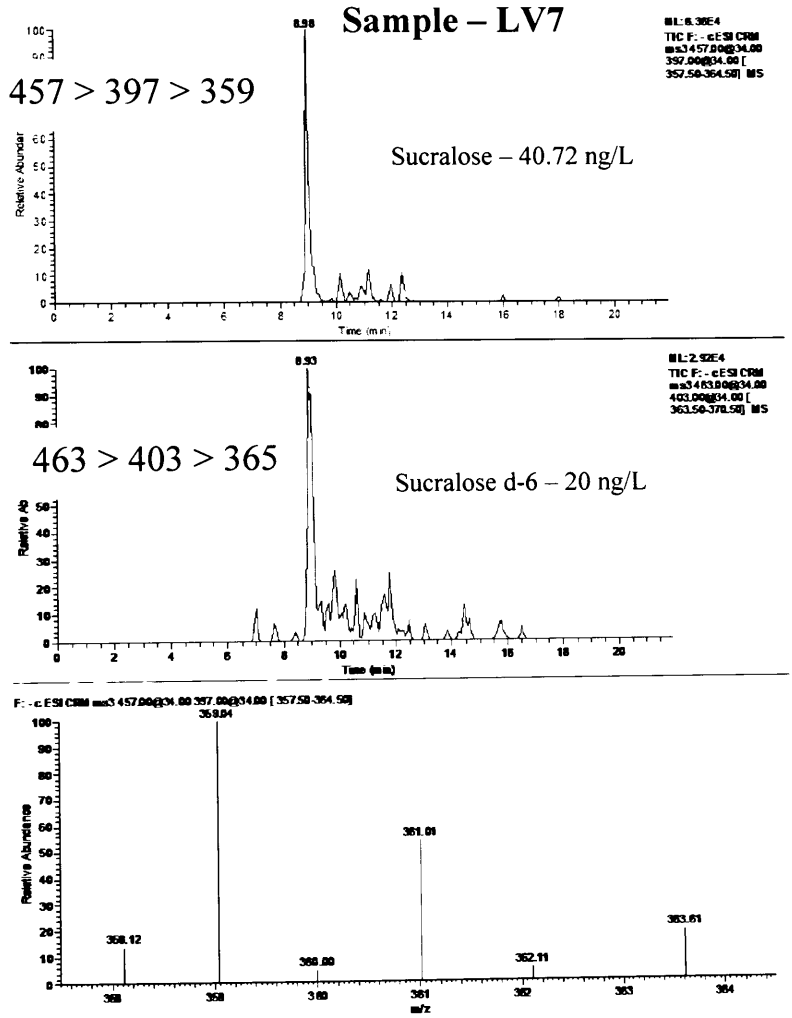

Figure 3.21. Sample chromatogram of sucralose analyzed with HPLC/MSMS – MS^3 transitions. April 2008 Little Venice (LV7).

Figure 3.22 below shows a chromatogram of sucralose occurrence from a sea water sample (LV2) acquired by GC/MS in selected ion monitoring mode (SIM) (section 3.3.6.6). The chromatogram illustrates sucralose at a concentration of 21.1 ng/L in; a level that is near the 20th percentile – 20.73 ng/L - from our environmental dataset.

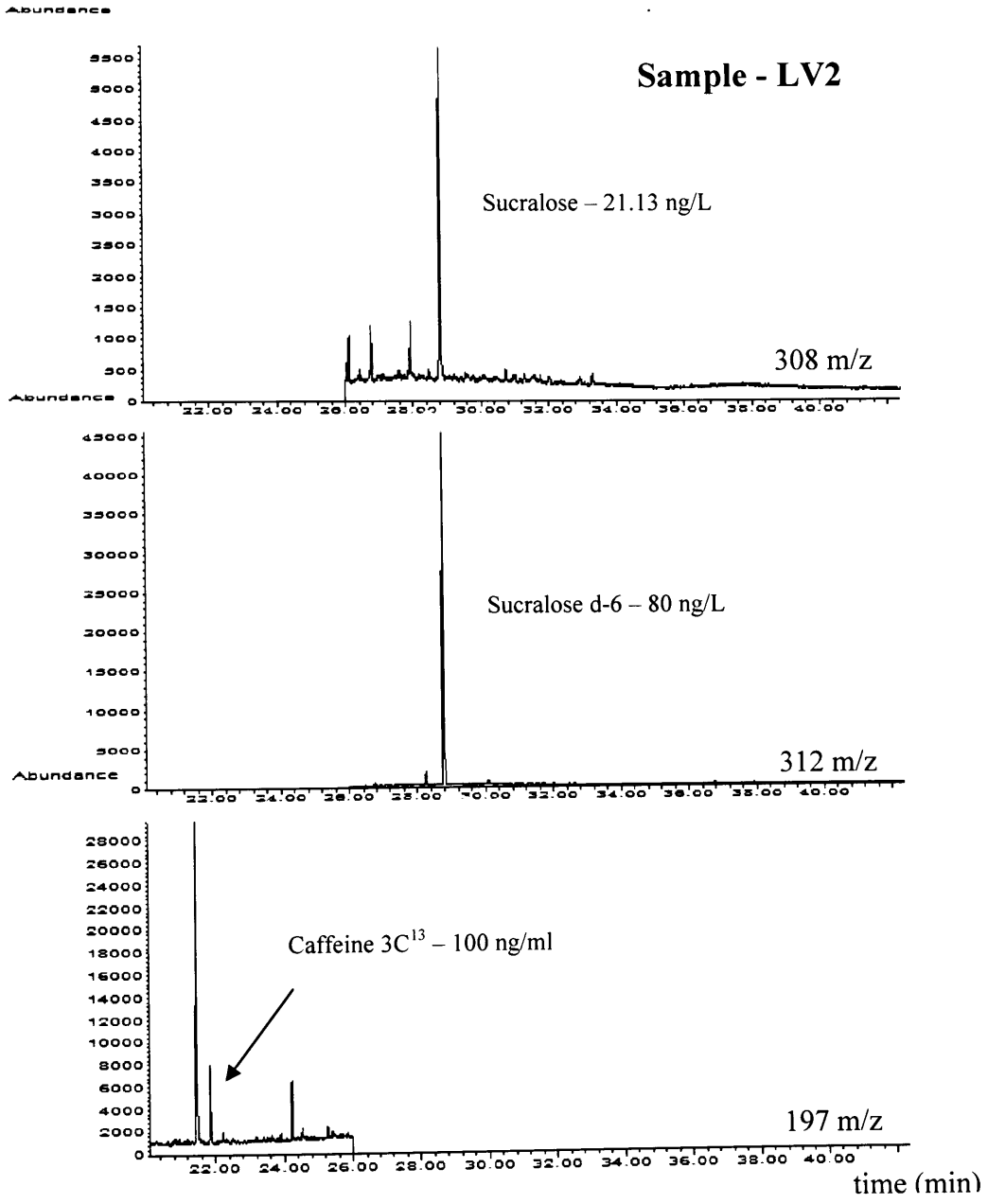

Figure 3.22. Sample chromatogram of sucralose analyzed with GC/MS – SIM mode. September 2008 Little Venice (LV2) sample.

Figure 3.23 & tables 3.13 & 3.14 show the results for the occurrence of sucralose in surface water samples collected in nearshore communities from the Florida Keys.

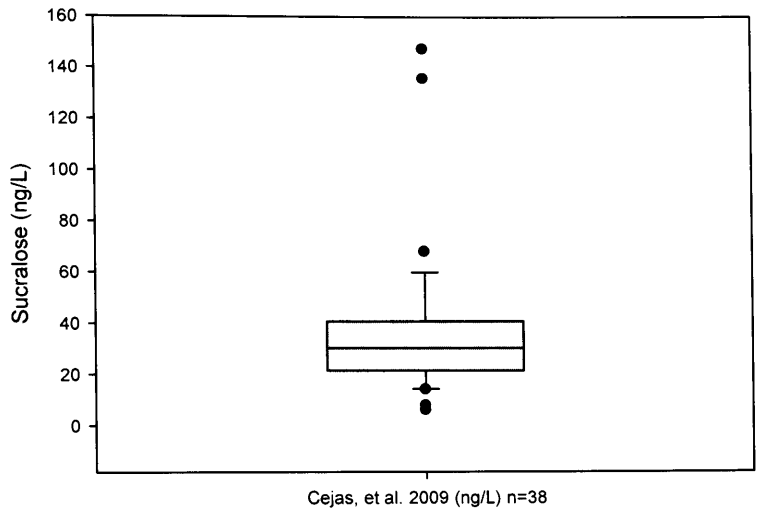

Figure 3.23. Distribution of sucralose data, percentiles distribution depicted as a box plot.

The figure presents a box plot of our sucralose data. Box plot graphs data as a box with representative statistical values. The lower boundary of the box represents the 25th percentile, a line within the box marks the median, and the top boundary of the box indicates the 75th percentile. Whiskers (error bars) above and below the box represent the 90th and 10th percentiles and the dots are outliers. The corresponding outliers and percentiles of our data are: minimum value = 6.02 ng/L; 10^{th} percentile = 14.49 ng/L; 25^{th} = 21.56 ng/L; 50^{th} = 30.28 ng/L; 75^{th} = 40.67 ng/L; 90^{th} = 58.69 ng/L; maximum value = 147.2 ng/L. Respectively, the tables show the data corresponding to three sampling trips to the Little Venice (LV) stations in Marathon Key – January, 2008; April, 2008; September, 2008 and one sampling trip to Lake Largo (LL) in Key Largo – September, 2008.

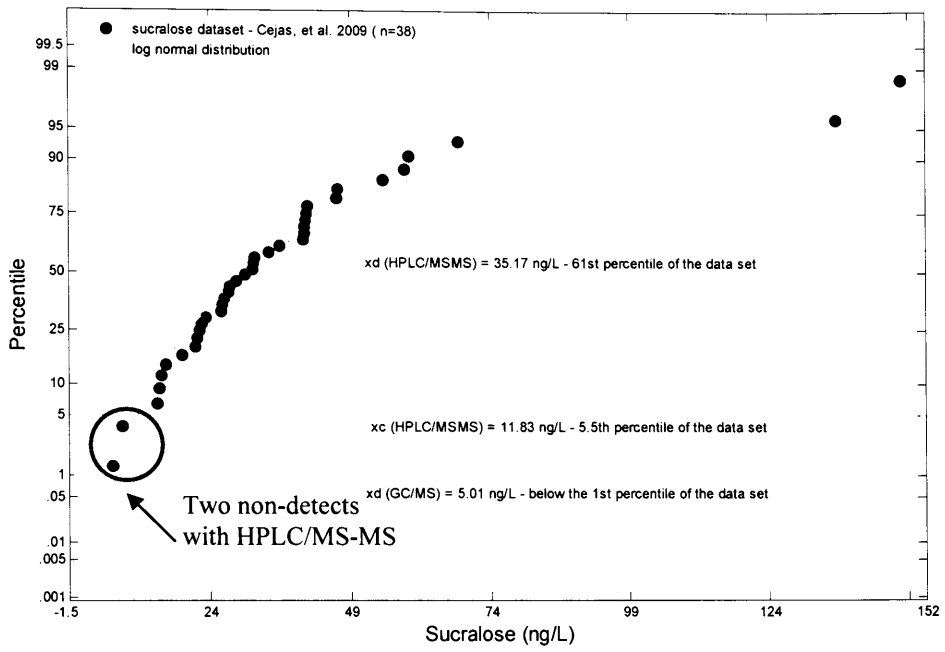

Figure 3.24. Probability distribution of the sucralose data set, presenting the percentiles corresponding to the detection limit X_d for the GC/MS method, the critical level x_c and the detection limit X_d for the HPLC/MSMS method.

The figure 3.24 above is a probability distribution of the Florida Keys sucralose data set. In this particular representation of the data, emphasis is placed on the percentile values of the calculated detection limits for both the GC/MS & HPLC/MSMS methods. The percentile distribution of the data set indicates that 100 % of the sample population is above the sucralose detection limit for the GC/MS approach. Furthermore 94.5 % of the sample population is above the decision limit – i.e., the critical level – for the HPLC/MSMS method, while only 39 % of the population is above the detection limit for the HPLC/MSMS method. This percentile distribution shows that the both methods are suitable for the trace analysis of sucralose in the Florida Keys nearshore environment. However, this claim is true, if applying the decision limit threshold Lc for the HPLC/MSMS approach.

Station	Date Collected	Latitude	Longitude	Volume Extracted (L)	Salinity	Sucralose Concentration (ng/L)
LV 1 - 1	1/14/2008	24 38.51 N	81 01.84 W	0.7	36.82	20.69
LV 2	1/14/2008	24 25.99 N	81 36.92 W	0.7	36.74	21.56
LV 3	1/14/2008	24 42.68 N	81 02.77 W	0.7	37.05	26.67
LV 4	1/14/2008	24 27.76 N	81 36.88 W	0.7	36.78	31.39
LV 5	1/14/2008	24 32.59 N	81 36.70 W	0.7	36.64	26.94
LV 6	1/14/2008	24 22.48 N	81 43.89 W	0.7	36.45	25.50
LV 7	1/14/2008	24 31.03 N	81 43.84 W	0.7	36.9	21.96
LV 8	1/14/2008	24 15.82 N	81 58.58 W	0.7	36.11	28.06
LV 9	1/14/2008	24 21.27 N	81 58.71 W	0.7	36.43	29.66
LV 10	1/14/2008	24 06.01 N	81 58.39 W	0.7	36.48	7.83
LV 1 - 2	4/15/2008	24 38.51 N	81 01.84 W	0.9	37.83	14.79
LV 2	4/15/2008	24 25.99 N	81 36.92 W	0.9	37.2	40.33
LV 3	4/15/2008	24 42.68 N	81 02.77 W	0.9	37.79	15.52
LV 4	4/15/2008	24 27.76 N	81 36.88 W	0.9	37.62	40.07
LV 5	4/15/2008	24 32.59 N	81 36.70 W	0.9	37.59	54.26
LV 6	4/15/2008	24 22.48 N	81 43.89 W	0.9	37.43	25.31
LV 7	4/15/2008	24 31.03 N	81 43.84 W	0.9	37.05	40.72
LV 8	4/15/2008	24 15.82 N	81 58.58 W	0.9	37.48	46.06
LV 9	4/15/2008	24 21.27 N	81 58.71 W	0.9	37.49	58.17
LV 10	4/15/2008	24 06.01 N	81 58.39 W	0.9	37.82	6.02

Table 3.12. Sucralose occurrence data from the Little Venice stations (LV) – January; April, 2008.

Station	Date Collected	Latitude	Longitude	Volume Extracted (L)	Salinity	Sucralose Concentration (ng/L)
LV 1 - 3	9/3/2008	24 38.51 N	81 01.84 W	0.7	35.71	40.16
LV 2	9/3/2008	24 25.99 N	81 36.92 W	0.7	35.83	21.13
LV 3	9/3/2008	24 42.68 N	81 02.77 W	0.7	35.98	40.67
LV 4	9/3/2008	24 27.76 N	81 36.88 W	0.7	35.96	35.77
LV 5	9/3/2008	24 32.59 N	81 36.70 W	0.7	35.63	147.20
LV 6	9/3/2008	24 22.48 N	81 43.89 W	0.7	35.91	30.90
LV 7	9/3/2008	24 31.03 N	81 43.84 W	0.7	35.54	46.27
LV 8	9/3/2008	24 15.82 N	81 58.58 W	0.7	35.54	67.77
LV 9	9/3/2008	24 21.27 N	81 58.71 W	0.7	35.88	58.91
LV 10	9/3/2008	24 06.01 N	81 58.39 W	0.7	35.92	14.36
LL 1		25 15.42 N	80 01.15 W	0.9		33.77
LL 2		25 15.78 N	80 07.51 W	0.9		40.23
LL 3		25 09.91 N	80 07.86 W	0.9		31.17
LL 4		25 15.42 N	80 14.83 W	0.9		22.73
LL 5		25 11.21 N	80 14.70 W	0.9		14.00
LL 6		25 12.97 N	80 22.36 W	0.9		25.92
LL 7		25 10.00 N	80 22.42 W	0.9		18.39
LL 8		25 14.31 N	80 27.65 W	0.9		135.56

Table 3.13. Sucralose occurrence data from the Little Venice (LV) and Lake Largo (LL) stations - September, 2008.

3.4.4.1. Sucralose: a molecular tracer of the sewage vector in the Florida Keys marine setting.

It was stated in chapter 1 that molecular sewage tracers should have the following physicochemical characteristics: 1) specificity – solely related to the sewage vector; 2) (2) be persistent and present at high (detectable) concentrations in contaminated environmental samples; 3) Do not undergo extreme rates of degradation in wastewater/water, if so degradation rates should be known. (4) Chemical tracers should have high water solubility, low K_{OW} and low volatility. Sucralose is certainly specific, only related to anthropogenic excrement sources. As evident in chapter 1, sucralose is remarkably persistent, resistant to metabolic transformation and soluble in water. Furthermore, results from our study indicate that sucralose is present in the Florida Keys nearshore environment at greater median concentrations than previously measured for other microconstituents in the Florida Keys (figure 3.25). (Singh, et al.)

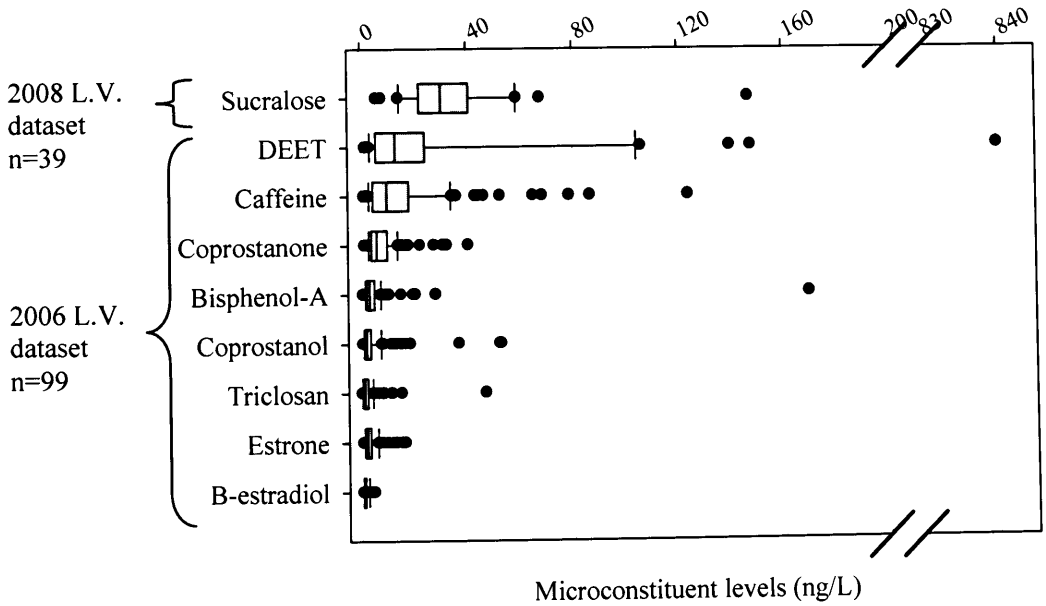

Figure 3.25. Occurrence of microconstituents in Little Venice, Marathon. Source: 2006 dataset, Singh, et al. accepted for ecotoxicology; 2008 dataset, current study.

The following box plots were designed to illustrate the observed dilution gradient of sucralose based on the distribution of the expected wastewater sources along the Florida Keys coastline (Figure 3.26), as well as the temporal changes of sucralose levels from different sampling trips to Little Venice throughout 2008 (Figure 3.27).

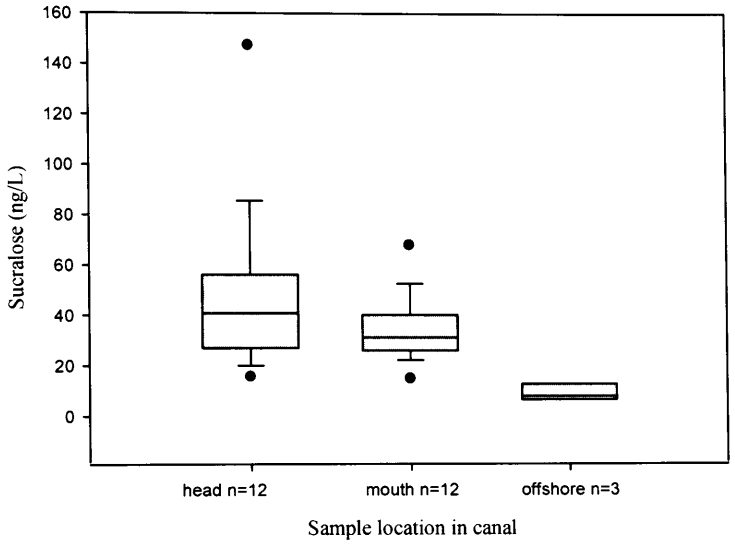

Figure 3.26. Box plots of sucralose occurrence from Little Venice stations – comparing head, mouth and offshore stations.

Figure 3.26 shows how sucralose levels generally decrease as the location of the sampling stations move further offshore. This pattern reflects a classic diffusion/dispersion transport process where a net diffusive flux of sucralose is observed from stations closest to the distributed wastewater point source along the coastline to the offshore sampling site.

The next box plot Figure 3.27 shows sucralose occurrence ordered by the three different sampling trips to Little Venice, which were designed to coincide with the peak dry season – January (winter/dry season); April (intermediate rainfall season);

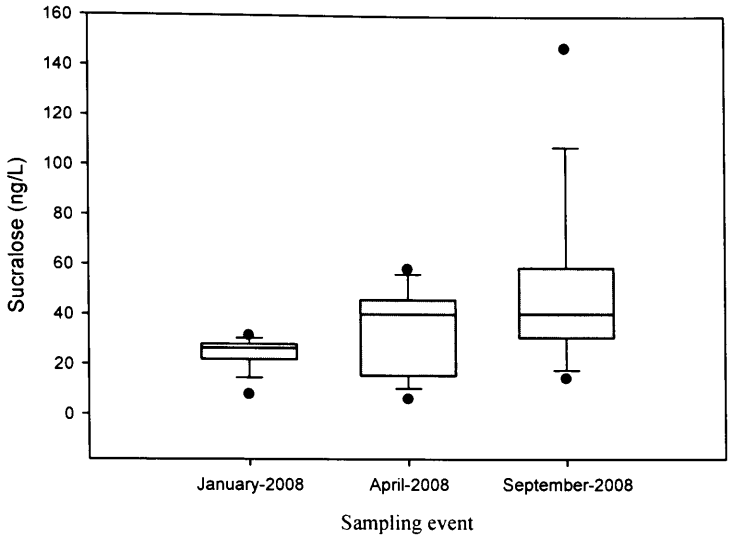

Figure 3.27. Box plots of sucralose occurrence from Little Venice stations – comparing results from three sampling trips.

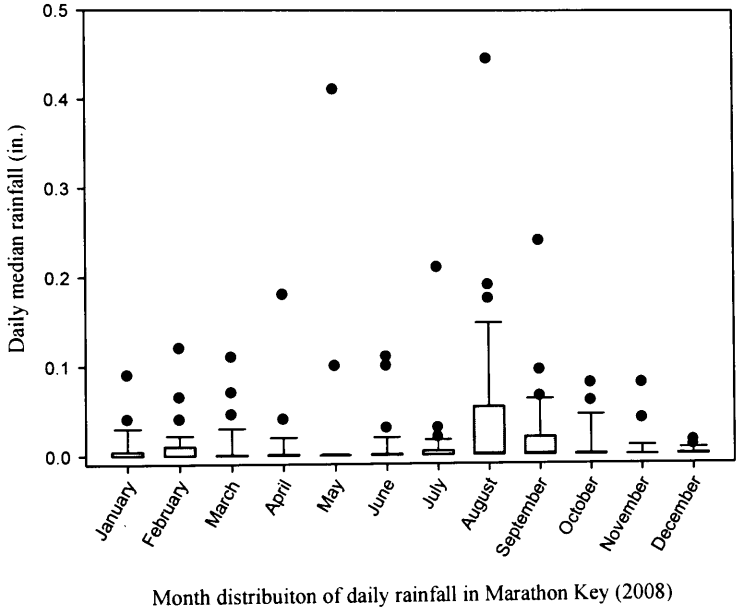

Figure 3.28. Box plots of daily median rainfall at Marathon Key throughout the sampling period - 2008

and the peak wet season September (wet season). Figure 3.27 & 3.28 indicates an observed trend of sucralose occurrence from the three sampling trips, where the highest

level is concurrent with the wet season, the mid sucralose levels coincides with the tourist season and the lowest levels are in accord with the dry season. Even though this study is simply a screening of sucralose occurrence with greater emphasis placed in analytical method development, the structure of the data raises some interesting and revealing questions about rainfall as a driver of wastewater intrusion into the Florida Keys watershed.

The figure 3.29 below illustrates the net diffusive flux of sucralose from the Lake Largo sampling site that is located in Key Largo. The high sucralose level of 135.56 ng/L represents the second highest concentration of our data set and signals a significant source of wastewater intrusion that should be further monitored to minimize the risk of health and ecosystem level risks in nearshore Florida Keys marine waters.

Figure 3.29. Satellite image of Lake Largo illustrating the diffusion/dispersion transport process from a distributed point source.

3.5 Conclusion

Two isotope dilution analytical methods were successfully developed and validated for the trace determination of sucralose from sea water samples. One method applies high pressure liquid chromatography coupled to an electrospray ionization quadrapole ion trap mass spectrometry system, while the other employs gas chromatography coupled to a single quadrapole mass spectrometry system in conjunction with selected ion monitoring scan mode. Both analytical methods were validated with statistically supported detection limits based on a calibration design from samples extracted with the complete analytical method. Furthermore, the methods were validated by their successful application to the determination of sucralose from key locations in the coastal marine environment of the Florida Keys – Lake Largo; a community adjacent to Key Largo Harbor and Little Venice – a high population residential zone in Marathon Key. Due to knowledge limitations of sucralose levels in U.S. waters, the more sensitive GC/MS-derivitized sucralose approach was chosen for the analysis of the complete set of environmental samples.

Detection limits for the two methodologies were as follows: for the HPLC/MSMS analysis, the critical level-decision limit Lc is 11.82 ng/L while the detection limit Ld is 35.17 ng/L. From a sea water sample 3 x S/N was calculated as 5 ng/L, while 10 x S/N was 16.6 ng/L. Detection limits for the GC/MS method were the following. The critical level-decision limit Lc was 2.24 ng/L while the detection limit Ld was 5.01 ng/L. Furthermore, from a sea water sample 3 x S/N was 0.48 ng/L and 10 x S/N was 1.6 ng/L. The corresponding outliers and percentiles of the Florida Keys sample set are: Sample size was n=38; minimum value = 6.02 ng/L; 10^{th} percentile = 14.49 ng/L; 25^{th} = 21.56

ng/L; 50^{th} (median) = 30.28 ng/L; 75^{th} = 40.67 ng/L; 90^{th} = 58.69 ng/L; maximum value = 147.2 ng/L. The percentile distribution of the data set indicates that 100 % of the sample population is above the sucralose detection limit for GC/MS. Furthermore 94.5 % of the sample population (36 samples – 2 non-detects) was above the decision limit – i.e. the critical level – for the HPLC/MSMS method, while only 39 % of the population is above the detection limit for the HPLC/MSMS method. Considering the decision limit Lc as the criteria for detection, both analytical approaches are suitable for monitoring sucralose occurrence in the nearshore marine environs of the Florida Keys.

Matrix suppression effect proved to be significant for the analysis of sucralose from sea water. Suppression effects were evaluated and minimized to a significant degree by optimizing the sucralose retention in the HPLC column, effectively resolving the endogenous matrix components from sucralose.

The primary hypothesis of this research was, due to the following unique physical attributes: specific to an anthropogenic source, resistance to degradation and high water solubility, sucralose is a powerful sewage tracer in the nearshore marine waters of the Florida Keys. This research has answered some important questions in regards to its environmental concentrations in the middle Florida Keys, and its utility as a tracer for the sewage vector. A classic diffusion/dispersion pattern was observed for sucralose, where a net diffusive flux of sucralose occurred from stations closest to the distributed wastewater point source along the coastline to the offshore sampling site. In addition, a concentration trend of sucralose was apparent in three sampling events conducted in the wet, intermediate and dry season; where the highest median values were detected in the wet season and lowest in the dry season. Finally, the median levels of sucralose from our

dataset 30.3 ng/L, was compared to the median levels of various microconstituents recorded in 2006 from the same study site – DEET 12.9 ng/L; caffeine 9.6; coprostanone 5.83 ng/L; bisphenol-A 3.01 ng/L; coprostanol 1.9 ng/L; triclosan 1.1 ng/L; estrone 2 ng/L; B-estradiol 0.665 ng/L.

In light of the above results, it is shown that sucralose is present at high detectable concentrations (relative to previously detected microconstituents) in the nearshore Florida Keys marine environment, an occurrence pattern typical for a distributed point source was observed. A common temporal trend was noted between sucralose and two nutrients. Given the evidence, sucralose appears to be a powerful and unique tracer of the sewage vector in the nearshore waters of the Florida Keys.

BIBLIOGRAPHY

Abian, J., A. J. Oosterkamp (1999). "Comparison of conventional, narrow-bore and capillary liquid chromatography/mass spectrometry for electrospray ionization mass spectrometry: practical considerations." Journal of Mass Spectrometry 34(4): 244-254.

Aronson, R. B. and W. F. Precht (2002). Evolutionary Paleoecology of caribbean coral reefs. Evolutionary Paleoecology: The Ecological Context of Macroevolutionary Change. New York, Columbia University Press: 171-233.

Baird, I. M., N. W. Shephard (2000). "Repeated dose study of sucralose tolerance in human subjects." Food and Chemical Toxicology 38(Supplement 2): 123-129.

Box, G. E. P. and J. S. Hunter (1957). "Multi-factor Experimental Designs for Exploring Response Surfaces." The Annals of Mathematical Statistics 28(1): 195-241.

Boyd, R. K., C. Basic (2008). Trace Quantitative Analysis by Mass Spectrometry West Sussex, Wiley.

Boyer, J. N., R. D. Jones (2004). "Little Venice Water Quality Monitoring Project: Phase 1 Results. Southeast Environmental Research Center." Florida International University.

Bruno, J. F., L. E. Petes (2003). "Nutrient enrichment can increase the severity of coral diseases." Ecology Letters 6(12): 1056-1061.

Calamari, D., E. Zuccato (2003). "Strategic Survey of Therapeutic Drugs in the Rivers Po and Lambro in Northern Italy." Environmental Science & Technology 37(7): 1241-1248.

Cech, N. B. and C. G. Enke (2001). "Practical implications of some recent studies in electrospray ionization fundamentals." Mass Spectrometry Reviews 20(6): 362-387.

Cochran, P. K., C. A. Kellogg (1998). "Prophage induction of indigenous marine lysogenic bacteria by environmental pollutants." Marine Ecology Progress Series 164: 125-133.

Currie, L. A. (1968). "Limits for qualitative detection and quantitative determination. Application to radiochemistry." Analytical Chemistry 40(3): 586-593.

Danovaro, R. and C. Corinaldesi (2003). "Sunscreen Products Increase Virus Production Through Prophage Induction in Marine Bacterioplankton." Microbial Ecology 45(2): 109-118.

Depledge, M. H. and R. D. Handy (1999). "Physiological Responses: Their Measurement and Use as Environmental Biomarkers in Ecotoxicology." Ecotoxicology 8: 329-349.

Desbrow, C., E. J. Routledge (1998). "Identification of estrogenic chemicals in STW effluent. 1. Chemical fractionation and in vitro biological screening." Environmental Science & Technology 32(11): 1549-1558.

Downs, C. A., J. E. Fauth (2005). "Cellular diagnostics and coral health: Declining coral health in the Florida Keys." Marine Pollution Bulletin 51(5-7): 558-569.

Dustan, P. and J. C. Halas (1987). "CHANGES IN THE REEF-CORAL COMMUNITY OF CARYSFORT REEF, KEY-LARGO, FLORIDA - 1974 TO 1982." Coral Reefs 6(2): 91-106.

Finn, J. P. and G. H. Lord (2000). "Neurotoxicity studies on sucralose and its hydrolysis products with special reference to histopathologic and ultrastructural changes." Food and Chemical Toxicology 38: S7-S17.

Fu, I., E. J. Woolf (1998). "Effect of the sample matrix on the determination of indinavir in human urine by HPLC with turbo ion spray tandem mass spectrometric detection." Journal of Pharmaceutical and Biomedical Analysis 18(3): 347-357.

Gardinali, P. R. and X. Zhao (2002). "Trace determination of caffeine in surface water samples by liquid chromatography-atmospheric pressure chemical ionization-mass spectrometry (LC-APCI-MS)." Environment International 28(6): 521-528.

Glassmeyer, S. T., E. T. Furlong (2005). "Transport of Chemical and Microbial Compounds from Known Wastewater Discharges: Potential for Use as Indicators of Human Fecal Contamination." Environmental Science & Technology 39(14): 5157-5169.

Grice, H. C. and L. A. Goldsmith (2000). "Sucralose--an overview of the toxicity data." Food and Chemical Toxicology 38(Supplement 2): 1-6.

Grotz, V. L. and I. C. Munro (2009). "An overview of the safety of sucralose." Regulatory Toxicology and Pharmacology 55(1): 1-5.

Haeckel, R., P. Hanecke (2009). "Experience with the Application of the German Standard DIN 32645 for the Determination of the Detection Limit." LaboratoriumsMedizin 22(5): 273-280.

Hao, C., R. Clement (2007). "Liquid chromatography–tandem mass spectrometry of bioactive pharmaceutical compounds in the aquatic environment—a decade's activities." Analytical and Bioanalytical Chemistry 387(4): 1247-1257.

Hatano, K. and A. Nakao (2002). "Determination of sucralose in foods by liquid chromatography/tandem mass spectrometry." J. Food Hyg. Soc. Japan(42): 267-272.

Holcapek, M., Volna, K. (2004). "Effects of ion-pairing reagents on the electrospray signal suppression of sulphonated dyes and intermediates." Journal of Mass Spectrometry 39(1): 43-50.

Hordern, B. K., R. M. Dinsdale (2009). "Illicit drugs and pharmaceuticals in the environment - Forensic applications of environmental data, Part 2: Pharmaceuticals as chemical markers of faecal water contamination." Environmental Pollution 157(6): 1778-1786.

Horne, J., H. T. Lawless (2002). "Bitter Taste of Saccharin and Acesulfame-K." Chem. Senses 27(1): 31-38.

Isidori, M., M. Bellotta (2009). "Estrogenic activity of pharmaceuticals in the aquatic environment." Environment International 35(5): 826-829.

Jackson, J. B. C. (1992). "Pleistocene Perspectives on Coral Reef Community Structure." American Zoology 32(6): 719-731.

John, B. A., S. G. Wood (2000). "The pharmacokinetics and metabolism of sucralose in the rabbit." Food and Chemical Toxicology 38(Supplement 2): 111-113.

Jonkers, N., H. Govers (2005). "Adduct formation in LC-ESI-MS of nonylphenol ethoxylates: mass spectrometrical, theoretical and quantitative analytical aspects." Analytica Chimica Acta 531(2): 217-228.

Khuri, A. I. and J. A. Cornell (1996). Response Surfaces (statistics: A Series Of Textbooks And Monographs) New York, CRC Press.

Kille, J. W., W. C. L. Ford (2000). "Sucralose: lack of effects on sperm glycolysis and reproduction in the rat." Food and Chemical Toxicology 38(Supplement 2): 19-29.

Kille, J. W., J. M. Tesh (2000). "Sucralose: assessment of teratogenic potential in the rat and the rabbit." Food and Chemical Toxicology 38(Supplement 2): 43-52.

King, R., R. Bonfiglio (2000). "Mechanistic investigation of ionization suppression in electrospray ionization." Journal of the American Society for Mass Spectrometry 11(11): 942-950.

Kolpin, D. W., E. T. Furlong (2002). "Pharmaceuticals, Hormones, and Other Organic Wastewater Contaminants in U.S. Streams, 1999-2000: A National Reconnaissance." Environmental Science & Technology 36(6): 1202-1211.

Kuhn, C., B. Bufe (2004). "Bitter Taste Receptors for Saccharin and Acesulfame K." J. Neurosci. 24(45): 10260-10265.

Kuster, M., M. López de Alda (2009). "Liquid chromatography-tandem mass spectrometric analysis and regulatory issues of polar pesticides in natural and treated waters." Journal of Chromatography A 1216(3): 520-529.

Labare, M. P. and M. Alexander (1994). "Microbial cometabolism of sucralose, a chlorinated disaccharide, in environmental samples." Applied Microbiology and Biotechnology 42(1): 173-178

Lapointe, B. E. (1997). "Nutrient thresholds for bottom-up control of macroalgal blooms on coral reefs in Jamaica and southeast Florida." Limnology and Oceanography 42(5): 1119-1131.

Lapointe, B. E. and M. W. Clark (1992). "NUTRIENT INPUTS FROM THE WATERSHED AND COASTAL EUTROPHICATION IN THE FLORIDA KEYS." Estuaries 15(4): 465-476.

Leon, S. J. (2006). Linear Algebra (with applications). New York, Prentice Hall.

Lesser, M. P. (2004). "Experimental biology of coral reef ecosystems." Journal of Experimental Marine Biology and Ecology 300(1-2): 217-252.

Loos, R., B. M. Gawlik (2009). "Sucralose screening in European surface waters using a solid-phase extraction-liquid chromatography-triple quadrupole mass spectrometry method." Journal of Chromatography A 1216(7): 1126-1131.

Mallet, C. R., Z. Lu (2004). "A study of ion suppression effects in electrospray ionization from mobile phase additives and solid-phase extracts." Rapid Communications in Mass Spectrometry 18(1): 49-58.

Manisali, I., D. D. Y. Chen (2006). "Electrospray ionization source geometry for mass spectrometry: past, present, and future." TrAC Trends in Analytical Chemistry 25(3): 243-256.

Mann, S. W., M. M. Yuschak (2000). "A carcinogenicity study of sucralose in the CD-1 mouse." Food and Chemical Toxicology 38(Supplement 2): 91-97.

Mann, S. W., M. M. Yuschak (2000). "A combined chronic toxicity/carcinogenicity study of sucralose in Sprague-Dawley rats." Food and Chemical Toxicology 38(Supplement 2): 71-89.

Matuszewski, B. K., M. L. Constanzer (1998). "Matrix Effect in Quantitative LC/MS/MS Analyses of Biological Fluids: A Method for Determination of Finasteride in Human Plasma at Picogram Per Milliliter Concentrations." Analytical Chemistry 70(5): 882-889.

Matuszewski, B. K., M. L. Constanzer (2003). "Strategies for the Assessment of Matrix Effect in Quantitative Bioanalytical Methods Based on HPLC - MS/MS." Analytical Chemistry 75(13): 3019-3030.

Mead, R. N., J. B. Morgan (2009). "Occurrence of the artificial sweetener sucralose in coastal and marine waters of the United States." Marine Chemistry 116(1-4): 13-17.

Navia, J. L., R. E. Walkup (1996). Production of sucralose without intermediate isolation of crystalline sucralose-6-ester http://www.freepatentsonline.com/5498709.html. I. McNeil-PPC. United States Patent 5498709.

Niessen, W. M. A. (1998). "Advances in instrumentation in liquid chromatography-mass spectrometry and related liquid-introduction techniques." Journal of Chromatography A 794(1-2): 407-435.

Pamela, K. C., A. K. Christina (1998). "Prophage induction of indigenous marine lysogenic bacteria by environmental pollutants." Marine Ecology Progress Series 164: 125-133.

Patterson, K. L. and J. W. Porter (2002). "The etiology of white pox, a lethal disease of the Caribbean elkhorn coral, Acropora palmata." Proceedings of the National Academy of Sciences of the United States of America 99(13): 8725-8730.

Paul, J. H., J. B. Rose (1995). "Viral Tracer Studies Indicate Contamination of Marine Waters by Sewage Disposal Practices in Key Largo, Florida." Appl. Environ. Microbiol. 61(6): 2230-2234.

Petrovic, M., M. D. Hernando (2005). "Liquid chromatography-tandem mass spectrometry for the analysis of pharmaceutical residues in environmental samples: a review." Journal of Chromatography A 1067(1-2): 1-14.

Porter, J. W., P. Dustan (2001). "Patterns of spread of coral disease in the Florida Keys." Hydrobiologia 460(1): 1-24.

Precht, W. F. and S. L. Miller (2007). Ecological Shifts along the Florida Reef Tract: The Past as a Key to the Future. In the Geological Approaches to Coral Reef Ecology. New York, Springer: 237-312.

Qiu, W., Z. Wang (2007). "GC–MS Determination of Sucralose in Splenda." Chromatographia 66(11): 935-939.

Roberts, A., A. G. Renwick (2000). "Sucralose metabolism and pharmacokinetics in man." Food and Chemical Toxicology 38(Supplement 2): 31-41.

Schwarzenbach, R. P., P. M. Gschwend (1995). Environmental organic chemistry : illustrative examples, problems, and case studies. New York, Wiley.

Shinn, E. A., R. S. Reese (1994). "Fate and Pathways of Injection-Well Effluent in the Florida Keys." U.S. Geological Survey Open-File Report 94-276. 116. p.

Shore, L. S. and M. Shemesh (2003). "Naturally produced steroid hormones and their release into the environment." Pure and Applied Chemistry 75(11-12): 1859-1871.

Sims, J., A. Roberts (2000). "The metabolic fate of sucralose in rats." Food and Chemical Toxicology 38(Supplement 2): 115-121.

Singh, S. P. and P. R. Gardinali Accepted for Ecotoxicology.

Singh, S. P. and P. R. Gardinali (2006). "Trace determination of 1-aminopropanone, a potential marker for wastewater contamination by liquid chromatography and atmospheric pressure chemical ionization-mass spectrometry." Water Research 40(3): 588-594.

Stokstad, E. (2001). "Humans to Blame for Coral Loss." Science 293:593.
USEPA (1984). "Guidelines establishing test procedures for the analysis of pollutants, analytical methods for biological Pollutants in wastewater and sewage sludge, final rule." Federal Register, 40 CFR Parts 136 and 503 72(57).

Wang, Z.-W. and X.-L. Liu (2008). "Medium optimization for antifungal active substances production from a newly isolated Paenibacillus sp. using response surface methodology." Bioresource Technology 99(17): 8245-8251.

Weigel, S., U. Berger (2004). "Determination of selected pharmaceuticals and caffeine in sewage and seawater from Tromsø/Norway with emphasis on ibuprofen and its metabolites." Chemosphere 56(6): 583-592.

Weinbauer, M. G., D. Fuks (1993). "Distribution of Viruses and Dissolved DNA along a Coastal Trophic Gradient in the Northern Adriatic Sea." Appl. Environ. Microbiol. 59(12): 4074-4082.

Wiet, S. G. and P. K. Beyts (1992). "Sensory Characteristics of Sucralose and other High Intensity Sweeteners." Journal of Food Science 57(4): 1014-1019.

Wommack, K. E. and R. R. Colwell (2000). "Virioplankton: Viruses in Aquatic Ecosystems." Microbiol. Mol. Biol. Rev. 64(1): 69-114.

Wood, S. G., B. A. John (2000). "The pharmacokinetics and metabolism of sucralose in the dog." Food and Chemical Toxicology 38(Supplement 2): 99-106.

Young, D. A. and W. H. Bowen (1990). "The Influence of Sucralose on Bacterial Metabolism." Journal of Dental Research 69(8): 1480-1484.

Zorn, M. E., R. D. Gibbons (1997). "Weighted Least-Squares Approach To Calculating Limits of Detection and Quantification by Modeling Variability as a Function of Concentration." Analytical Chemistry 69(15): 3069-3075.

Appendix

A.1 APLICATION OF RESPONSE SURFACE METHODOLOGY FOR IONIZATION TUNING OF SUCRALOSE ADDUCT IONS

A.1.1 Central Composite Design of Experiment

As introduced in the previous section, ion formation, is influenced by source geometry, mobile phase composition and (relevant to this section) ESI parameters of the acceleration region. In addition, we report a distinct ESI ion profile of sucralose compared to the previous studies. The goal of this section is to answer the following questions: 1.) can multi-parameter tuning of ESI parameters, that control the behavior of ions in the acceleration region, optimize ion formation for each of the following sucralose ions - deprotonated molecular ion $[M-H]^-$ – 397 m/z, hydrated adduct $[M+2*H_2O-H]^-$ – 433 m/z and acetate adduct $[M+C_2H_3O_2]^-$ – 457 m/z? 2.) What are the ESI parameter values that optimize ionization efficiency for the sucralose-acetate adduct?

An orthogonal four factor CCD was applied in this research (Khuri and Cornell, 1996). The main ESI parameters of the source acceleration region were selected as the variables. These parameters are: tube lens voltage, capillary voltage, capillary temperature and nebulizing gas flow. It was effectively used as a design matrix to fit a second order model, including interaction terms, on the experimental data. The orthogonal rotatable central composite design (CCD) gives almost as much information and requires many fewer tests than the full factorial design. For instance, a full factorial

test with four factors requires 3^4= 81 runs, while the CCD with four factors requires only $N = 2^k + 2k + n_0 = 36$ runs (n_0 is the number of replicate center points).

Also, the CCD was developed to minimize the variance of the β coefficients – the coefficients of the linear equation - for the selected linear model. The CCD consists of the following: 1.) Factorial (cube) portion: A complete or fraction of a 2^k factorial design where the factor levels are coded to the standard -1, +1 values. 2.) Replicate n_0 center points ($n_0 \geq 1$) on the design matrix. 3.) Axial portion: Two axial points on the axis of each design variable at a distance α from the design center. The main idea in this section is to review practical aspects of the central composite design that are relevant for our study concerning the ESI sucralose ionization tuning. In essence, a major criterion for usefulness of an experimental design is the distribution of the variance function. The variance function for an orthogonal second order rotatable design is given by the following equation.

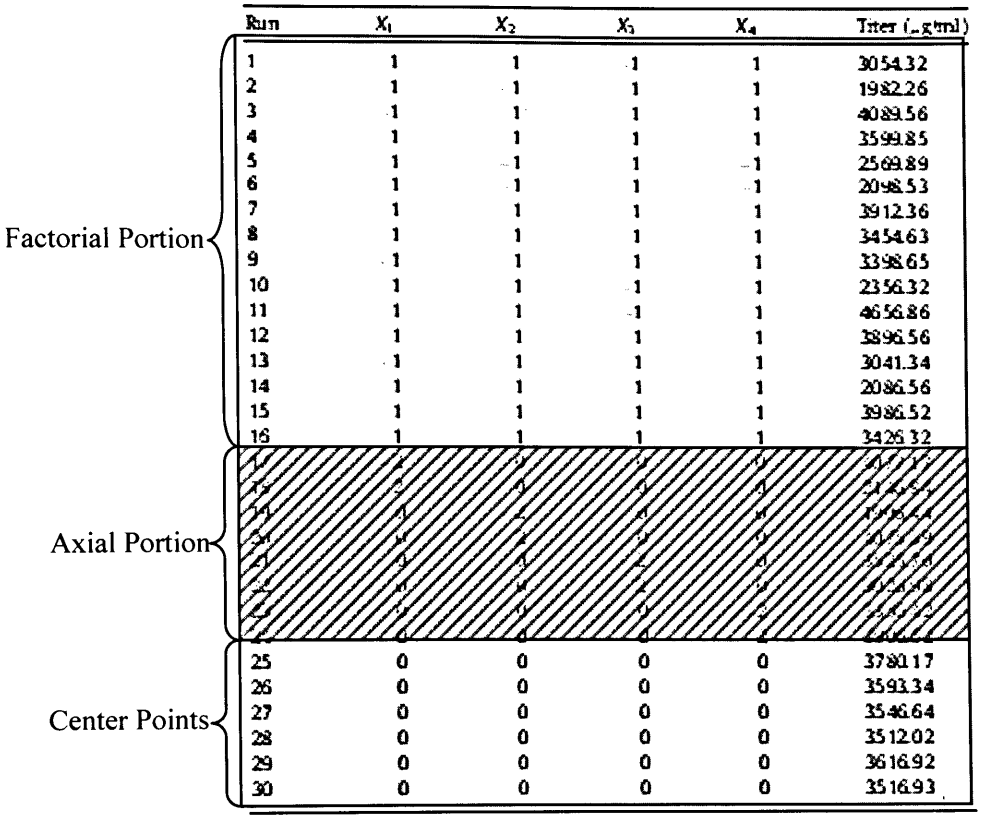

Run	X_1	X_2	X_3	X_4	Titer (μg/ml)
1	1	1	1	1	3054.32
2	1	1	1	1	1982.26
3	1	1	1	1	4089.56
4	1	1	1	1	3599.85
5	1	1	1	1	2569.89
6	1	1	1	1	2098.53
7	1	1	1	1	3912.36
8	1	1	1	1	3454.63
9	1	1	1	1	3398.65
10	1	1	1	1	2356.32
11	1	1	1	1	4656.86
12	1	1	1	1	3896.56
13	1	1	1	1	3041.34
14	1	1	1	1	2086.56
15	1	1	1	1	3986.52
16	1	1	1	1	3426.32
25	0	0	0	0	3780.17
26	0	0	0	0	3593.34
27	0	0	0	0	3546.64
28	0	0	0	0	3512.02
29	0	0	0	0	3616.92
30	0	0	0	0	3516.93

Figure A.1. A tabular representation of a central composite design in $k = 4$
Source: Wang and Liu, 2008.

(1) $$V(\rho) = \frac{1}{2}\left(k + 2 + \rho^4\right)$$

k is the number of variables; ρ is radii of the design space.

The variance function indicates a general condition whereby variance is proportional to the number of factors in the model as well as distance from the design center.

Central composite designs that are rotatable, whether orthogonal or not, ensure constant variance of the predicted response at all points that are equidistant from the center of the design. Uniform precision CCD's produce prediction variance stability in the

vicinity of the design center. The figure 2.7 below helps to clarify the condition of uniform precision. The standardized weight function is simply the inverse of the variance function, given by

(2) $$W(\rho) = \{V(\rho)\}^{-1}$$

The figure 2.7 below is a measure of precision (weight function) as a function of ρ, which are the radii of a sphere from the design center. A uniform precision CCD has a design chosen (select values of axial points α and replicates of center points n_0) so that the value of $V(\rho)$ at $\rho = 0$ is equal to the variance at $\rho = 1$ (Box and Hunter, 1956). This property provides approximately a uniform value of prediction variance inside a sphere of radius 1. To remain within the scope of this report, I will simply introduce the definition of λ and it's relevance in the case of orthogonal rotatable designs. The variance function $V(\rho)$ for a rotatable design depends only on $\lambda_0, \lambda_2, \cdots, \lambda_{2d}$ (d = design order), which are the elements of the moment matrix $N^{-1}X^TX$.

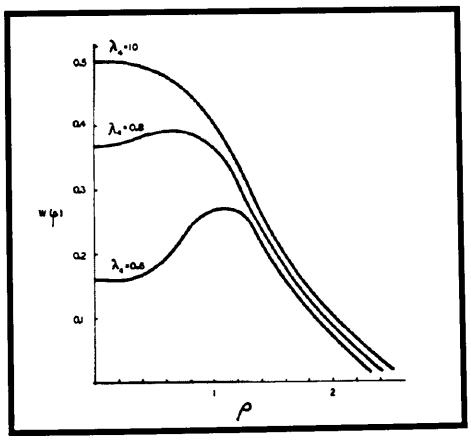

Figure A.2. Weight functions for second order rotatable designs having various values of λ when k=2. Source: Box and Hunter, 1956.

It will suffice to say that a CCD is orthogonal if the mixed fourth order moment, [*iijj*], or equivalently λ_4 is equal to unity, and generally the highest precision is afforded from such a design (Khuri and Cornell, 1996).

Uniform precision and orthogonal CCD are dependent on the number of replicates selected for the center points of the design matrix n_0 as well as the value selected to define the axial portion of the design matrix α. The table above concerns the appropriate values for these parameters to produce the desirable qualities of either uniform precision or an orthogonal rotatable CCD. The current research employed the orthogonal design. Some fundamental aspects of the role of these parameters will be reviewed.

Central composite rotatable second order designs

k	2		3		4		5		5(½ rep)		6		6(½ rep)		7		7(½ rep)		8		8(½ rep)		8(½ rep)	
n_c	4		8		16		32		16		64		32		128		64		256		128		64	
n_a	4		6		8		10		10		12		12		14		14		16		16		16	
n_s (Table 1)	5		6		7		10		6		15		9		21		14		28		20		13	
n_s (Orthogonal)		8		9		12		17		10		24		15		35		22		52		33		20
N total	13	16	20	23	31	36	52	59	32	36	91	100	53	59	163	177	92	100	300	324	164	177	93	100
$\alpha = n_c^{\frac{1}{4}}$	1.414		1.682		2.000		2.378		2.000		2.828		2.378		3.364		2.828		4.000		3.364		2.828	
λ_4 Table 1	0.81		0.86		0.86		0.89		0.89		0.91		0.90		0.92		0.92		0.93		0.93		0.93	
λ_4 Orthogonal		1		0.99		1		1.01		1		1		1.01		1.00		1		1		1.00		1
ρ_a/ρ_c	1.000		0.971		1.000		1.064		0.894		1.155		0.971		1.271		1.069		1.414		1.189		1.000	

Figure A.3. Prescribed values for a uniform precision and orthogonal rotatable CCD. Source: Box and Hunter, 1956.

Fortunately, the Central composite models were thoroughly investigated and improved over 45 years ago by G.E.P. Box and J.S. Hunter. Their work was a major part of the foundation of designs of experiments in statistics (Box and Hunter, 1956). The figure 2.8 above is from their seminal work in CCD's and provides the user key values to

construct the efficient uniform precision or orthogonal design matrices. Furthermore, this resource was applied for the current study.

The following is a brief introduction of some key equations to provide a basic idea of the relationship between λ_4, α and n_0. The objective was to generate an orthogonal CCD. As such, the following values were calculated. The mixed fourth order moment, [*iijj*], or equivalently, λ_4, is equal to unity as follows.

(3) $$\lambda_4 = \frac{FN}{\left(F + 2\alpha^2\right)^2} = 1$$

F, N and *k* are respectively: the number of points in the factorial portion of the design matrix, the total number of points in the design matrix and the number of independent variables of the linear model. Given that we are choosing to construct a design matrix that is both orthogonal and rotatable we must choose an appropriate value of center point replicates n_0 as follows. This is the first step. Calculation of n_0 : We only need to replace α^2 in equation 3 by $\sqrt{F}$, since $\alpha^4 = \sqrt{F}$ is a condition for a CCD to be rotatable.

(4) $$\left(F + 2\sqrt{F}\right)^2 = F\left(F + 2k + n_0\right)$$

Solving equation 4 for n_0 we get the number of center point replicates required for the orthogonal design

(5) $$n_0 = 4\sqrt{F} + 4 - 2k$$

F is easily calculated as follows.

(6) $$F = 2^k$$

N is calculated from the following equation

(7) $$N = F + 2k + n_0$$

Finally, the axial setting α is solved by rearranging equation 3

(8) $$\alpha = \left(\frac{(FN)^{1/2} - F}{2} \right)^{1/2}$$

Test	Coded level of variables				Actual level of variables			
	X1	X2	X3	X4	Capillary (V)	Ion spray voltage (kV)	Tube lens (V)	Sheath gas (psi)
1	0	0	0	0	-5	4	10	35
2	0	0	0	0	-5	4	10	35
3	0	0	0	0	-5	4	10	35
4	0	0	0	0	-5	4	10	35
5	0	0	0	0	-5	4	10	35
6	0	0	0	0	-5	4	10	35
7	0	0	0	0	-5	4	10	35
8	0	0	0	0	-5	4	10	35
9	0	0	0	0	-5	4	10	35
10	0	0	0	0	-5	4	10	35
11	0	0	0	0	-5	4	10	35
12	0	0	0	0	-5	4	10	35
13	-1	-1	-1	-1	-15	3	-5	25
14	1	-1	-1	-1	5	3	-5	25
15	-1	1	-1	-1	-15	5	-5	25
16	1	1	-1	-1	5	5	-5	25
17	-1	-1	1	-1	-15	3	25	25
18	1	-1	1	-1	5	3	25	25
19	-1	1	1	-1	-15	5	25	25
20	1	1	1	-1	5	5	25	25
21	-1	-1	-1	1	-15	3	-5	45
22	1	-1	-1	1	5	3	-5	45
23	-1	1	-1	1	-15	5	-5	45
24	1	1	-1	1	5	5	-5	45
25	-1	-1	1	1	-15	3	25	45
26	1	-1	1	1	5	3	25	45
27	-1	1	1	1	-15	5	25	45
28	1	1	1	1	5	5	25	45
29	-2	0	0	0	-25	4	10	35
30	2	0	0	0	15	4	10	35
31	0	-2	0	0	-5	2	10	35
32	0	2	0	0	-5	6	10	35
33	0	0	-2	0	-5	4	-20	35
34	0	0	2	0	-5	4	40	35
35	0	0	0	-2	-5	4	10	15
36	0	0	0	2	-5	4	10	55

Table A.1. Central composite design matrix includes actual and coded values.

Code	Actual value of a variable
$-\beta$	x_{min}
-1	$[(x_{max}+x_{min})/2]-[(x_{max}-x_{min})/2\alpha]$
0	$(x_{max}+x_{min})/2$
+1	$[(x_{max}+x_{min})/2]+[(x_{max}-x_{min})/2\alpha]$
$+\beta$	x_{max}

Table A.2. Relationship between coded and the actual values of the design matrix

The equations in the table above were applied to calculate the factorial points (-1,1), center point (0) and axial point $(-\beta,\beta)$ of the design matrix. The table 2.1 below is the orthogonal central composite design matrix for the current study. Notice the three segments of the design: factorial portion, center points and axial points. The following section is a brief overview of least squares analysis, analysis of variance and their application to response surface methodology.

A.1.2 Least Squares Estimates and Analysis of Variance

Response surface methodology (RSM) is a collection of statistical and mathematical models that are useful for understanding various types of processes and engineering problems (Khuri and Cornell, 1996). For the current study of ESI and sucralose, a second order four parameter linear model was used to fit a response surface on the actual data. To effectively answer these questions, the four parameters selected are: tube lens voltage, capillary voltage, capillary temperature and nebulizing gas flow. Given the goal is to optimize the response variable (sucralose response); the key is to find a suitable approximation for the true functional relationship between ion current and the

four independent variables above. A full quadratic model was used to consider the contribution of quadratic curvature and interaction effects.

(9)
$$Y = \beta_0 + \beta_1 X_1 + \beta_2 X_2 + \beta_3 X_3 + \beta_4 X_4 + \beta_{11} X_{11}^2 + \beta_{22} X_{22}^2 + \beta_{33} X_{33}^2 + \beta_{44} X_{44}^2 + \beta_{12} X_1 X_2 + \beta_{13} X_1 X_3 + \beta_{14} X_1 X_4 + \beta_{23} X_2 X_3 + \beta_{34} X_3 X_4 + \varepsilon$$

The prior section introduced some fundamental aspects of the CCD: importance of designing a suitable matrix for the experimental region and the conversion of actual selected experimental values to coded form. Two sets of response vectors were obtained from the experiments. Moreover, each run was applied to answer each question above. Regression analysis was then carried out in matrix notation to determine the coefficients of the response model. The response data is the *actual* response variable Y.

(10)
$$Y = \begin{bmatrix} Y_1 \\ \vdots \\ Y_n \end{bmatrix}$$

The matrix of independent variables is called the X matrix and is constructed of a column of ones (intercept vector), a column for each model parameter and n number of rows (each test run is a row). The X matrix has the following form for a four factor full quadratic model with n runs

(11)
$$X = \begin{bmatrix} 1 & X_{1i} & X_{2i} & X_{3i} & X_{4i} & X_{11i}^2 & X_{22i}^2 & X_{33i}^2 & X_{44i}^2 & X_{12i}^2 & X_{13i}^2 & X_{14i}^2 & X_{24i}^2 & X_{34i}^2 & X_{23i}^2 \\ \vdots & \vdots & \vdots & \vdots & \vdots & \vdots & \vdots & \vdots & \vdots & \vdots & \vdots & \vdots & \vdots & \vdots & \vdots \\ 1 & X_{1n} & X_{2n} & X_{3n} & X_{4n} & X_{11n}^2 & X_{22n}^2 & X_{33n}^2 & X_{44n}^2 & X_{12n}^2 & X_{13n}^2 & X_{14n}^2 & X_{24n}^2 & X_{34n}^2 & X_{23n}^2 \end{bmatrix}$$

The coefficients β, for each parameter in the second order equation 9, are then easily calculated from the matrices above with the following equation

(12) $$\hat{B}' = \begin{bmatrix} \hat{\beta}_0 \\ \vdots \\ \hat{\beta}_{34} \end{bmatrix} = \left(X^T X\right)^{-1} X^T Y$$

It follows that the *estimated* response variable from the regression model $\hat{Y}$ is easily calculated as follows

(13) $$\hat{Y} = X\left(X^T X\right)^{-1} X^T Y = X\hat{\beta} = \begin{bmatrix} \hat{Y}_1 \\ \vdots \\ \hat{Y}_n \end{bmatrix}$$

Analysis of variance is applied to further understand the significance of particular aspects of the regression model. In this study a second order linear equation has been fit to the data containing four input variables; whereas each input variable is a particular ESI controlling parameter and the response variable is the response of the sucralose deprotonated molecular ion $[M-H]^-$ – 397 m/z, or a particular sucralose adduct ion: hydrated adduct $[M+2*H_2O-H]^-$ – 433 m/z or the acetate adduct $[M+C_2H_3O_2]^-$ – 457 m/z. The overall purpose of applying least squares analysis and analysis of variance to this particular investigation is to fit an approximate model on the data set - to understand the functional relationship between the independent variables and the response variable. Analysis of variance provides a framework to assess the contribution of either individual parameters, or groups of terms to the overall regression model.

The contribution of linear, quadratic and crossproduct terms must be assessed (The order grouping of terms includes all terms of a particular order, irrespective of the variable assignment) to select a suitable regression equation for the data. Further insight about the regression model will be acquired from evaluating the contribution of each

factor to the regression model (Each factor includes all orders of terms that correspond to each independent variable). In essence, ANOVA provides metrics to evaluate how well the regression terms *explain* the data set.

Given that the scope of this report places greater emphasis on statistics, as applied to chemometrics, we will briefly review the basic equations for ANOVA in matrix notation: sum of squares for regression $SS(reg)$, sum of squares for residual $SS(res)$ and R^2. The sum of squares for regression is a measure of variation in the response variable Y about their mean, ascribed to the regression.

(14) $$SS_{reg} = \hat{\beta} X^T Y$$

The mean square for regression provides an estimate based on (*n-2*) degrees of freedom of the variance about the regression. The value is simply the $SS(reg)$ divided by the degrees of freedom

(15) $$MS_{reg} = \frac{SS_{reg}}{n-2}$$

The sum of squares for residual is a measure of variation in the response variable Y about their mean, ascribed to the variation not explained by the regression, the error.

(16) $$SS_{res} = Y^T Y - \hat{\beta} X^T Y$$

Also, the mean square for residual is the SS_{res} normalized by the degrees of freedom as such

(17) $$MS_{res} = \left(\sqrt{\frac{SS_{res}}{n-2}} \right)^2$$

R^2 Statistic, or the correlation coefficient, is the proportion of total regression explained by the mean. It is calculated as follows

(18) $$R^2 = 1 - \frac{SS_{reg}}{Y^T Y} = 1 - \frac{SS_{reg}}{SS_{total}}$$

In the results section, these measures will be applied to evaluate the contribution of particular parameter groupings - e.g. order of terms (linear, quadratic or crossproduct terms, variable terms (that include all term orders) and individual coefficient terms - to the variation of the response variable about their mean. ANOVA analysis will elucidate the ESI parameters that significantly affect the response of sucralose and sucralose acetate adduct.

A.1.3 Canonical Analysis – Exploration of the Fitted Response Surface

The sections above were an overview of the techniques applied to fit and evaluate a second order linear model on the dataset. This section will introduce canonical analysis (Khuri and Cornell, 1996), a technique used to find the values of the input variables e.g. capillary voltage, tube lens voltage, ion spray voltage and sheath gas flow, which produce the maximum ionization of sucralose and the sucralose acetate adduct. The canonical equation for a k variable system will be developed. This is accomplished by translating the origin of the response system $(x_1, x_2, ..., x_k) = (0, 0, ..., 0)$ to the stationary point x_0. To

follow through with this process, intermediate variables must first be defined that express the second order linear model (equation 9) in terms of the values of z_i. The intermediate variables are $(x_1 - x_{10}, x_2 - x_{20}, ..., x_k - x_{k0}) = (z_1, z_2, ..., z_k)$. First, the standard second order linear equation will be written in matrix notation. This form of the equation corresponds to the origin of the response system $(x_1, x_2, ..., x_k) = (0, 0, ..., 0)$

(19) $$\hat{Y}(x) = b_0 + x^T b + x^T Bx$$

It follows that the second order response system expressed in terms of the values of z_i is

(20) $$\hat{Y}(z) = b_0 + (z + x_0)^T b + (z + x_0)^T B(z + x_0)$$

$$= \hat{Y}_0 + z^T Bz$$

The z^T variable is the transpose of the z vector (an expression of the difference between the x variable at the origin and the stationary point). The elements of the $(k \times 1)$ vector b are the estimated coefficients of the first order terms, while the elements of the $(k \times k)$ symmetric matrix B are the estimated coefficients of the second order terms. In this form of the linear model, the predicted response $\hat{Y}(z)$ is a linear function of estimate of the response at the stationary point $\hat{Y}_0$ plus a quadratic form in the values of z_i.

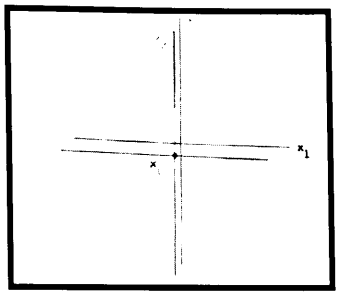

Figure A.4. Graphical representation of a stationary point x_0 relative to the origin of the response system $(x_1, x_2, ..., x_k) = (0, 0, ..., 0)$ Source: Khuri and Cornell, 1996.

The figure 2.9 above is a hypothetical arrangement between the standard origin of a response system $(x_1, x_2, ..., x_k) = (0, 0, ..., 0)$ and the values of the response system at which the slope of the response surface is zero in all directions x_0. As one can see, this step is just a translation of the center of the design to the stationary point, which can be either a maximum or a minimum of the response surface.

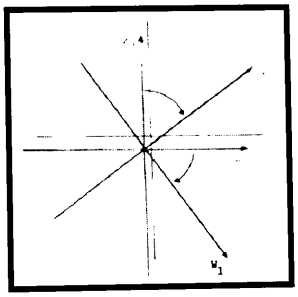

Figure A.5. Rotation of the z_i axes to form the W_i axes. Source: Khuri and Cornell, 1996

The following step is to obtain the canonical form of the predicted response equation. To do so eigenvectors and eigenvalues must be defined. Again, given the context of this report, I will refrain from an in depth discussion of these terms. If one wishes to delve into a deeper coverage of linear algebra please refer to (ref X). A new set

of variables $(W_1, W_2, ..., W_k)$ must be defined to obtain a canonical form of the equation 20 - such that $W = (W_1, W_2, ..., W_k)^T$

(21) $$W = M^T z$$

M is an $(k \times k)$ orthogonal matrix whose columns are eigenvectors of the matrix B, the estimated coefficients of second order terms. The matrix M provides important information about the dataset. For example, when multiplied with B (second order coefficients of the response system) in the following way - $M^T BM = diag(\lambda_1, \lambda_2, ..., \lambda_k)$, it produces a symmetric matrix with diagonal elements as the eigenvalues of the coefficients in B. The importance of this relationship will now become clear.

The axes of this canonical form are illustrated in the figure 2.10 above and are called the principal axes of the response system. Basically, the transformation of equation 21 is a rotation of the z_i axes (the z variables were explained earlier and has to do with the stationary point x_0) to form the W_i axes. This transformation is now applied to express the quadratic term of equation 20 (response system in terms of z_i) in the W_i variables as follows

(22) $$z^T Bz = W^T M^T BMW$$

$$= \lambda_1 W_1^2 + \cdots + \lambda_k W_k^2$$

The eigenvalues λ_i of the equation above are the coefficients in the canonical linear equation below

(23) $$\hat{Y} = \hat{Y}_0 + \sum_{i=1}^{k} \lambda_i W_i^2$$

This equation is laden with information about the shape of the response surface. For instance, if all of the eigenvalues (remember these values are the coefficients of the canonical form of the response system) are negative then the response surface is a maximum. If all of the values are positive, then the surface is a minimum. If all of the values are of mixed signs, then the fitted surface is a saddle point.

As might be evident by this point, the matrix M encodes information about the fitted response system: shape of the fitted surface in terms of the W_i axes, which provides a functional basis to derive the stationary point x_0. A good metaphor for the M matrix is that of a bridge. The M matrix serves as a bridge between the W_i axes and the x_i axes as follows

(24) $$\begin{aligned} W &= M^T z \\ &= M^T (x - x_0) \end{aligned}$$

Respectively, between the eigenvalues λ_i that provide information about the shape of the fitted surface and the stationary point in terms of the original x_i axes, the corresponding maximum or minimum values of the fitted response surface. The techniques above were applied to optimize the ESI response of sucralose ions and derive the parameter values that correspond to the maximum response.

A.2 Calculating Limits of Detection and Quantification by Modeling Variability as a Function of Concentration

A.2.1 Introduction

To calculate the lower limits of the measurement process for sucralose, two specific lower levels were determined. The first level is the critical level (L_C) and is "a decision limit at which one may decide whether or not the result of an analysis indicates detection". This has a specifically defined false positive (type 1) error rate (α) that results from the hypothesis test H_0: X=0 at the lowest detectable concentration (Currie, 1968). The critical level (L_C) minimizes the risk of only Type 1 error. The second level is a detection limit (L_D); Currie defined this as "the true concentration at which a given analytical procedure may be relied upon to lead to detection". At the detection limit, a second hypotheses test H_0: $X=L_D$ allows the false negative (type 2) error rate (β) to be set at the critical level (L_C) which effectively increases the confidence of detection by minimizing Type 1 and Type 2 error rates. This procedure will be explained in some detail.

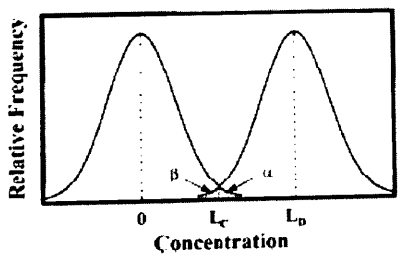

Figure A. 6. Relationship between a blank (X=0), the critical level (L_C) and the limit of detection (L_D). The distributions from both hypothesis tests overlap at L_C with false positive type 1 error (α) and false negative type 2 error (β) values are equivalent. Source: Zorn, et al. 1997.

Thus, if a suitable approach to model the variability of the target analyte as a function of concentration is applied - and properly accounted for by a weighted least squares regression model - then the true detection limit of a particular compound in a particular set of conditions (complete extraction and analytical system) can be systematically determined.

Current techniques derive detection and quantification limits from variability in analyte response at a single arbitrary spiked concentration e.g. U.S. EPA's MDL (U.S. EPA, 1984). Nonetheless, raw calibration data is characteristically heteroscedastic, meaning that the standard deviations of replicate responses - $s(Y_i)$ - are non-constant and increase as a function of concentration x_i as depicted in the figure 3.3 below. Thus, these single concentration designs are inconsistent with the heteroscedastic condition and result in calculated limits that are directly dependent on the variability of the spiking concentration, usually much higher than the actual limit of detection and not from the variabilility of the actual L_D or L_Q.

In order to accurately assess lower limits of detection, a calibration design by Zorn, et al. 1997, was carefully followed that applied a weighted least squares approach to calculate the two lower detection levels - the critical level (L_C) and the detection limit (L_D) - by modeling variability as a function of sucralose concentration (Figure 3.4). The purpose of applying weighted least squares regression is to accommodate the condition of non-constant variance that is observed in the actual data, by normalizing least squares estimates with weights: the inverse relationship of the actual variance of the response variable. In doing so, greater weight is given to the lower end of the concentration range

(Figure 3.3 bottom). Subsequently, detection limits can be derived from the actual variability of the analyte, at the statistically determined detection limit, rather than from the variability at an arbitrary concentration.

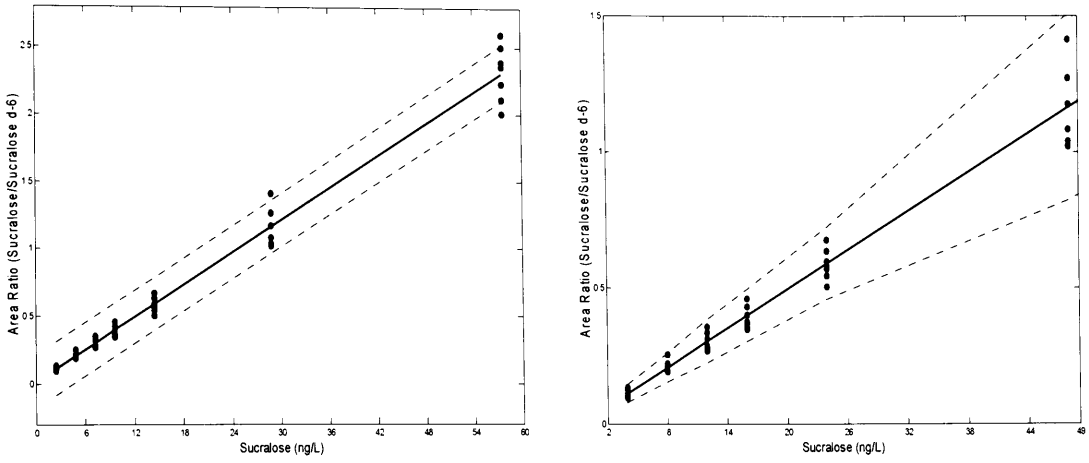

Figure A.7. Unweighted least squares regression analysis (left) and weighted least squares regression analysis (right). The widths of the weighted confidence intervals change with concentration, accurately representing the actual variance structure of the data.

A.2.2 Weighted Least Squares Regression

A calibration design was applied to calculate complete method detection limits for two analytical methods e.g. HPLC-ESI-MSMS and GC/MS. Meaning that the detection limits consider the bias and error from the complete analytical methodology, not just the measurement error from the instrumental analysis. The following sequence of equations was applied to calculate detection limits for both instrumental approaches. Complete method detection limits were calculated by spiking a series of sucralose concentration levels and sucralose d-6 at a constant concentration to serve as a deuterium labeled surrogate internal standard, into a series of 500 ml deionized water samples. The samples

were then extracted and processed in the same manner as a real sample. For each sample concentration, seven replicates were then analyzed in random order. Subsequently, sample chromatograms were integrated and peak area ratios were calculated as peak area of sucralose over peak area of sucralose d-6. The variability of sucralose peak area ratios were then assessed for each concentration level as pure error sum of squares (variance). Furthermore, equations applied to calculate important weighted regression estimates will be listed below. Their utility will become clear at the later stages of this section, where the detection limit calculations are explained. The pure error sum of squares was calculated first in the following manner.

(2) $$SS_{p.e.} = \sum_{u=1}^{n_j} y_{ju}^2 - \frac{\left(\sum_{u=1}^{n_j} y_{ju}\right)^2}{n_j}$$

The pure error mean square is a variance measure and was then calculated.

(3) $$MS_{p.e.} = SS_{p.e} / d.f._{p.e} = s_e^2$$

The weights are the inverse of the pure error mean square and were calculated for each sucralose concentration level as such.

(4) $$\hat{w}_i = \frac{1}{s_e^2}$$

The application of matrix notation will simplify calculations for the necessary weighted regression estimates. The diagonal matrices V^{-1} and P^{-1} were generated from the weights as follows.

(5) $$V^{-1} = \begin{bmatrix} \hat{w}_1 & & 0 \\ & \ddots & \\ 0 & & \hat{w}_J \end{bmatrix}$$

(6) $$P^{-1} = \begin{bmatrix} \sqrt{\hat{w}_1} & & 0 \\ & \ddots & \\ 0 & & \sqrt{\hat{w}_J} \end{bmatrix}$$

The response variable for the linear model is the vector Y_i and is simply the area ratios.

y_i = ith calibration level (sucralose area)/ ith calibration level (sucralose d-6 area)

(7) $$Y = \begin{bmatrix} y_1 \\ \vdots \\ \vdots \\ y_n \end{bmatrix}$$

The concentration values for the sucralose calibration design are encoded in the following independent variable matrix.

(8) $$X = \begin{bmatrix} 1 & x_1 \\ \vdots & \vdots \\ \vdots & \vdots \\ 1 & x_n \end{bmatrix}$$

The weighted sum of squares for regression was calculated in the following manner.

(9) $$SS_{Wregression} = Y^T V^{-1} X \left(X^T V^{-1} X \right)^{-1} X^T V^{-1} Y$$

And the weighted total sum of squares as such.

(10) $$SS_{Wtotal} = Y^T V^{-1} Y$$

The weighted residual sum of squares is then calculated by the difference between the above two values.

(11) $$SS_{Wresidual} = SS_{Wtotal} - SS_{Wregression}$$

The weighted residual standard deviation reflects the deviation from the regression line, which is actually the variability among the samples, and is calculated with the following equation.

(12) $$s_W = \sqrt{\frac{SS_{Wres}}{n_j - 2}}$$

The coefficients β, of the weighted linear regression equation $Y = b_{0W} + b_{1W}X + \varepsilon$, are also required to calculate detection limits and were calculated in the following manner.

(13) $$b = \hat{\beta} = \left(X^T V^{-1} X\right)^{-1} \left(X^T V^{-1} Y\right)$$

The weighted mean concentration value is calculated in the following manner.

(14) $$\bar{X}_W = \frac{\sum\left(P^{-1}X\right)}{\sum \hat{w}_i}$$

A.2.3 Modeling the Variability of Sucralose Response and calculating Detection Limits

The calculated pure error mean square values s_e^2 were modeled and fit with a suitable polynomial, exponential or power function (Figure 3.4). One way to evaluate the quality of the fit is to ensure that the dependent variable (s_e^2) does not tend to an unrealistic negative values as the x variable approaches zero concentration.

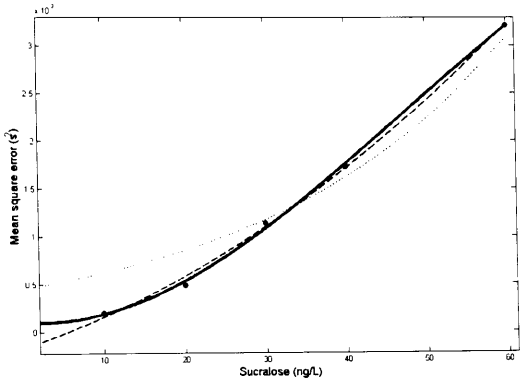

Figure A.8. Standard deviation as a function of concentration. Fit using a quadratic model, a cubic model and an exponential model.

Once a good model fit was attained, the desired weight and the weighted least squares estimates were applied to calculate L_C and L_D. The following one sided weighted prediction interval was applied to calculate R_C – the response unit value at the critical concentration (the decision limit that leads to detection) (Figure 3.5).

(15) $$R_C = b_{0w} + t_{(1-\alpha,n-p-2)} s_W \left[\frac{1}{w_0} + \frac{1}{\sum w_i} + \frac{\bar{X}_W^2}{Sxx_W} \right]^{1/2}$$

b_{0w} is the weighted intercept term of the linear equation and $t_{(1-\alpha,n-p-2)}$ is directly acquired from a standard t table, w_0 is the inverse of the variance at the lowest possible measurement of the analyte and was acquired from the variability model. The rest of the equation terms were calculated from the weighted least squares estimates that were described above.

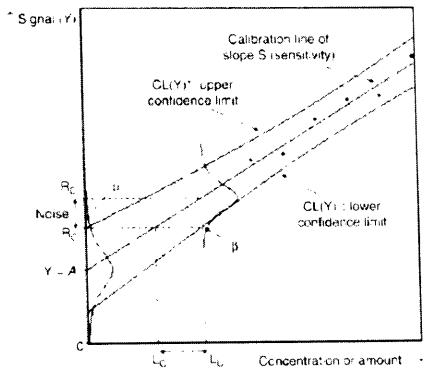

Figure A.9. Calibration design critical level in response (R_C) and concentration units and limit of detection in concentration units (L_C). Source: Boyd, et al. 2006.

The response units were converted to concentration units (L_C) by simply subtracting the intercept coefficient from the response, then dividing the difference by the first order coefficient of the weighted linear model in the following way (Figure 3.5).

(16) $$L_C = \frac{Y_C - b_{0w}}{b_{1w}}$$

The following step was to calculate the concentration unit value at the detection limit (L_D). As explained in the opening paragraph of this section, and clearly illustrated in figure 3.2 & 3.5, the detection limit corresponds to a pure error mean square value that is

twice the pure error mean square value of the target analyte at the critical level (L_C) (Currie, 1968). As such, the weight corresponding to 2* $s_{C^*}^2$ was entered into the following one sided equation, as were the weighted least squares estimates, to calculate the detection limit of the target analyte.

(17)
$$L_D = L_{C^*} + \frac{t_{(1-\beta,n-p-2)} s_W}{b_{1w}} \left[\frac{1}{w_{Ld}} + \frac{1}{\sum w_i} + \frac{\left(2 * L_{C^*} - \bar{X}_W\right)^2}{Sxx_W} \right]^{1/2}$$